Chair of Ferrous Metallurgy

Master's Thesis

MgO-C Refractory-Slag interaction: A Study on the effect of antioxidants and slag MgO content on MgO-C refractory-slag interactions in Si-killed steel refining

Oluwabukunmi Omotola Otegbeye

December 2022

MONTANUNIVERSITÄT LEOBEN
www.unileoben.ac.at

AFFIDAVIT

I declare on oath that I wrote this thesis independently, did not use other than the specified sources and aids, and did not otherwise use any unauthorized aids.

I declare that I have read, understood, and complied with the guidelines of the senate of the Montanuniversität Leoben for "Good Scientific Practice".

Furthermore, I declare that the electronic and printed version of the submitted thesis are identical, both, formally and with regard to content.

Date 06.12.2022

otegbeyetola

Signature Author
Oluwabukunmi Omotola Otegbeye

Abstract

Magnesia-carbon (MgO-C) refractories are typically used in secondary metallurgy applications because of their excellent corrosion resistance against basic slags and high thermal strength. The contact area of the refractory and slag is usually the area of the refractory susceptible to corrosion during secondary metallurgy processes. In this master's thesis work, the degradation mechanisms of different MgO-C refractory materials were investigated by using a lab-scale static crucible testing method. The major differentiating factor for the refractories is the different antioxidant composition of the refractories. Antioxidants are metallic additives like aluminium (Al) and silicon (Si) added to the MgO-C refractory to prevent carbon oxidation. Also, different slags with varying MgO slag content (wt. %) were used for the experiments. After the different experiments, samples from the reacted and infiltrated refractories were taken and used for the analysis of the main corrosion/ degradation phenomena.

Before structuring the design of the experiment, it was critical to have in-depth knowledge and understanding of different literature studies that had investigated similar topics. In chapter 2 of this thesis, a literature review was done to highlight various relevant topics ranging from steel cleanliness, non-metallic inclusions (NMIs) and their characterisation, secondary metallurgy processes, types of slags and refractory materials used in secondary metallurgy and the interaction between refractory (MgO-C) and slag/steel.

Based on the different inferences drawn from the literature review, an approach of the refractory/ slag interaction investigation was adopted, and the design of the experiment was done accordingly. Chapter 3 gives an overview of the research methodology used to perform the experimental part. Characterisation and analysis of the experiment results was the main feature of chapter 4. The analysis was made on sub-topics on refractory and slag interaction at the interface, slag composition evolution and penetration of the slag into the refractory. Discussions on the various effects of the different parameters like dwelling time, slag composition and antioxidant composition of the refractory were done in chapter 5.

Table of contents

List of Figures

List of tables

1. Introduction

Environment-friendly and economically efficient production of steel requires efficient use of energy and materials. The key to achieving this goal is to design and produce steel with a minimal amount of inclusions i.e., producing relatively clean steel. Steel cleanliness is an important factor for high-quality steel grades, as certain metallic residuals or non-metallic impurities have a significant impact on the steel's physical and mechanical properties of these steel grades like their optics, fatigue strength, and fracture toughness amongst others. The general quality of a steel grade is determined by the chemical composition, amount, and nature (morphology, size) of inclusions present in the steel. Steel quality and cleanliness can be improved during secondary metallurgy in the ladle, where the steel can be

desiliconized, dephosphorized, desulfurized, degassed, and be alloyed. The refractory quality in this ladle can be important as the refractory can be a source of exothermic inclusions in the steel. One of the major roles of ladle slag, for example, is to minimize or absorb inclusions formed in the steel via the steel`s interaction with the refractory. This highlights the effect of the ladle's refractory lining on steel cleanliness, as it could cause exogenous inclusions in the steel and changes in slag chemistry and composition. So, it is critical that these reactions or interactions are identified and analysed, to minimize the effects of the refractory in producing high-quality steel grades.

There is a correlation between the dissolution of solid oxides into the molten slag and the refractory lining lifetime. In recent years, the use of refractory bricks composed of more than one refractory component has increased as it improves the durability of the brick. To have a better understanding of the dissolution behaviour of such composite materials, it may be necessary to investigate and clarify the dissolution mechanism and kinetics of each component.

So far, there have been several experiments that have shown clear evidence of interaction between liquid steel and refractory materials which is dependent on both the steel composition and the type of refractory material. Also, several studies have highlighted the interaction between slags and refractory[1, 2]. Therefore, the reactions that transfer elements between the refractories and molten steel, and between slag and refractories are closely related to the product quality.

This thesis aims at investigating and having a better understanding of how the interaction of molten steel, slag and refractory materials affects steel cleanliness. The thesis will be applied to an industrial case study involving refractories from Calderys and flux from Imerys.

2. Literature Review

2.1 Steel cleanliness

Clean steel is categorized as steel with a relatively low content of inclusions and tramp elements like S, total oxygen (T.O.), N, H, and sometimes C. Steel cleanliness is a critical determinant of the quality of steel. There is a growing market demand for clean steel in the industry because of its better mechanical properties. Individually or in combination, the effects of these impurities can negatively influence the properties of the steel, such as tensile strength, formability, welding capability, cracking resistance, corrosion resistance, fatigue resistance [3, 4]. According to studies, Ultra Low Carbon (ULC)

and Low-Carbon (LC) steels used for aerospace and automotive applications, as well as linepipe and spring steels are seen as cleanness sensitive steel grades. To meet the growing demand of clean steel for these applications, more focus has been drawn to the subject of steel cleanliness [5]. It is quite difficult and unrealistic to control the number of impurities and inclusions during primary metallurgical processes e.g., in the blast furnace or oxygen converter. However, secondary metallurgy processes give an avenue for controlling these impurities and inclusions. In the past, secondary metallurgy processes were limited to carburization, deoxidation and minor alloying of the molten steel. However, due to higher demand for high quality steel and improved properties, various types of molten steel treatment in ladle have been developed. Some of these treatment techniques are highlighted below [6].

- Hot metal desulphurization is used to obtain low S contents in BOF-produced steel grades. Hot metal desulphurisation is commonly conducted in a ladle using a desulphurisation reagent that is either injected into the metal bath or added on top of it. The sulphur in the molten steel is reduced in the slag and it is accompanied by oxidation in the steel bath. Calcium is a common reagent that is added to react with sulphur.
- Tundish metallurgy to precipitate and remove non-metallic inclusions
- Vacuum treatment of liquid steel helps in achieving the lowest contents of C and S as well as the removal of dissolved gases like H and N.
- Vacuum steel degassing process amongst other processes allows steelmakers to obtain lower overall inclusion contents and a higher degree of steel cleanness.

The inclusion size distribution in steel is very critical. Large macro-inclusions are harmful to the mechanical properties of the steel. One kg of typical LCAK steel contains 10^7– 10^9 inclusions, with sizes between 80 to 270 µm [7]. Large inclusions may be difficult to detect as they are rare in comparison to the smaller inclusions. A single large inclusion in an entire steel melt could cause catastrophic defects to the steel. Clean steel, therefore, requires not only monitoring the steel's average inclusion number but also preventing inclusions with large sizes that are harmful to the product. The maximum size of inclusion a particular steel grade is allowed to have is referred to as its critical inclusion size [8].

2.2 Secondary metallurgy process

In the production of steel from either ores or scrap, secondary refining is required to reduce the tap-to-tap time in the converter or electric arc furnace (EAF) and to adjust the liquid steel composition and temperature to the desired level before casting. Depending on the amount of deoxidation or 'killing' required, secondary metallurgy starts with deoxidation. By floating out, the oxides produced during deoxidation can be removed from the steel. The oxide particles which remain in the steel are called non-metallic inclusions. These inclusions have different melting points and mechanical properties than the steel. During casting, the inclusion’s liquidus temperature is very important,

because in the small size casting channels (such as the ladle nozzle or tundish nozzle) certain oxides with higher liquidus temperature than the steel might accumulate and clog the casting channels. Inclusions have low formability compared to the steel matrix, hence they may create cracks in the steel during the rolling process[9, 10]. **Error! Reference source not found.** show typical secondary metallurgy processes during steel making. After the melting of steel in the converter/EAF, the molten steel is treated in the ladle to reduce inclusions. Finally, it is transferred to the continuous caster where it is transformed into semi-finished steel products [9].

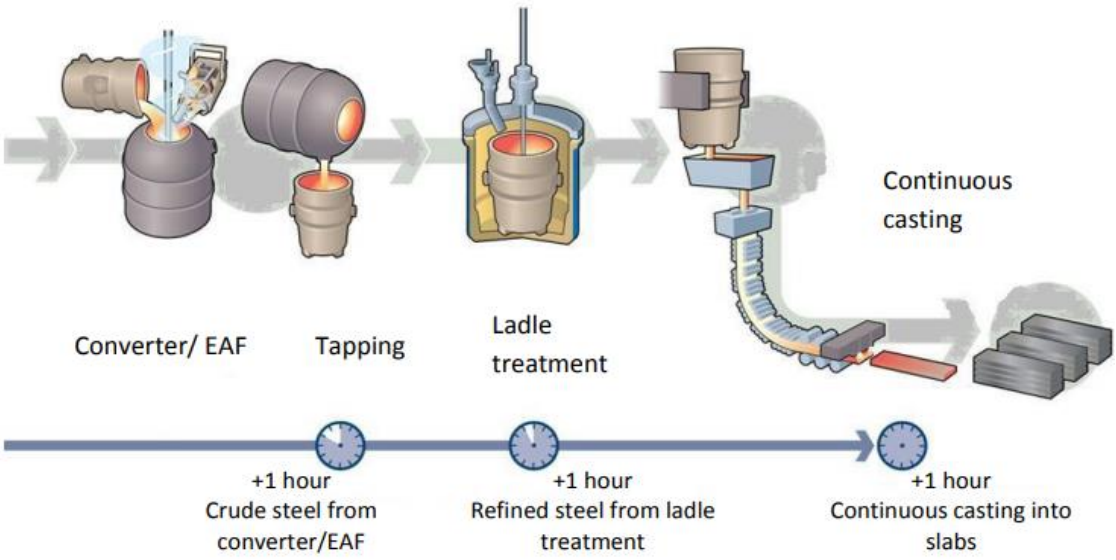

Figure 2. 1. Steps in secondary steelmaking [9]

The main processes in secondary metallurgy are [10]:

• **Desulphurization**: interactions between steel and slag will eliminate S dissolved in the steel. Desulphurization is a function of steel composition and slag interaction. Additionally, other thermodynamic conditions such as the sulfide capacity of the steel and oxygen in the steel also affect desulphurization. Another essential parameter in desulphurization is the temperature at which the desulphurization process is carried out. The temperature consequently also influences the slag viscosity, as well as the sulfide capacity of the slag. In desulphurization, an optimum slag composition is saturated with CaO, to facilitate the exchange of the dissolved S in the steel with O from the slag [11].

• **Alloying**: the chemical composition of steel could be modified by the addition of alloying elements like Ni and Cr amongst others. Alloying is carried out in the heating and wire feeding position of the ladle station.

• **Degassing**: this treatment is done via specialized equipment under vacuum conditions. It eliminates C and produces very low-carbon steel that cannot be achieved in the BOF or EAF. Degassing is also used to achieve low amounts of dissolved N and H.

• **Removal of inclusions**: coagulation and flotation of inclusions extract them from steel during the process. This is a very important mechanism for achieving steel cleanliness.

• **Modification of calcium inclusion**: remaining ones can be altered or modified with a process called calcium treatment. Calcium treatment is a common procedure used before the continuous casting of low carbon steel. Conventionally, calcium is introduced into the steel bath by steel-clad calcium wire injection. Because calcium has a lower melting point in comparison to steel, calcium can be introduced into the steel while the steel is in the molten state. Once calcium is added to liquid steel, Ca dissolves into the steel and forms calcium aluminates. These calcium aluminates are liquid, hence do not form clusters, thereby preventing the nozzle from blocking[12].

Secondary metallurgy processes include different methods and different types of equipment are used. Some of these equipments are [10]:

• **VOD (Vacuum Oxygen Degassing)**: it is an oxygen-injected Vacuum Degasser. Oxygen injection over the steel bath surface favors the decarburization reaction. Since O reacts with C before Cr, it is mainly used mostly to produce stainless steel.

• **LMF (Ladle Metallurgical Furnace)**: the steel is heated by electric arcs in this equipment; the furnace has three graphite electrodes that form an electrical arc with the liquid steel that transfers the thermal energy to the rest of the steel from the steel surface. Adjustment of the chemical composition by ferroalloy addition is possible. To homogenize and achieve a strong slag-steel contact, bubbling is carried out by inert gas injection through porous plugs at the bottom of the ladle. It is ideal for desulphurization.

• **CAS-OB (Composition Adjustment by Sealed argon bubbling with Oxygen Blowing):** in this system, a bell goes down to the steel to create an inert region over the "slag eye" (area without slag because it was pushed aside by the bubbling plume). Underneath this bell, the alloy addition and chemical reheating by oxygen and aluminum injection are made. It generates more Al_2O_3 than an LMF, and to obtain clean steel, it must float out.

• **RH (Ruhrstahl - Heraeus)**: it is a vacuum vessel with two legs immersed in liquid steel. Argon is injected into one leg and creates the flow of steel. Decarburization is performed in this vessel. This equipment is quicker than VD and has greater efficiency.

2.3 Non-Metallic Inclusions (NMIs)

NMIs are non-metallic substances with different chemical compositions compared to the surrounding matrix. Theoretically, it is also possible to have metallic inclusions present in the steel matrix. A typical example of metallic inclusions is incompletely dissolved alloying elements. Non-metallic inclusions can be critical to the steel properties, especially concerning their effect on the steel mechanical properties [13, 14]. Generally, NMIs in steel have a negative effect on the mechanical properties of steel with exception of a few special steel grades. An example of such steel grade is ODS (Oxide dispersion strengthened) steels, where inclusions like TiO_2, Y_2O_3 have positive effects on their mechanical properties like hot strength and yield strength [15].

2.3.1 NMIs classification

NMIs can be characterised mainly according to their sources, size, distribution (clustering), chemical composition, and time/temperature.

2.3.1.1. Source

The origin of the inclusion is a criterion used to classify steel inclusions. Inclusions could find their way into the steel bath endogenously or from outside the steel bath.

Endogenous inclusions: Particles that are products of the reactions inside the steel melt, during cooling or solidification. An example of this form of inclusion as shown in **Error! Reference source not found.** is alumina inclusions formed in a high oxygen environment [16].

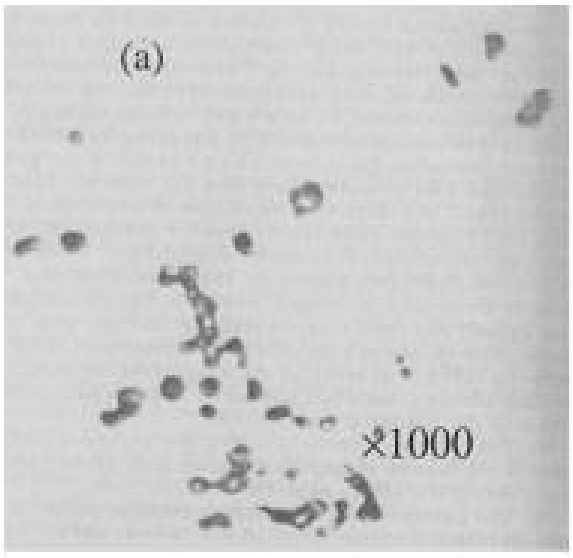

Figure 2. 2. Microscopy image of an example of endogenous inclusions [16].

Exogenous inclusions: Particles that intruded the steel melt from outside, e.g., small parts of refractory material, entrapped slag droplets, or particles from reoxidation of the steel by the atmosphere. An example of this form of inclusions as shown in **Error! Reference source not found.** is a complex calcium aluminate inclusion created by calcium addition to the molten steel to modify alumina inclusions to prevent nozzle clogging in continuous casting [16].

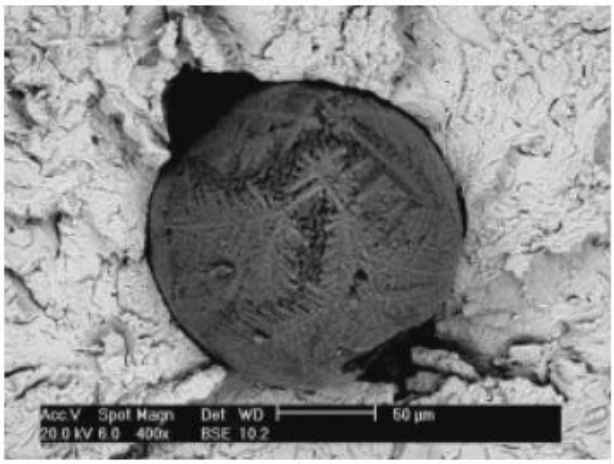

Figure 2. 3. Microscopy image of calcium aluminate inclusion (exogenous inclusions) [16].

2.3.1.2. By size

The size of the inclusion is a very important parameter that could be used for steel inclusion classification. The effect of inclusions on the properties of steel could vary depending on their size. The various size classification of NMIs is[17].

- Macro inclusions (≥ 100µm).
- Meso inclusions (≥ 15µm to < 100µm).
- Micro inclusions (≥ 1µm to < 15µm).
- Sub micro inclusions (< 1 µm).

An overview of the microscopic images of the size distribution of inclusion is shown in **Error! Reference source not found.** [17]

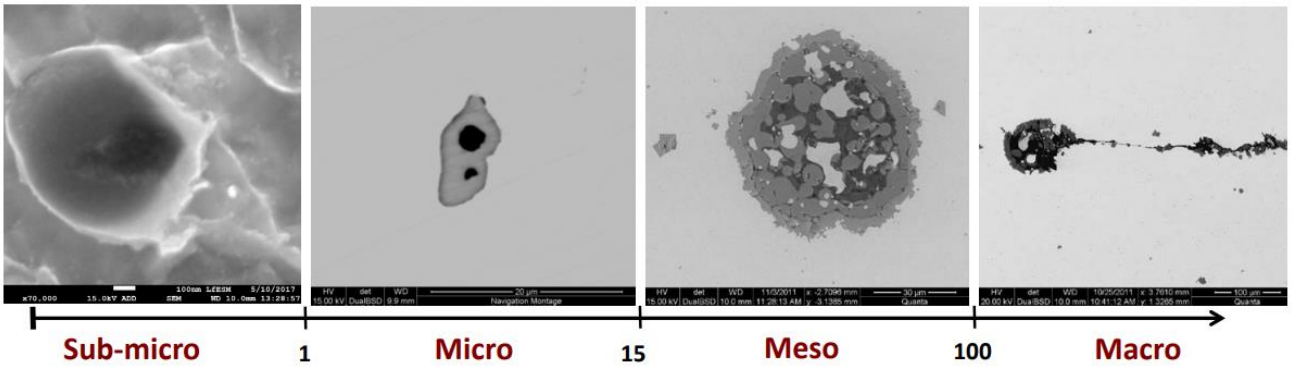

Figure 2. 4. Microscopic images of different size ranges of NMIs [17].

2.3.1.3. Clustering degree

NMIs are generally not good for steel, especially when these inclusions are in clusters. Steel cleanliness is not dependent on total oxygen (Otot), but it also depends on the size and the distribution of these inclusions. The individual spinel inclusions are usually small in size and are not considered to be very harmful unless they appear as clusters. Such clusters may be several individuals and small particles (micro-inclusions) in the cross-section of the steel matrix. Large size to analyze the degree of clustering there must be an understanding on how closely these inclusions are to each other. The degree of clustering is measured using the DIN 50602 standard. This method of measurement relies on the length, width, and diameter of the inclusions individually or as a cluster. Inclusions based on this

measurement are either spherical (d ≥ 3 µm) or elongated (l ≥ 3 to 1410 µm and w ≥ 2 µm). Examples of the degree of clustering include [18, 19]:

- **Single inclusion:** these are relatively isolated inclusions. Based on microscopic distance measured, the closest inclusion to these inclusions is more than 40 µm away in the y-direction (vertical) and 10 µm in the x-direction (horizontal). Single inclusions are usually having both elongated (α) and spherical (β) shapes.
- **Double inclusion**: this class occurs when two inclusions have a closeness of less than 40 µm away in the y-direction and 10 µm in the x-direction with the next inclusion or set of inclusions. Furthermore, they are more than 40 µm away in the y-direction and 10 µm in the x-direction from the next inclusions or set of inclusions. Double inclusions could have either elongated (α) or spherical (β) shapes.
- **Inclusion Lines**: this is made up of three or more particles close to each other in a range less than 40 µm away in the y-direction and less than 10 µm in the x-direction. Inclusion lines could have either elongated (α) or spherical (β) shapes.
- **Inclusion Clusters**: are made up of multiple inclusion lines or several single inclusions in proximity. These inclusion lines must less than 40 µm away in the y-direction and 10 µm in the x-direction.

Figure 2. 5. Degree of inclusion clustering according to EN 10247:2007 [18]. Figure 2. 5 illustrates the measurement of the degree of inclusion clustering according to EN 10247:2007. Figure 2. 6 show clusters of alumina during the processing in the liquid state [13].

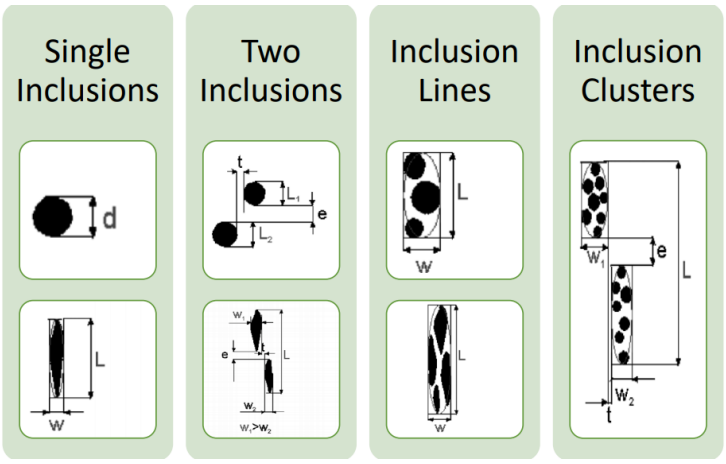

Figure 2. 5. Degree of inclusion clustering according to EN 10247:2007 [18].

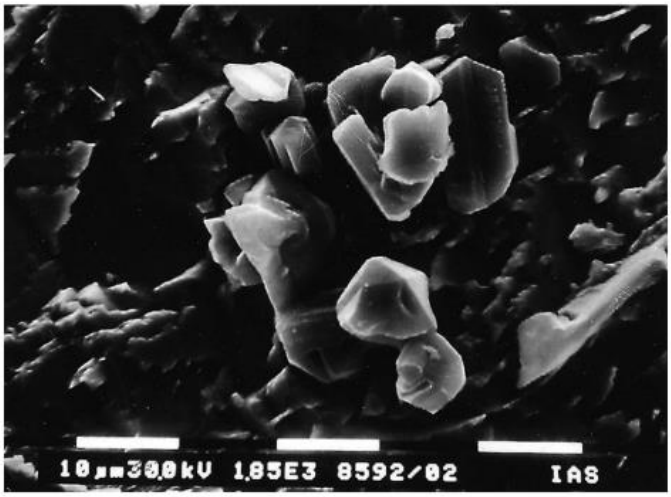

Figure 2. 6. SEM image of alumina cluster in steel after deep etching [13].

2.3.1.4. Chemical composition

Another typical way to classify NMIs is by their chemical composition. Some of the elements that make up NMIs are:

- **Oxides**: Alumina (Al_2O_3) inclusions are usually found in LCAK steel, and silica (SiO_2) inclusions in Si-killed steel are common examples of oxide non-metallic inclusion. They are formed by the reaction of dissolved oxygen and the added aluminium and silicon deoxidants [20].
- **Sulphides**: The sulphide inclusions formed during solidification of steel are predominantly manganese sulphide. MnS as a common inclusion adversely influences the mechanical properties, physical properties and corrosion resistance of the steels [21].
- **Nitrides:** Nitrides are usually formed in the steel melt or during solidification. These nitrides may be considered as non-metallic inclusions and do not have beneficial effects on the steel quality. For example, nitrides are known to inhibit grain growth. Some elements that typically form nitride non-metallic inclusions are Al, Nb, Ti, V, and Zr [22].
- **Carbides:** Carbide particles like TiC are known fatigue crack initiators and can also cause surface defects.

2.3.1.5. Time/Temperature of formation

Inclusions can form at various steps, temperatures, and different process conditions. The time and temperature at which the inclusions are formed are a way to classify them:

- Primary inclusions: Particles that are formed in the liquid steel by deoxidation or desulfurization reactions.
- Secondary inclusions: Particles that emerge above the temperature that the steel phase starts solidifying.
- Tertiary inclusions: Particles which form during solidification between liquid and solid temperature.
- Quaternary inclusions: Particles which appear in the solid state.

2.3.2 Characterization of inclusions

To effectively characterize the inclusions in a matrix, we must generally evaluate physical characteristics like their size, morphology, distribution, as well as their chemical composition. To identify the inclusions, present in a steel sample, several methods are employed conventionally within the steel-making industry. The size of the inclusions, the volume of the specimen examined, and the time taken for inspection are essential parameters used to differentiate the various possible methods for characterization. If the material volume requiring examination increases, the minimum amount of the measurable inclusions typically increases. This limits the use of ultrasound methods to classify steel inclusions in steel grades like bearing steel, as the detection limit is larger than the inclusions size which needs to be controlled. Thus, the use of smaller representative steel samples is becoming increasingly common for analysis methods that encompass smaller inclusions in their detection range. Indeed, to characterize the total population of inclusions, more than one technique is required [14]. Methods based on the sample surface characterization like OES/PDA, identify inclusions of a maximum size of 20 µm. This method is appropriate to classify the micro-inclusion population. For inclusions with a size greater than 20 µm, other methods like MIDAS (Mannesmann inclusion detection by analyzing surfboards) as will be explained later in the chapter, can be used to identify inclusions of this size. Large inclusions greater than 20 µm can potentially cause devastating effects during production processes or at the beginning of the life cycle of a steel component. Methods with a satisfactory detection limit are required for steel with low inclusion content and small permissible size ranges. Scanning electron microscopy coupled with energy-dispersive X-ray spectrometry (SEM/EDS), which simultaneously offers metallographic images and elementary chemical analysis , is among the most used techniques to study micro-inclusions [23]. More modern equipment requires an automated system as an extra upgrade, which allows the whole sample to be scanned. Indirect methods are used to estimate the number of inclusions. It is often commonly adopted in the industry as it is relatively cheaper, faster, and simpler in comparison to the direct methods. Measuring the total oxygen content of steel samples, which is directly related to the presence of inclusions, is a conventionally used process [24]. Figure 2. 7Figure 2. 7. Assessment techniques of various sizes of inclusions [17] shows the classification of the various assessment techniques of inclusions based on their testing capacity and time taken to analyse the samples [17].

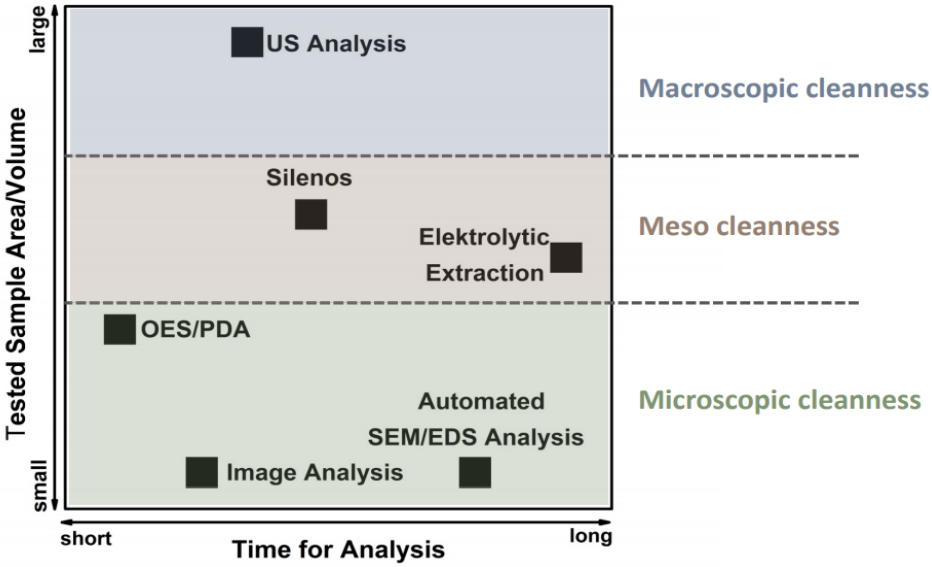

Figure 2. 7. Assessment techniques of various sizes of inclusions [17]

2.3.2.1 Direct methods of inclusion characterization.

There are various direct methods of inclusion analysis and characterization. They include:

- **Optical microscopy**

Optical microscopy is a conventional method that can be used to analyze 2-dimensional sections of inclusions by using an optical microscope. However, inclusions are generally 3-dimensional. Hence, this method is unsuited to analyze complexed-shaped inclusions. Furthermore, relatively small inclusions are difficult to count using this method [25].

- **MIDAS (Mannesmann inclusion detection by analyzing surfboards)**

The MIDAS method is used in the steelmaking industry to detect macroscopic inclusion particles in large volumes of steel. MIDAS could be used to investigate steel volume with weight as high as 45kg, and the result gotten in a relatively short period. The introduction of MIDAS for defining macrocleanness has resulted in major improvements in secondary metallurgy and casting technology processes in the steelmaking industry [26].

MIDAS is an off-line macroscopic inclusion identification system. It increases the probability of finding macro inclusions which are less frequent in steel in comparison to normal metallographic methods. Figure 2.8 highlights the the rolling procedure for a round billet, initially with a twofold lateral spread, and then a fivefold elongation. The rolling procedure is optimised for flat-rolling of the inclusions or clusters, grain refinement, and for a high yield of ultrasonic detection [27].

The MIDAS method of assessment of cleanness is usually used in combination with metallography and SEM/EDX-analysis to get more detailed information about the type, morphology, and chemical composition of oxide inclusions and their origin. Figure 2. 8 shows an example of MIDAS analysis technique as represented in a deformed ladle slag inclusion in a slab surfboard. An SEM analysis of the disintegrated inclusion in form of an elliptical shape (102×312 mm) confirms the chemical composition of the inclusion and ladle slag [27].

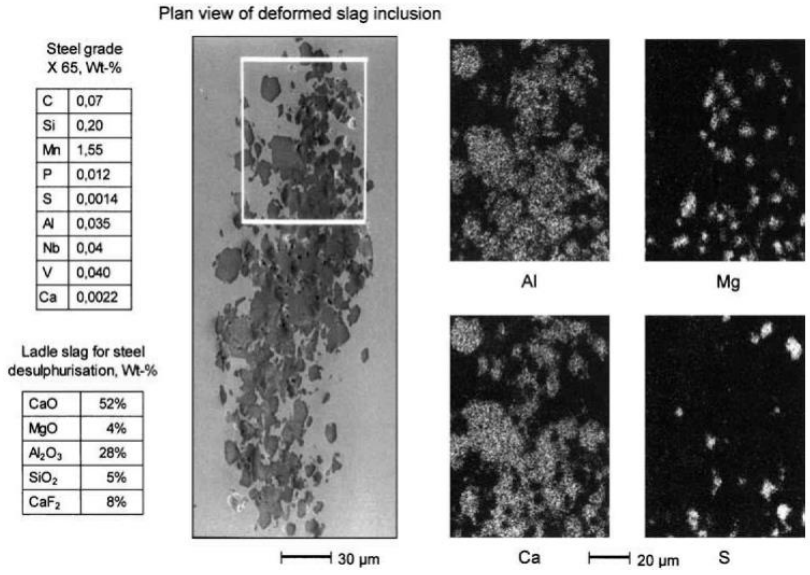

Figure 2. 8. SEM analysis of ladle slag inclusion in MIDAS sample from desulphurisation of plate grade steel X65 [27].

- **Steel Inclusion Level Evaluation by Numerical Optical Systems (SILENOS)**

SILENOS was designed for quick quantification and characterization of non-metallic inclusion of continuously cast steel materials with the aid of images of steel samples milled off in layers. It involves the use of an imaging system, design, and development of efficient algorithms for image analysis, as well as the transfer of the results obtained to the modeling. Computer Graphics are used for visualization and analysis. Afterward, image processing is done, and finally, the method is optimized for use in an industrially usable testing machine [28]**.** Figure 2. 9 shows an imaging machine and the processing methodology of the SILENOS [28].

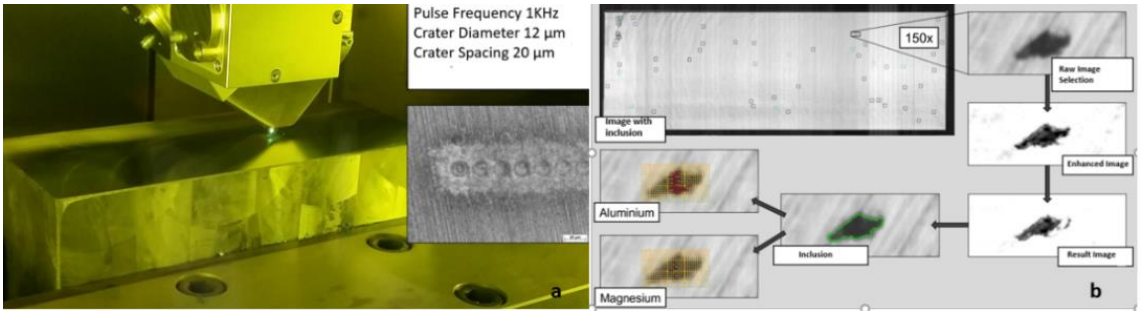

Figure 2. 9. (a) SILENOS imaging machine (b) SILENOS image processing steps [28]

- **Electrolytic extraction**

Electrolytic extraction is done by immersing the steel into an electrolyte. The steel matrix is dissolved using an electric current. The electrolyte which acts as a solvent separates the inclusions from the steel matrix. Afterward, the electrolyte is filtered. The inclusions remaining on the filter are then analyzed using a scanning electron microscope[19]. Figure 2. 10 (a, b and c) shows images of the setup of an electrolytic extraction process. Figure 2. 10a shows filtrates that are produced after the extraction process. Figure 2. 10b shows a simple extraction equipment used for the process, and Figure 2. 10c shows a schematic diagram of the different components of an electrolytic extraction process.

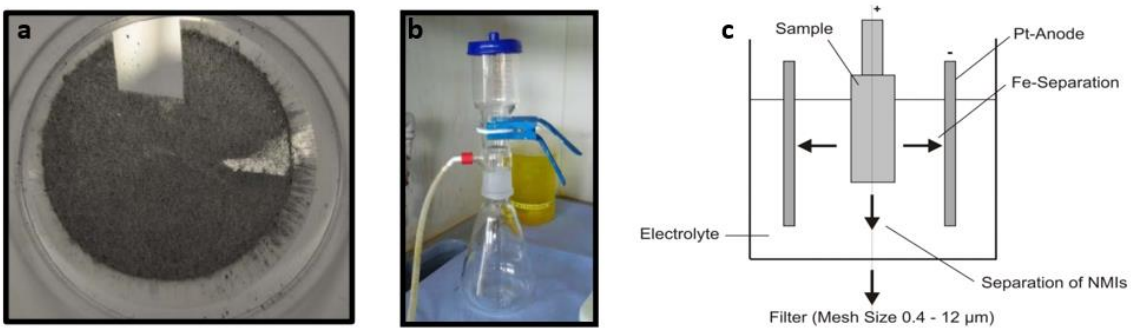

Figure 2. 10. (a) inclusion residue after filtration. (b) Filter device. (c) Schematic of electrolytic extraction [19].

- **Scanning electron microscope (SEM) and Energy Dispersive X-ray microanalysis (EDS)**

In connection with an EDS probe, the automated SEM is one of the most used tools used to measure steel cleanliness. Using the SEM helps to visualize the three-dimensional morphology and the composition of the inclusions that are being examined. To make the 3-dimensional morphological examination, the particles must be extracted, while for the compositional analyses, the inclusions are preferentially analyzed on a flat polished surface. The possibility to obtain data for all the particles scanned within the sample is one of the major advantages of using the automated SEM process. The automated SEM working principle is that due to a difference in greyscale in the BSE Image (backscattered electron image), non-metallic inclusions are detected and their sizes and/or compositions are automatically analyzed. The contrast in the BSE image is hugely dependent on the atomic number of the material, as the color gets brighter with increasing atomic number. In contrast, manual SEM procedures are generally restricted to studying only the inclusions identified by the equipment operator. There is little certainty that the sample will be analyzed equally and in its totality. Unlike manual SEM, the automated SEM scans the sample uniformly and further analyses all recognizable inclusions within the sample. The analysis period depends, amongst other things, on the SEM characteristics, the degree of the automation, the parameters of the analysis, the sample area assessed, and the cleanliness of the sample itself. However, characteristics like phase and morphology, are better analyzed via the manual SEM method in comparison to the automated SEM method, as the manual SEM method analyses each detail in accordance to the operator's specifications [7, 24].

Nevertheless, a combination of manual SEM and automated SEM analysis is an effective way to characterize inclusions. A combination of both SEM techniques provides a detailed analysis of the identified inclusions, as well as helps to statistically characterize the inclusions in number and size. This gives a robust and comprehensive overview of these inclusions [29]. Figure 2. 11 (a, b and c)shows a SEM setup in combination with an EDS probe. The SEM image shows the cross-sectional morphology of the inclusions and the EDS give more details about the inclusion chemistry [19].

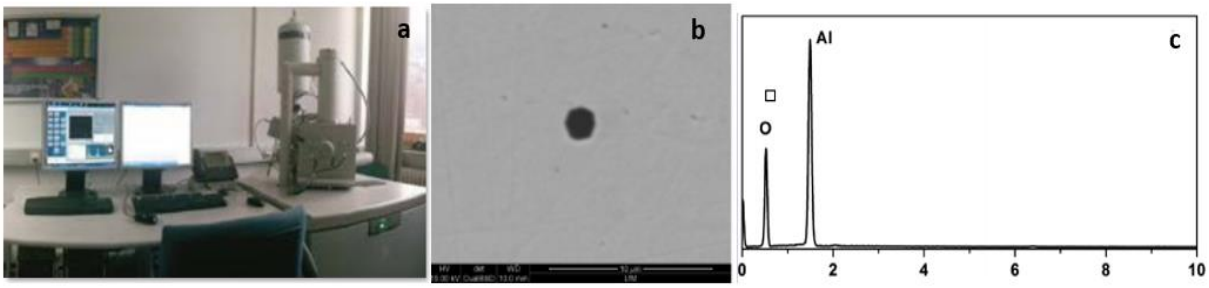

Figure 2. 11. (a) SEM/EDS setup. (b) SEM-images of detected Al_2O_3particles on the analysed sample area. (c) Corresponding EDS analyses to Al_2O_3 particles [19]

- **Image analysis (IA)**

The Image Analysis (IA) method is a software use to evaluate video-scanned microscope images. It differentiates dark and light regions based on a greyscale cut-off. This approach can easily test large areas and higher inclusion numbers. Moreover, for non-metallic inclusions, it is prone to depicting errors such as error scratches, pitting, and stains in its analysis [30].

- **Optical emission spectrometry/pulse discrimination analysis (OES-PDA)**

Optical emission spectroscopy (OES) is used in combination with pulse discrimination analysis (PDA). This combination is one the quickest methods which are employed to estimate cleanliness. Samples used in this method are taken during the manufacturing process. OES-PDA is a relatively common technique that has been successfully used over the years to characterize cleanliness at a microscopic level and to evaluate an inclusion's chemical composition. Inclusions invariably cause high-intensity peaks which are counted to give the PDA index. PDA indexes represent intensities of peaks that exceed the average intensity of the metallic background [31].

- **Laser microprobe mass spectrometry (LAMMS)**

Using microprobe analysis is an effective method for the evaluation of inclusions. Laser microprobe mass spectrometry (LAMMS) is a type of microprobe analysis. It provides high lateral resolution, as well as high elemental sensitivity, and at the same time, structural information. LAMMS is a very useful and efficient method in carrying out investigations and analysis of fine inclusions, specifically oxides. The working principle of LAMMS is that a pulsed laser beam radiates individual particles, and the ones with the lowest laser intensity above an ionization threshold value are chosen for their characteristic pattern of spectrum due to their chemical states. Intensity spectra in LAMMS are associated to specific elements based on already obtained results from a reference sample.

Table 2. 1 Comparison of direct methods for evaluating steel cleanliness.Table 2. 1 compares the direct methods of evaluating steel cleanliness, highlighting their advantages and disadvantages [32].

Table 2. 1 Comparison of direct methods for evaluating steel cleanliness.

Method	Advantages	Shortcomings
MMO	-Inclusion Amount, size, distribution and possibly morphology	-No composition data -Two dimensional -Time consuming
Image Analysis	-Inclusion size distribution measured	-No composition data -morphological data -Two dimensional
SEM and EPMA	-3D morphology -Composition measured	-Measure only individual inclusion -Time consuming
OES-PDA	-Measure total oxygen, size distribution and composition -Fast	-No morphology data -Only for inclusions smaller than 12µm
LAMMS	-Inclusion composition measures	-No morphological data -No size distribution data

2.3.2.2 Indirect methods of NMIs characterisation.

- **Total oxygen**

Total oxygen (T.O) content is an indirect method that is commonly used to estimate steel cleanliness based on the evaluation of oxide inclusions in the steel. The total oxygen in liquid steel is the amount of soluble oxygen in the steel and oxygen present in form of oxide inclusions in the steel. The total oxygen (T.O) in the steel is derived by the summation of the free oxygen (dissolved oxygen) and the oxygen in oxidic non-metallic inclusions. This so-called “free oxygen”, or “active” oxygen can be measured using oxygen sensors [7].

The main benefit of this approach is its simplicity and the speed to obtain values that are directly linked to cleanliness. Its values can be easily correlated with parameters like processing time from the steelmaking process. Although this is a relatively fast and simple method to evaluate the cleanliness of steel during the different stages of production, it only refers to oxide inclusions and does not give details on the inclusions’ chemical composition and morphology. However, the final analysis is much more detailed when data from this technique is used in combination with the results of SEM-EDS research for example [33] [34].

- **Nitrogen pickup**

Nitrogen is an undesirable element in steel, especially in interstitial-free (IF) steel grades. It reduces the steel’s toughness, ductility and increases brittleness at room temperature. The difference in nitrogen content of the molten steel between steelmaking vessels (ladle and tundish) is usually used as an indicator of the air entrained during transfer operations. After deoxidation, the low dissolved oxygen content of the steel makes it susceptible to the rapid absorption of air. Hence, nitrogen pickup serves as an indirect method to measure total oxygen, steel cleanliness, and quality problems from reoxidation inclusions [35, 36].

2.4 Slag for Secondary Steelmaking

The importance of slag in steelmaking cannot be over-emphasized as slags play a significant role in the steelmaking process. Amongst these important functions of slags are [37, 38]:

- Acts as an insulator to prevent the oxidation of the metal,
- Limits heat losses through radiation,
- Removes impurities from the molten metal,
- Prevents nitrogen pickup, and
- Helps dephosphorization and desulfurization.

Over the years, there has been relatively little effort to understand and optimize the slag systems in steelmaking. More recently, with an understanding that the interaction of steel/slags/refractories affects steel quality, there is a more thorough approach to slag design. This approach is tailoring the slag by altering its chemistry using slag engineering or slag optimization. Slag engineering helps to improve the steelmaking process by optimizing the functionality of the slag. Furthermore, it helps to achieve a more cost-effective and quality steel production. Slag engineering has also been utilized to reduce the corrosion rate of the ladle refractory lining. Consequently, this increases the lining’s lifetime. Features of slag engineering include [37–39]:

- Using different slags at the different processing stages,
- Adjusting slag chemistry to adapt to the steel grade produced,
- Altering the slag practice in accordance with the type of refractory used,
- Monitoring the slag compositions continually and,
- Designing slag addition practices and calculations to be done simultaneously as the metallurgical alloying practice is established.

Some of the basics of slag engineering in secondary steelmaking for process optimization are [40, 41]:

- Limiting slag carryover to the ladle,
- Reducing refractory bricks corrosion by lowering FeO and MnO content of slag to less than 1%, and
- Maintaining basic slag composition by keeping the slag basicity ratio at 2.5 or higher

2.4.1 Calcium Aluminate Flux

As mentioned earlier, slag engineering must be done in secondary steelmaking to tackle refractory degradation. Basic slags with a $CaO\text{-}Al_2O_3$ (CA) composition are commonly used to achieve low rate of refractory corrosion. This type of slag is used generally in low carbon low alloy steel production, because of its low oxidation potential, low melting point (1350~1450°C), high sulphide capacity, and low viscosity at high temperatures. Calcium aluminate fluxes, also known as LDSF synthetic slag, are used as slag conditioners during steel refining, due to their relatively rapid formation of a liquid phase. This property helps to adjust the chemistry of the slag and also the slag's viscosity [42, 43]. Also, as a result of the increasing demand for high-quality clean steels, slags are designed primarily to optimize inclusion removal. Calcium Aluminate Fluxes are quite important for steel refining processes like desulphurization processes. The quick modification of the Al_2O_3 /SiO_2 ratio by pre-reacted Calcium Aluminate phases plays an essential role in this regard [44, 45].

The chemical composition of calcium aluminate flux is like those of the typical slag used in secondary steelmaking, therefore it can trap non-metallic inclusions as soon as the ladle is filled. It is therefore possible to remove these impurities when they are formed, hence reducing the need for subsequent processing. The fact that calcium aluminate flux is consistent, increases its predictability and performance reproducibility [46].

2.4.2 Calcium Magnesium Aluminate (CMA) Flux

Different degradation phenomena occur in the zone at which refractory and slag are in contact. These phenomena are combinations of thermo-chemical and thermo-physical mechanisms. Although factors like time, temperature, and turbulence enhance the corrosion rate of magnesia–carbon refractory material, the thermochemical degradation mechanism is viewed as a more critical cause of degradation. The slag compositions are typically under-saturated with MgO. Hence, this creates a chemical gradient between the MgO-containing bricks and the slag. Eventually, this under-saturation of MgO leads to the possibility of a dissolution reaction in the MgO-containing brick [47–50].

CMA flux is a synthetic calcium magnesium aluminate that forms basic slags. The main aim of this type of flux is to increase the MgO content in the slag. This must be achieved as fast as possible to decrease the MgO-dissolution rate at the slag and refractory contact zone. The CMA flux contains MgO in microcrystalline phases and is added to the slag in form of dust-free aggregates. As can be seen in Table 2. 2, CMA flux has a high MgO content of about 12 wt% [46].

Table 2. 2 Chemical composition of CMA in wt% [46].

CaO	MgO	Al_2O_3	SIO_2	FeO	TiO_2	CaF	H_2O	CO_2
32.9	12.5	40.9	3.6	1.7	2.2	0	<0.15	<0.1

The increased MgO content compared to the regular calcium aluminate fluxes has no negative impact on the slag's metallurgical efficiency like inclusion removal. The melting behavior of a calcium aluminate flux is highlighted in Figure 2. 12. It starts to flow at 1360°C. CMA has the comparative advantage of having an increased MgO-level in the slag right from the onset, compared to a normal calcium aluminate or a CaF_2 practice [51].

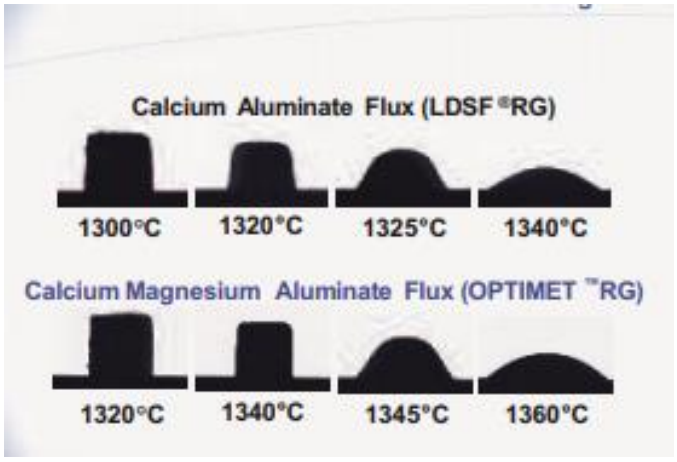

Figure 2. 12. Melting behaviour of Calcium Aluminate flux and Calcium Magnesium Aluminate flux [51].

Typically, in Al-killed steel production at the beginning of the steel treatment in the ladle, adding 20 wt.% CMA results in a final slag composition as presented in Table 2. 3 [46].

Table 2. 3 Chemical composition of slag after addition of 20 % CMA in wt%

CaO	MgO	Al2O3	SiO2	FeO
53.5	7.0	27.2	9.2	3.1

Figure 2. 13 illustrates the slag MgO evolution behaviour of different flux materials. The figure indicates a high initial MgO saturation level can be achieved with very little increase of MgO from the refractory matrix, which results in a low corrosion rate [46].

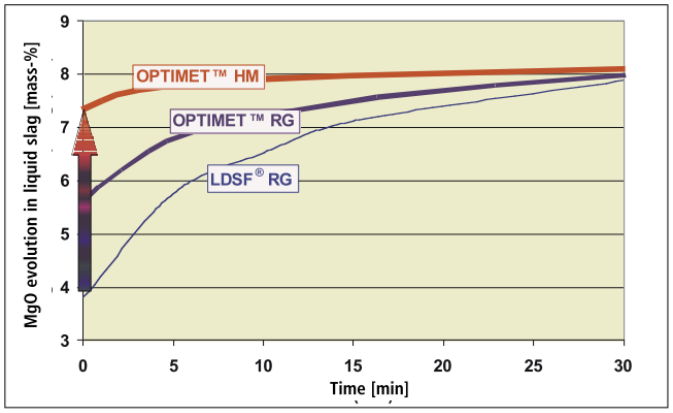

Figure 2. 13. Evolution of MgO content in slag (mass %) in contact with MgO-C bricks as function of flux material [46].

2.5 Refractories for secondary metallurgy applications

2.5.1 Overview of refractories for Secondary Metallurgy

Refractories are materials with relatively high melting points. They can also maintain their structural properties at very high temperatures. Refractories are used in both ferrous and non-ferrous metallurgy industries, where furnaces or kilns are needed [52]. As discussed earlier, refractories are the primary materials used to line the walls of the ladle for steelmaking. Figure 2. 14 shows the different zones of a steel ladle [53].

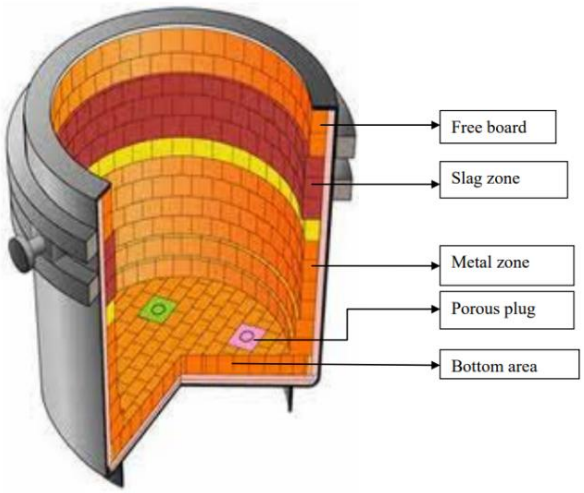

Figure 2. 14. Schematic view of a typical ladle lining [53].

Refractory compounds can be classified based on their chemical compositions as acidic, basic, or neutral [54].

- **Acidic refractories**

Acidic refractories is a class of refractory material with silica and alumina as primary component. Acidic refractory can withstand the corrosion of acid slag, but at high temperatures, it can react easily to alkaline slag erosion. Several subclasses, such as alumina-silicate, alumina-chrome, and alumina-spinel bricks, can be distinguished within this class [54]. Acidic refractory is widely used in the metallurgy industry for coke ovens, open-hearth regenerators and furnace roofs, refractory firing kilns, and glass tank furnaces [55].

- **Basic refractories**

Basic refractories consist mainly of basic oxides like magnesium oxide and calcium oxide. They chemically react with acidic slags, especially at high temperatures. Hence, basic refractories are attacked or corroded by acidic slags but are generally stable to alkaline slags, dust, and fumes. This type of refractory is often used for furnace linings where the environment is alkaline, for example, non-ferrous metallurgical operations and in many secondary steelmaking processes [54, 56].

- **Neutral refractories**

Neutral refractories can be composed of oxides or non-oxides elements such as silicon, aluminum, magnesium, calcium, and zirconium. The environments (acidic or basic) are usually determined using

a ratio of CaO /SiO_2 of the slag. Slags can corrode the brick it comes in contact with if it is not compatible with the brick. Neutral refractories are chemically stable to both acidic and basic environments at high temperatures. They are used in high temperature processes and under acidic or basic atmospheres. The common substances of neutral refractories are carbon, chromites ($FeCr_2O_4$), and alumina (Al_2O_3) [57]. A general rule of thumb for brick selection according to refractory brick basicity is presented in Figure 2. 15 [57].

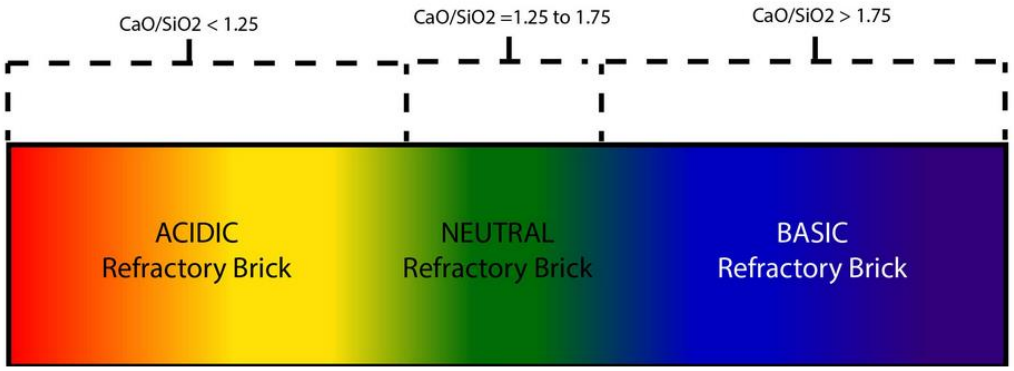

Figure 2. 15.Refractory brick categories according to slag basicity [57].

2.5.2 Metallurgical demands on refractories

In an evolving market like the refractory industry, refractory producers must continuously modify their products to meet the customers changing requirements and needs. An optimal refractory design should satisfy the criteria of quality, productivity, and cost simultaneously. Quality, in this case, refers to the level of metallurgical integrity like strength, ductility, formability etc. of the process, while the term productivity represents the demands on safety, availability, and reliability. The cost represents a satisfactory price/result relation. From a secondary metallurgical standpoint, are presented below some major refractory lining expectations or properties customers demand include [58, 59].

- Inert lining
- Durable lining
- Low specific refractory consumption
- High slag resistance
- Short heat-up time
- Low loss of liquid steel temperature
- Environmentally harmless refractories
- Reliable stirring performance of purging plugs

It is important to note that there is hardly a single refractory that satisfies all the requirements, and that explains the continuous evolution of refractory lining designs. Refractory design must be tailored to specific service conditions of the steel plants.

Unique requirements are required for the various processes or stages of steelmaking. For example, secondary refining of stainless steel using the AOD, or VOD is a very aggressive process for the refractory ladle lining. It must be able to withstand the increased severity of service conditions due to longer dwelling period of the liquid melt in the refractory at higher temperatures, that are generally associated with secondary steelmaking [38].

Secondary metallurgical treatment requires a longer time in comparison to primary metallurgy and this results in an increase in the residence time (tap to open time) of the steel in the ladle. For example, vacuum treatment requires approximately 1 to 3 hours of residence time. The temperature at which steel is tapped from the melting unit into the ladle must be factored in since the steel cools down in the ladle. Hence, the refractory ladle needs higher thermomechanical stability and corrosion resistance than the basic oxygen furnace (BOF). The tapping temperature can be increased with the aid of reheating facilities such as ladle furnace or aluminothermic heating. Some sections of the lining, e.g., the slag line, are areas of increased thermal and chemical attack on refractories in parallel [60, 61].

Intensive stirring of molten steel is a common feature of steel refining in the ladle. This stirring can be done by using several methods among which are gas stirring using inert gases like argon and Electro-Magnetic Stirring (EMS). Gas stirring with purging plugs placed at the ladle bottom is conventionally used in secondary metallurgy. Depending on the metallurgical requirements, the stirring time with purging plugs ranges from 10 to 20 minutes. However, they may take as long as 80 minutes, with a gas flow rate of 1000 l/min or more. Due to the induced turbulence caused by stirring at such a high flowrate, the refractory linings might become susceptible to mechanical attack in form of erosion. A complex combination of corrosion, degradation, spalling and cracking causes refractory wear, which is the result of the thermal, mechanical, and chemical stresses on the lining. It is critical that the refractory lining is resistant to this erosion [62, 63]. Table 2. 4 highlights some of the important property requirements of refractories used in steel ladle.

Table 2. 4 Refractory requirements of different metallurgical processes

Process characteristics	Refractory Requirements
Corrosive slag	High corrosion resistance
Intensive ladle stirring	High erosion resistance
Deoxidation, alloying	Thermodynamical stability
Heating (electrically or chemically)	High thermal stability and corrosion resistance
Long residence/dwelling time of melt	High thermomechanical stability
High temperature	High thermal stability

2.5.3 Magnesia-Carbon Refractory

Magnesia-carbon (MgO–C) refractory is widely considered as the most reliable lining material in steel refining furnaces. With its main composition being magnesia (>90 wt.%), MgO-C is a basic refractory. Furthermore, MgO-C has a relatively high slag/metal corrosion resistance and excellent thermal shock properties at high temperatures. Another component of the MgO-C refractory besides magnesia is carbon. It generally has a carbon content of 8-20 wt.%, when used in steel ladle applications. Since

MgO-C refractory is widely used in secondary metallurgical applications, it is subject to extreme circumstances. Some of these conditions include temperatures higher than 1600°C, severe convection, and oxidizing atmospheres. These conditions make the refractory prone to failure and shorten the refractory life due to chemical corrosion, thermal shock, and mechanical erosion. Hence, carbon is a very critical component of the MgO-C composition [64, 65]. The importance of carbon was highlighted in experiments conducted by Yong Cheng *et al*. [66], which showed that as carbon content increased, the thermal expansion rate of the MgO-C specimen decreased while its thermal conductivity increased, resulting in much-improved thermal shock resistance. The experiment also showed that an increase in carbon content gradually reduced the flexural and cold rupture modulus of MgO-C bricks. However, there was an increase in their fracture displacements due to graphite flakes good sliding ability, hence increasing their resistance to mechanically induced corrosion [66].

A prominent feature of the MgO-C refractory is its susceptibility to oxidation of its carbon component. This characteristic is a drawback in the use of MgO-C refractory. In MgO-C refractories, carbon oxidation occurs in two ways: (a) direct oxidation and (b) indirect oxidation.

Direct carbon oxidation occurs when the carbon and oxygen atoms directly combine to form CO (gas) at around 1400°C. Indirect carbon oxidation happens via the reaction of carbon with MgO to form Mg (g) and CO (g).

The resulting Mg (g) from the indirect carbon oxidation oxidizes again and produces MgO(s). This MgO is a nascent dense layer that limits the penetration of slag/metal components. Consequently, it improves the penetration resistance and resistance to corrosion. Carbon oxidation could be prevented by using antioxidants. These antioxidants react with incoming oxygen, hence preserving carbon and maintaining the structure and properties of the brick [67–69].

2.5.4.1 Main constituents of MgO-C bricks

As highlighted previously, the raw materials components like magnesia, carbon content, and antioxidants play a major role in refractory optimization and the refractory lifespan. As well as the listed components, the binder is also a component of the MgO-C refractory.

2.5.4.2 Magnesia

Magnesia mainly consists of burned MgO but does not occur naturally. It can easily be made by calcining magnesium carbonate or magnesium hydroxide, which are available commercially. Alternatively, synthetic magnesia could be produced using the Aman process. The Aman process produces high-purity synthetic MgO by steam pyrohydrolysis of hydrous magnesium chlorides. The principle behind it is decomposing hydrous magnesium chloride in a furnace by injecting steam into the furnace. The overall reaction can be represented by equation 2.1 [70].

$$\mathrm{MgCl_2.6H_2O \rightarrow MgO + 2HCl + 5H_2O} \qquad 2.1$$

Synthetic magnesia generally has smaller particles and crystals in comparison to magnesia obtained by magnesium carbonate or hydroxide calcination. However, the bulk density is greater for calcined magnesite [70]. Magnesia typically contains more than 97 wt.% MgO. The weight percentage of impurities are typically as follows: Fe_2O_3 < 0.2, Al_2O_3 < 0.3, SiO_2 < 0.5, and CaO < 1.0 wt.% [71]. Magnesia is the most important component of the MgO-C refractory, constituting more than 80 wt%

of the batch. Properties of magnesia that make it so critical include high resistivity to chemical attack in basic environments, low susceptibility to abrasion, and high thermal strength. Figure 10 below show a diagram of the molecular crystal structure of MgO [53].

2.5.4.3 Solid Carbon

The primary source of carbon in MgO-C refractories is graphite. An alternative source of carbon is carbon-black. Carbon black is formed during the incomplete combustion of hydrocarbons during their thermal decomposition (e.g. oil or natural gas) [72]. Usually, carbon from carbon-black has an average composition of about 99.5 wt.% C; particle size: 10 – 500 nm [73]. Graphite has a carbon content of 93 – 96 %, and in some applications, this content could go up to 99 %. Among the different sources of carbon, graphite shows the highest oxidation resistance, and, due to the flaky nature, it gives the refractory brick higher thermal conductivity and lowers the thermal expansion. Resistance against oxidation is a critical criterion in carbon selection for the MgO-C refractory. Hence, flaky graphite is the most used carbon source for MgO-C refractory production [72, 74–76]. Figure 2. 16 shows that natural graphite is flaky in nature and the graphene layers are attached together [77].

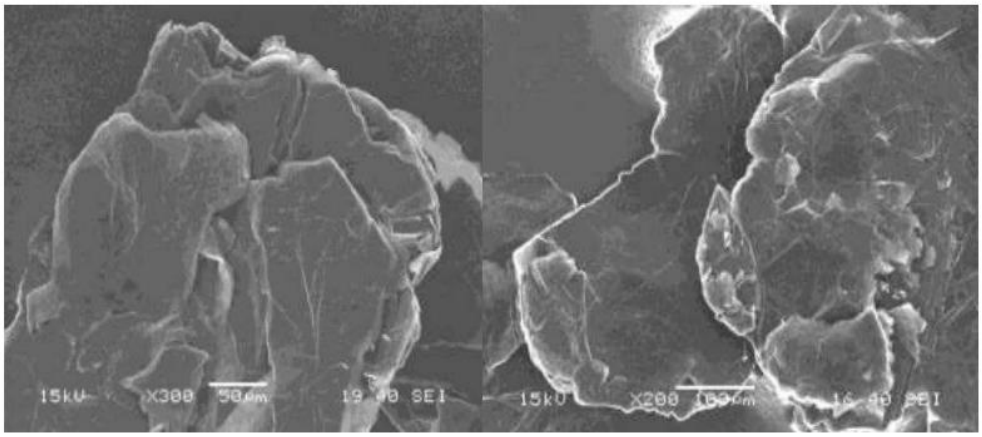

Figure 2. 16. SEM images of flaky graphite [77]

Regardless of its source, carbon's high melting point improves the thermal resistance of the refractory. Furthermore, carbon's low affinity (wettability) to molten metal and slag improves the corrosion resistance of the refractory. There had been the tendency to use more carbon in the MgO-C brick to maximize its corrosion resistance and thermal shock resistance properties. But more research conducted about it has made it clear that higher carbon content in the brick has its drawback. Oxidation of carbon within the MgO-C refractory matrix is problematic because it causes increased porosity. Consequently, these pores become penetration channels for liquid slag. These liquid slag that fill up the pores could inherently corrode the refractory, iincrease the shell temperature, and cause significant carbon pickup in the steel [78–80].

2.5.4.4 Antioxidants

Antioxidants are metals and their alloys (such as Al, Si, Al-Mg, Al-Si), carbides (such as B_4C and SiC), and boron-based compounds (such as CaB_6 and ZrB_2) added to the MgO-C refractory to slow down the oxidation of carbon. These antioxidants react at various temperatures with refractory constituents and gases within the environment. These reactions induce changes in the MgO-C refractory microstructure and its thermo-mechanical properties [81–83].

Antioxidants react with both C and O, and the resulting reactions lead to the plugging of pores, hence mitigating carbon oxidation by forming a solid phase [84].

Some of the parameters used for selecting the antioxidant to be used in a given application are [79, 85]:

- Refractory composition,
- Process conditions (atmosphere and target temperature),
- Slag chemical composition, and
- Thermomechanical stresses that develop during the process.

Al antioxidants are the most used antioxidants in MgO-C refractory because of their capacity to conserve mass, decrease porosity, increase the hot mechanical rupture module (HMOR), and form a protective surface layer on the refractory that reduces slag corrosion [86].

At high temperatures (> 1200° C), Al reacts with graphite and/or nitrogen (N_2) to form a metallic carbide (Al_4C_3) and/or AlN. Occasionally, Al can be oxidized to Al_2O_3 directly by CO. The Al_4C_3 formed further then reacts with N_2 to form AlN whiskers. Al_4C_3 also reacts with CO to form Al_2O_3, which goes on to reacts with MgO to form $MgAl_2O_4$ (MA) as seen in equations 2.2, 2.3, and 2.4.

$$4Al_{(l)} + 3C_S = Al_4C_{3(s)} \quad 2.2$$

$$Al_4C_{3(s)} + 6CO_{(g)} = 2Al_2O_3 + 9C_{(s)} \quad 2.3$$

$$Al_2O_{3(s)} + MgO_{(s)} = MgAl_2O_4 \quad 2.4$$

Al(g) is also involved in the reaction processes, as their presence explains reaction products like AlN (whiskers) and MA, which precipitates on large periclase grain surfaces. The amount of MA formed is time dependent as shown in Fig. 2. 17. More amounts of MA are formed as the dwelling time of the reaction increases. If Al_4C_3 is not quickly oxidised by CO, it will nucleate and finally form a solid Al_4C_3 grain. However, fast oxidation of Al_4C_3, which is more often the case, will lead to volumetric expansion. The resultant Al_2O_3 from Al_4C_3 oxidation may contain some cracks and micropores [85].

Si when used as an antioxidant in a MgO-C sample initially reacts with C to form silicon carbide (SiC) as shown in equation 2.5.

$$4Si_{(s)} + 3C_S = SiC_{(s)} \quad 2.5$$

As more CO diffuses into the reactive system, CO reacts with SiC to form SiO_2, which further reacted with MgO to form Mg_2SiO_4 (M_2S), as shown in equation 2.6, 2.7.

$$SiC_{(s)} + 2CO_{(g)} = SiO_2 + 3C_{(s)} \quad 2.6$$

$$SiO_{2(s)} + MgO_{(s)} = Mg_2SiO_{4(s)} \quad 2.7$$

Figure 2. 17 (a and b) show SEM images of MgO-C refractory samples containing Al and Si additives fired for 3 hrs. The product phases of Al2O3, Al4C3 and MA formed in the MgO-C refractory matrix with Al additive is revealed in Fig 2. 17a. Fig. 2. 17b shows the product phases of SiC and M2S formed in the fired MgO-C matrix [85].

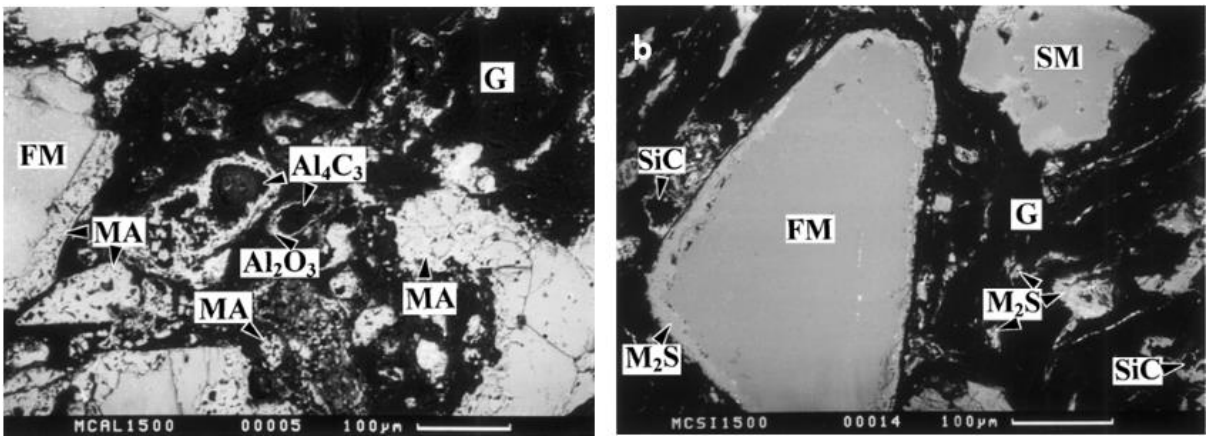

Figure 2. 17. Higher magnification SEM backscattered electron images (BEI) of MgO-C refractory samples with Al and Si additives (a) with Al additive fired at 1500° C (b) with Si additive fired at 1500° C. FM; fused magnesia, SM: sintered magnesia [85].

Figure 2. 18 (a and b) show carbon loss curves (wt. %) of MgO-C refractories with different antioxidants (Al, Si, SiC and B_4C) ranging from 0- 3wt. %. The carbon loss curves indicate that all the specimens with antioxidants had similar results at 1300 °C, except for the specimen with SiC addition. It can be seen from the result that carbon losses of specimens containing particularly Al, Si and B_4C are like each other [81].

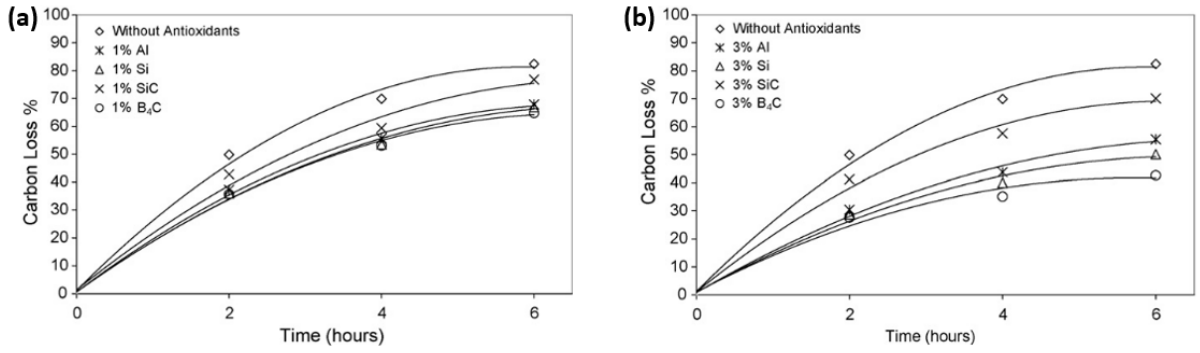

Figure 2. 18. Carbon losses % of MgO–C specimens (a) with/without 1 wt.% antioxidant at 1300 °C (b) with/without 3 wt.% antioxidant at 1300 °C [81].

As the carbon content, the number of antioxidants added to the MgO-C refractory matrix must be limited. Although antioxidants are beneficial to oxidation resistance, they can also have harmful effects on steel cleanliness. For example, research conducted by L. Chen *et al*. [86] showed that high-carbon steel used for saw wire had a drastic increase in Al_2O_3 inclusions originating mainly from the dissolution of Al antioxidant particles within the MgO–C refractory. This increased number of inclusions lead to reduced mechanical properties and ultimately caused wire breakage [86].

2.5.4.4 Binders

Binders are an important component of the MgO-C refractory. The main functions of binders are:

- Shaping of the refractory grains,
- Ensuring the dimensional integrity of the MgO-C refractory when installed in the refractory brick, and the subsequent initial heating.

The main types of binder used for MgO-C refractories are coal tar pitch and phenolic resin. Previously, the pitch was widely used as binders for MgO-C brick. Pitch-bonded bricks have an anisotropic, graphite-like coke structure after carbonization. This inherent coke microstructure makes pitch binders mechanically flexible. MgO-C refractories with pitch as binder, have relatively higher spalling resistance, better thermal shock resistance, and higher strength at temperatures to MgO-C refractories without binders. However, this type of binder must be first heated. Initially, heating of the binder results in the softening of the binding agent. During the curing process of pitch or tar bonded MgO-C refractories, massive amounts of toxic fumes containing high content of Polycyclic Aromatic Compounds (PAC) are liberated. Also, hot pressing of the mixture is required for using pitch. Hence, due to the drawback of using pitch, the use of resin as the preferred binder for MgO-C refractory rose to prominence [87, 88].

Resins allow molding and mixing at room temperature. Unlike pitches, resins do not go through a thermoplastic phase during heating, and this results in the possibility of greater accuracy of the products [89]. Phenolic-formaldehyde (PF) resin is the most effective binder used in carbon-containing refractories. Another advantage of using resin as the binder for MgO-C bricks production is that it is environmentally acceptable. In contrast to pitch binders, they do not emit toxic fumes. However, the maximum cold compressive strength of resin-bonded MgO-C bricks occurs after hardening, which is then reduced during pyrolysis. Therefore, pitch binders normally guarantee higher strength after heating in comparison to resins. Pitch-bonded MgO-C refractory bricks tend to expand after tempering. The tendency of resin-bonded bricks to shrink depends on the carbon content of the refractory brick [90–92].

Another type of resin is Resol. Resol resin has the advantage of low viscosity, low volatility, and low porosity after heating to high temperatures. The desired viscosity of resin used for MgO-C brick is usually about 8000 cps at 25 °C. However, the viscosity of resol resin increases with a decrease in temperature. This could lead to low dispersion of ingredients in the mixer machine compared to the dispersion during production in warmer seasons [89].

2.6 Interaction between refractory (MgO-C) and liquid phase (slag and/or liquid steel)

The corrosion of refractory materials in pyrometallurgical operations or specifically secondary metallurgy by the liquid phases (molten metal, slag) is a concern to refractory wear. Due to the relatively high temperature of the process, any reactions would be expedited and may result in significant refractory wear. The most predominant form of refractory attack by the liquid phase is a chemical attack and must be considered in the refractory design. This type of attack occurs because the reaction system attempts to establish equilibrium, especially when the liquid phase is undersaturated in a refractory component [93–95]. The attack of the refractory is much complex than just its chemical reaction with the liquid phases. It also involves physical and mechanical wear (erosion, abrasion). The direct contact between liquid phases and refractory enables the reaction to occur and ensures product transport between liquid phases and refractory. Other factors that shed more light on the corrosion mechanisms of refractories are refractories microstructure, melt properties, wetting properties, and interactions at high temperatures [38].

Few molten metals can wet refractory, but in contrast, most slags wet refractory. Hence, the most critical area of refractory wear is usually where slag and refractory are in contact. Slag penetration of the refractory is directly proportional to the porosity of the refractory. Once the slag penetrates the refractory, it dissolves the refractory matrix via chemical reactions and consequently corrodes the refractory components by flowing liquids [95, 96]. Figure 2. 19 shows a schematic representation of the overall corrosion mechanism of magnesia refractory caused by slag [47].

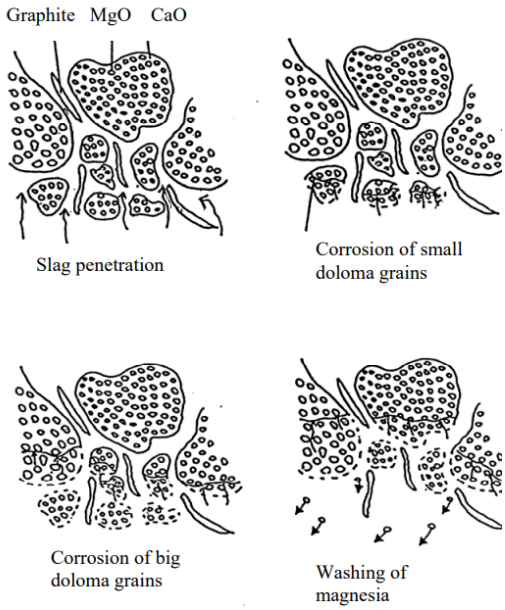

Figure 2. 19. Corrosion mechanism of doloma refractory [47].

Furthermore, wettability between the refractory and slag also causes the local erosion of refractories at its interface with slag, see Figure 2. 20. This erosion occurs because of slag film motion against the refractory. This motion induces the abrasion of the refractory [96].

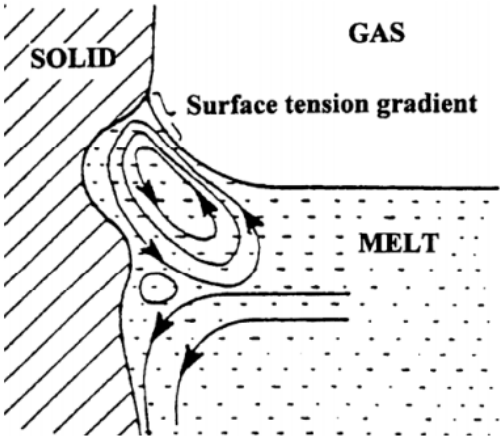

Figure 2. 20. Motion of the slag film caused by the surface tension phenomena between the refractory and slag [96].

The active film motion is due to the Marangoni effect, and also due to change in the form of the slag film with variation in the surface tension and the density of the slag film[97]. The *Marangoni effect* is a hydrodynamic phenomenon that best describes the mass transfer at the interface between two phases due to a gradient of the surface tension [98].

Some experiments have shown that the nature of the interaction between the liquid phase (slag, molten steel) and refractory materials is dependent on the steel composition, flux type, temperature, turbulence, and the type of refractory material. The interaction between the refractories, slag, and molten steel is closely related to the quality of steel produced. For example, non-metallic inclusions could form inside the steel from antioxidants used in a MgO-C refractory brick. Another possibility is the change in the chemistry of slag due to its reaction with the refractory. Therefore, when the molten steel is being treated in a ladle, the reaction between molten steel, slag, and the refractory lining has a massive influence on the steel purity [99–101].

It has become imperative to understand the dissolution mechanism and kinetics of each component of a slag/molten steel/refractory system to explain the dissolution behavior of the refractory due to its interaction with the liquid phases [102–104]**.** Figure 2. 21 shows a schematic diagram of the interaction between steel, slag, refractory, and non-metallic inclusions [17]. The diagram depicts molten steel which has a density just below the slag. Additionally, the diagram shows nonmetallic inclusions moving from the molten steel into the slag.

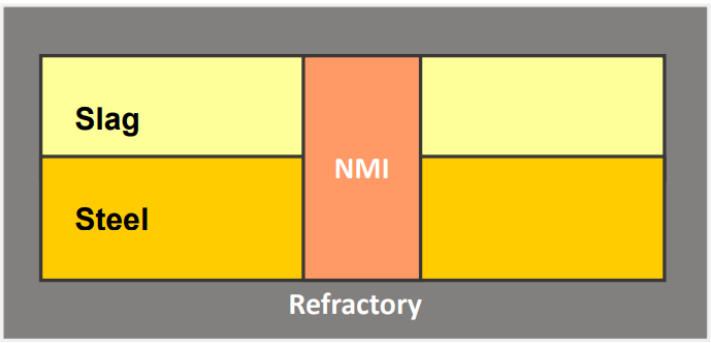

Figure 2. 21. Schematic diagram of the interactions between steel, slag, refractory, and non-metallic inclusions [17].

2.6.1 Thermodynamics and Kinetics of slag/molten steel/refractory (MgO-C)

The resistance to chemical corrosion or thermomechanical erosion is critical to the designing of the refractory materials. To achieve an optimal refractory design, it is necessary to understand the fundamentals of the thermodynamics and kinetics of the slag/molten steel/refractory system interactions that drive refractory wear [105].

2.6.2 Overview of thermodynamics of MgO and carbon reaction

Although carbon in MgO–C bricks restricts slag penetration, carbon oxidation poses a significant challenge. Carbon could be oxidized by the gas phase, liquid phase, or MgO in the refractory brick. Gas-phase oxidation is due to the presence of oxygen or CO_2 in the surrounding atmosphere. To reduce this type of oxidation, special care must be taken during heating and the ladle must be properly maintained before tapping. Liquid-phase oxidation could be due to the presence of unstable oxides in the slag like SiO_2 or MnO[106]. Some experiments have shown that there is a possibility of carbon oxidation by magnesia according to the following reaction in equation 2.8, 2.9 [99, 104, 107]:

$$\mathrm{MgO_{(s)} + C_{(s)} = Mg_{(g)} + CO_{(g)}} \quad 2.8$$

$$\Delta G^{\circ} = 624032 - 295.95T \quad \mathrm{J/mol} \quad 2.9$$

Where T is the temperature in Kelvin. The reduction reaction of MgO by carbon is a phenomenon that does not occur often in secondary metallurgy processes because this reaction would happen at a higher temperature than the refining temperature. However, a partial pressure decrease for magnesium gas and CO can occur at a lower temperature. This could be the case during vacuum degassing.

Figure 2. 22 relates the free energy for the formation of MgO and CO to temperature and partial pressure. The sudden deviation in the line 2Mg + O_2 = 2 MgO is due to magnesium metal reaching its boiling point. The free energy of formation above this temperature is evaluated based on the metal vapour at 0.1013 MPa. The three other lines in the magnesia group highlight the three lines highlight de dependency on the partial pressure of magnesium metal. From figure 2.20, the various partial pressures and temperatures at which the reduction of MgO by carbon will be thermodynamically feasible can be predicted. It can be seen that MgO is stable in contact with carbon below 2124 K. However, at lower temperatures and reduced P_{Mg} and P_{CO}, the reaction MgO(s)+C(s) = Mg(g) + CO(g) can take place [99].

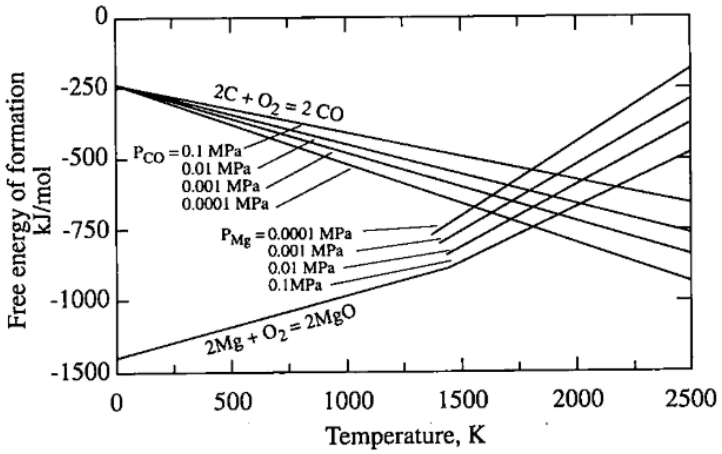

Figure 2. 22. Equilibrium relations for carbon monoxide and magnesium as a function of temperature [99].

2.6.3 Reaction at refractory/steel interface

Corrosion of the refractory by molten steel is not prominent at the refractory/steel interface due to a dense $MgO_{(s)}$ protective layer that forms on the surface of the brick, which is in contact with the molten steel. The resultant $Mg_{(g)}$ from carbon oxidation diffuses through the pores of the refractory and reacts with oxygen in the steel [99, 107–109]. $Mg_{(g)}$ oxidizes to MgO, which condenses to form a dense layer at the refractory/steel interface. The reaction that forms the $MgO_{(s)}$ layer is shown in equation 2.10 [107].

$$\mathrm{MgO_{(s)} + C_{(s)} = Mg_{(g)} + CO_{(g)}, Mg_{(g)} + O = MgO_{(s)}} \quad 2.10$$

The equilibrium constant for the above reactions may be written as in equation 2.11.

$$\ln K_1 = \ln\left[\frac{P_{(\mathrm{Mg})} * P_{(\mathrm{CO})}}{a_{(\mathrm{MgO})}} * a_{(C)}\right] = 34.87 - 74079/\mathrm{T} \quad 2.11$$

In Al-killed steel, the formation of spinel is an important aspect of the reaction between MgO-C refractory and the molten steel. CO(g) that is formed as a result of MgO reduction to Mg, reacts with dissolved aluminium in the steel and forms aluminium oxide [99, 109–111]. As the Mg(g) diffuses into the molten steel the following reaction as shown in equation 2.12 takes place [106].

$$\mathrm{2[Al] + 3CO_{(g)} = Al_2O_{3\,(s)} + 3[C]} \quad 2.12$$

The formed aluminium oxide consequently reacts with MgO, forming a spinel inclusion as shown in the following equation 2.13 [106]:

$$\mathrm{Al_2O_3 + MgO_{(s)} = MgO.Al_2O_{3\,(s)}} \quad 2.13$$

Figure 2. 23 shows microscopic images of the MgO-C crucible/steel interface when Al killed molten steel was held in a MgO-C crucible at 1873 K for 30 and 60 min, respectively. An oxide layer (spinel) can be seen been the steel and refractory. The oxide layer build up is as a result of spinel formation composing of $MgO{\cdot}Al_2O_3$ [99].

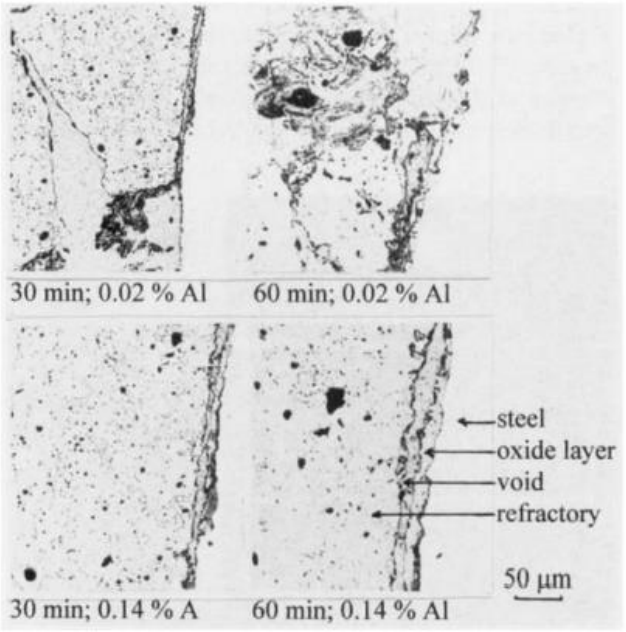

Figure 2. 23. Optical micrographs of MgO-C refractory/steel interface showing the layers formed in the presence of liquid steel [99]

Evidence of the reactions at the refractory/steel interface is the increased presence of MgO and Al_2O_3 in the steel. An example of a SEM-EDS distribution map of molten steel in Figure 2. 24 shows MgO and Al_2O_3 inclusions within the steel matrix [106].

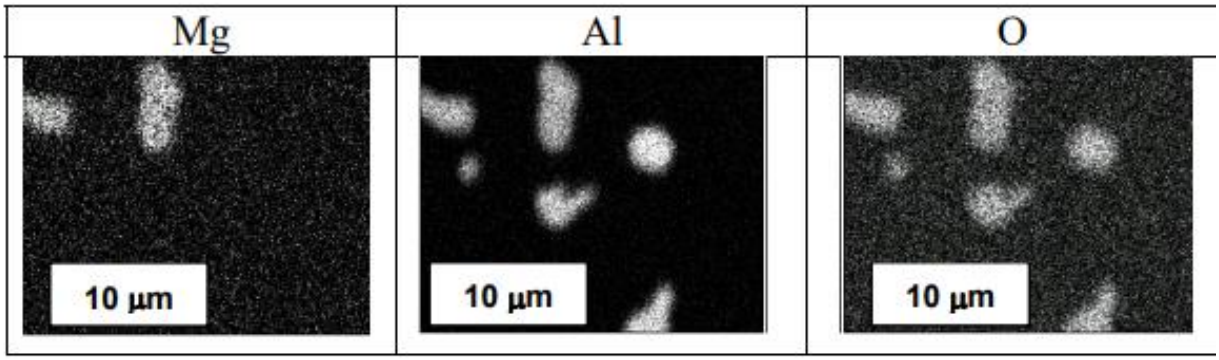

Figure 2. 24. SEM/EDS images of molten steel with Mg, Al and O inclusions [106].

2.6.4. Slag-Refractory Interaction

The reaction at the slag/refractory interface is the most critical with regards to refractory corrosion. Understanding the corrosion mechanism in this region cannot be over-emphasized as it gives us a better insight into the wear rate and general wear mechanism of the refractory. A refractory's resistance to slag is primarily determined by the equilibrium relationship between the slag and the refractory. This process can be divided into two main wear phenomena namely, continuous, and discontinuous. Continuous wear is characterized by continuous mass loss over time. It is dependent on thermal, chemical, and mechanical loading. Thermal loading happens because the reactions that induce continuous wear must occur at relatively high temperatures. Chemical loading occurs due to the dissolution of the refractory material by slag and oxidation of carbon bonds. Mechanical loading occurs with mass loss due to abrasion of the refractory material as a result of its exposure to gas and slag movement [112, 113].

In this review, a focus will be made on the continuous wear mechanisms as they are the most crucial aspect of the interaction that occurs in this region. The principle behind such wear is the initial penetration of the refractory by the slag, then the dissolution, and diffusion of the refractory material.

2.6.4.1 Penetration of MgO-C Refractories by Slag

Slag penetration of refractory is the infiltration of the refractory by liquid slag via open porosity. Slag penetration into the MgO-C refractory can be described by primary and secondary penetration. Primary penetration is a rapid liquid slag infiltrating of the refractory via the pores created at the decarburized zone of MgO-C. Secondary penetration occurs slowly at the grain boundaries of the MgO-C refractory matrix [114]. Slag penetration of the refractory was described by Siebring et al. using the equation 2.14 [115].

$$\Delta P = \frac{4\gamma\, cos\theta}{d} \qquad 2.14$$

where γ is the surface tension between the penetrating slag and the gas phase, θ is the contact angle, and d is is the diameter of the pores.

With the cylindrical capillary model, we can also describe the penetration rate dl/dt of slag into a pore of the refractory as shown in equation 2.15 [38].

$$\frac{dl}{dt} = \frac{r\gamma\, cos\theta}{4\eta l} r \qquad 2.15$$

where r is the capillary radius, γ is the surface tension between the penetrating slag and the gas phase, θ is the contact angle, η is the slag viscosity, and l is the slag penetration depth.

The equation 9 highlights the importance of the slag viscosity to the penetration rate. An increase in the slag viscosity reduces the rate of penetration of the slag into the refractory. Hence, the slag composition just like temperature is important to the rate of penetration of slag into the refractory matrix. The boundary layers between grains are relatively easily attacked in comparison to the matrix of the grain, except in cases whereby the slag is very aggressive. For example, a slag with very low magnesia content will attack the large periclase grains of a MgO refractory it is in contact with easily. Furthermore, when the slag begins to dissolve some refractory components, the slag viscosity will increase. This attack by the slag can only be possible via diffusion of the refractory particles through the viscous slag layer at the interface between the refractory and slag [38, 116, 117].. Furthermore, the slag penetration rate could be reduced when there is lower surface tension or an increased contact angle to above 90° [106]. The larger the wetting angle of the slag to the refractory, the more difficult it is for slag penetration to occur in the refractory matrix. Wetting angle between slag and refractory also plays a critical role also in slag penetration depth. However, other parameters like viscosity and temperature gradient equally have an influence on slag penetration depth. Figure 2. 25 illustrates the penetration of refractory by slag at different penetration conditions [96]. It depicts that if a refractory has a hot face (high temperature gradient), penetration will increase. Likewise, if the slag has a high temperature, there will be increase in penetration of the refractory by the slag.

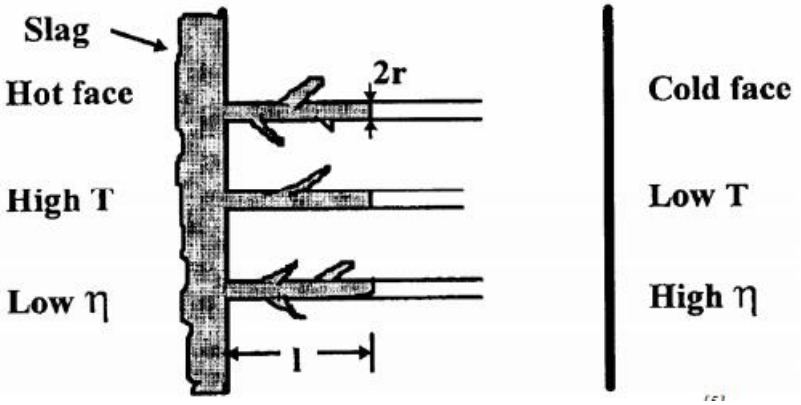

Figure 2. 25. Slag penetration of refractory at different penetration conditions [96].

The microstructure of the refractory grains (grain size, shape, and adjacent porosity level) also affects the penetration of refractory material. Invariably, it is the porous matrix that is attacked initially. Usually, veins of penetrating liquid spread through the porous matrix. A porous refractory has a higher tendency to get penetrated by the slag, which soaks into the pores, in comparison to a denser refractory [118, 119]. Finally, if the slag temperature drops below its solidus temperature, penetration would stop. Hence, the solidification temperature or break temperature would influence the penetration rate or penetration depth of slag into the refractory [114].

2.6.4.2 Dissolution of MgO-C Refractories by Slag

One of the significant mechanisms that influence refractory wear rate is dissolution. Dissolution is a phenomenon whereby a solid such as the refractory matrix is dissolved by liquid phases (slag, steel). Dissolution at the slag/refractory interface is either driven by chemical reactions or diffusion controlled. In almost all cases, refractory material dissolution in the liquid phase is controlled by the latter[120]. Furthermore, refractory wear is predominant at the refractory/slag interface. The major reason why a refractory material would be dissolved by the slag is the difference in concentration of the dissolved refractory component and the saturation concentration of that component in the slag [120]. Fick´s 1st law as shown in equation 2.16, can be used to describe the dissolution phenomena that relate the mass flux of an ion species j with the gradient of the concentration c and diffusion coefficient (D) of the considered ion [121].

$$j = -D\ grad\ c \qquad 2.16$$

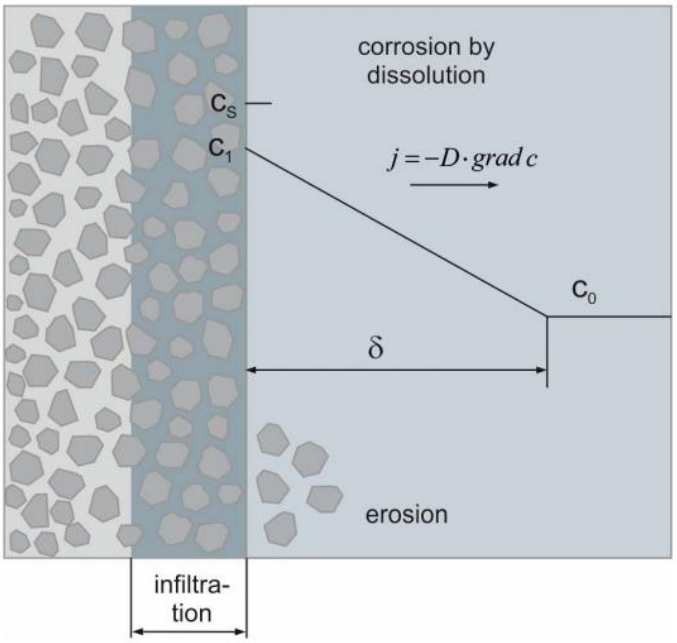

Figure 2. 26. illustration of the dissolution process that leads to refractory corrosion [121].

Figure 2. 26 shows an illustration of the dissolution of refractory material in contact with liquid slag. Refractory dissolution occurs at the hot face and within the infiltrated area of the material. Dissolution of the refractory material degrades the grain/matrix-bonds and consequently leads to erosive wear. Hence dissolution is a facilitates for erosion wear.

In Fig 2.24., C_s represents the saturation limit of the dissolving component of the refractory brick at the refractory/slag interface, for example, MgO in a MgO-C refractory. C_0 represents the initial slag MgO concentration far enough from the hot face [121]. Hence represented in equation 2.17 below is a one-dimensional form.

$$j = D * \frac{C_s - C_0}{\delta} = D * \frac{\Delta c}{\delta} \qquad 2.17$$

Hence, according to the equation 2.18, the ion flux j is:

$$j = \beta * \Delta c \qquad 2.18$$

Where β is the mass transfer coefficient, since the mass transfer coefficient is the ratio of D and δ, i.e., D/δ.

Some studies have shown that parameters like dissolution time, temperature, and rotation speed are the drivers of the MgO dissolution rate [122–124]. Using a finger test experiment, Sune Jansson [106] illustrated how these parameters listed above can be related to the corrosion rate of the refractory material. [106]. Studies by Mikio Umakoshi *et al*, [124] show that the dissolution rate increases with increasing revolving speed. This study supports the fact that the dissolution rate is primarily controlled by mass transport. It also shows that the dissolution rate of solid in a liquid is exponentially proportional to the stirring intensity [124]. Also, studies conducted by R. J. Fruehan *et al.* show that the dissolution rate of MgO-C refractory increase linearly as the holding time increase. With increase in holding time more carbon get oxidized and dissolution of the refractory occurs at a faster rate [122].

Another important factor that affects the dissolution rate is the slag composition. Besides the concentration differential of the dissolved component in the slag and refractory which is the primary driving force of dissolution rate of refractory materials, the basicity of slag also affects the dissolution rate. R. Wei *et al.* [119] showed for their studies that the MgO dissolution rate was found to be negatively correlated to the Fe_2O_3/CaO mass ratio and the MgO content in the initial slag. Furthermore, they also found that the dissolution rate of MgO in the MgO refractory decreased with increasing SiO_2 content. Additionally, the dissolution rate is also affected by the melt viscosity [119, 125]. Figure 2. 27 depicts the effect of the MgO mass percentage on the viscosity and magnesium ion diffusivity. Hence, the MgO dissolved in the slag, the higher the slag viscosity gets [119].

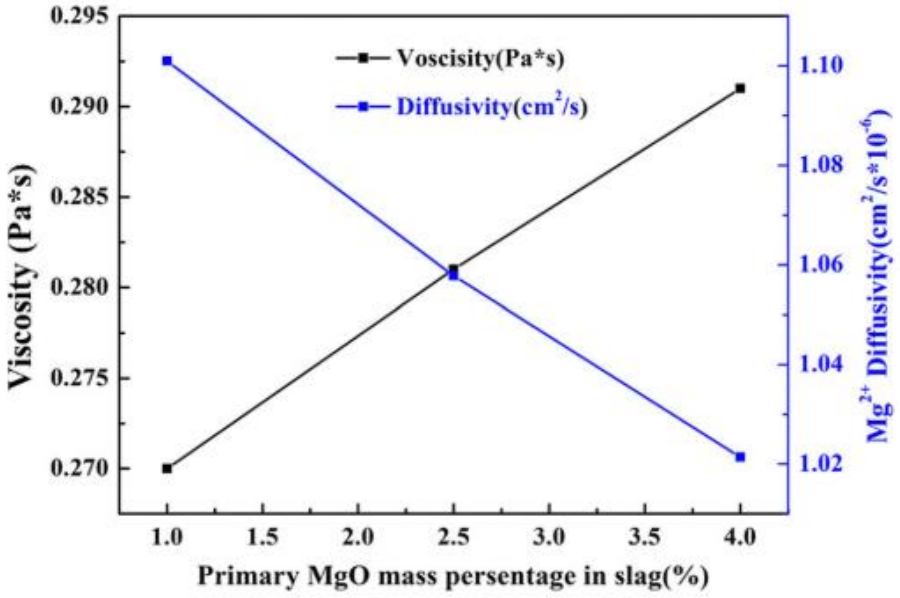

Figure 2. 27. Dependence of viscosity of melts and Mg2+ diffusivity on slag MgO composition (wt. %) at 1673 K (1400 °C).

2.7 Refractory corrosion test method

To investigate the behavior of the refractory in contact with a liquid phase (slag, metal), different corrosion tests methodology can be employed. These different methodologies can be divided into two categories: static and dynamic tests [38, 96, 126]. A common feature of both categories of corrosion testing is that changes will occur in the slag during the test as a result of selective infiltration of specific elements into the refractory brick, and the dissolution of brick into the slag [127].

2.7.1 Static tests

Static tests are tests in which there is no agitation of the testing system. The liquid phase is not stirred, neither is the refractory brick rotated. Hence, a parameter like revolution per minute(rpm) does not apply[128]. Consequently, these tests usually give lower corrosion rates in comparison to dynamic tests. Besides, most static tests have a drawback of the slag quickly becoming saturated at the refractory/ slag interface with reaction products with the refractory. This scenario would be unlikely when slag is moving relative to the refractory. The slag motion would continually refresh the system with slag free of corrosion products. However, static tests are very useful to study the chemical reactions that take place at the interface [96, 127].

2.7.1.1. Crucible (cup) test

The crucible test is also commonly known as the cup test. As shown in Figure 2. 28, the refractory bricks are cored out to form hollow cylinder shapes. The National Standards Authority of Ireland (NSAI) standard refractory sample for the crucible test is a cylinder of 76 mm in total height, 100 mm in outer diameter, 55 mm in inner diameter, and 55 mm in depth. Nevertheless, static tests are easier to implement than dynamic tests and remain very useful to study the chemical reactions that take place at the interface [120, 126].

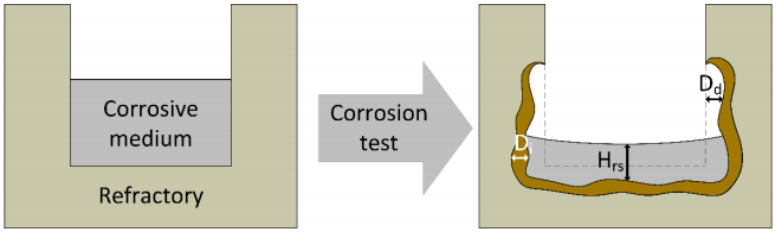

Figure 2. 28. Schematic of crucible test; where D_d is the dissolved brick thickness, D_i the infiltration depth and H_{rs} is the remaining slag level [128].

The test is carried out by filling the refractory crucible with slag and/or steel. The crucible is then heated up to a pre-determined temperature for several hours in a furnace. After a selected dwelling time, the samples can either be quenched or cooled down slowly in the furnace. It is typical for the test to be carried out in a controlled atmosphere. After the crucible and its content are cooled, the crucible can be embedded in resin to fixate the crucible and bath material so that a vertical cross section can be cut. The cut parts are studied to estimate the extent of degradation and possibly the corrosion rate [48, 100, 129, 130]. The corroded zones of the crucible (cup) just like the other testing methods can be analyzed using different characterization tools like X-ray diffraction and SEM/EDS. Additionally, parameters like mass loss, dissolution rate, infiltration depth, and oxidation thickness

can be measured considering different variables. Some of these variables include the amount of a specific oxide in the slag, time, and temperature [128].

2.7.1.2. Static finger test

The static finger test is also called dipping test. For this test, the refractory brick is shaped into a cylindrical rod and immersed into a vessel containing liquid slag and/or steel. Although the amount of liquid used for the experiment is not defined, caution must be taken as a large amount of refractory material in reaction with a comparably small amount of liquid slag and/or steel could lead to quick saturation of the liquid phase. Conventionally, the rods are maintained above the crucible and are heated before dipping to prevent thermal shock. Afterward, about 30 to 70% of their length is immersed into the molten liquid during a given amount of time [38, 131]. The standard dimension of the refractory rod is 10 to 30 mm in diameter and approximately 50 to 120 mm in length [126]. Figure 2. 29a shows a typical experimental setup of the static finger test and Figure 2. 29b. illustrates the evolution of the shape of the refractory rod sample during this test [128]. D_i represents the original sample dimension in the transverse direction, D_m indicates the dimension of the thinnest part (corrosion neck), and D_c the dimension of the corroded refractory rod in a transverse direction sufficiently far off the corrosion neck.

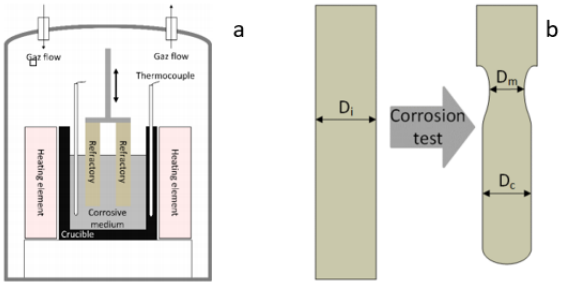

Figure 2. 29. Experimental setup for the finger test under a control atmosphere (a), sample evolution during the finger test (b) [128].

The advantage of the finger test is that it is relatively easy to set up. Additionally, in cases where we have a big enough furnace, multiple samples can be tested at the same time. Just like the crucible (cup) test, the atmosphere of the experimental setup is controlled. However, the finger test requires more slag and/or molten steel to form the corrosive medium compared to the crucible test. If the quantity of slag is not sufficient, the slag will be saturated.

2.7.2 Dynamic tests

A static test with a non-agitated or stirred corrosive medium (slag and/or molten) does not depict a real industrial case. Hence, to improve the static testing method, more dynamic approaches were developed and nowadays, dynamic tests are more used than static tests for corrosion testing.

2.7.1.1. Rotating finger test

The rotating finger test is very similar to the static finger test concerning its setup and experimental procedures. However, to simulate more realistic working conditions, the rods are rotated inside the slag and/or molten steel at a defined angular speed. Figure 2. 30 shows a schematic of the setup of the rotating finger test.

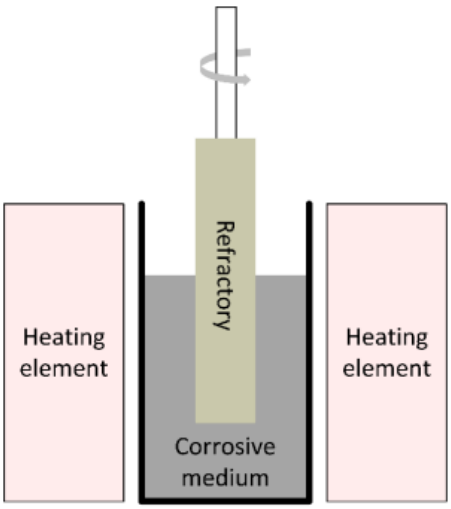

Figure 2. 30. Schematic of a rotating finger test [128]

The rotating finger test according to literature, is the most frequently used corrosion testing method to study and investigate the corrosion rate of refractory in the presence of a corrosive medium (slag, molten steel) [50, 106, 132–134].

2.7.1.2. Rotary slag test

The rotary slag test is a type of dynamic test where solid slag and/or steel is introduced into a refractory brick-lined cylindrical chamber and melted with a burner as illustrated in Figure 2. 31. To carry out this test, the cylindrical chamber is rotated horizontally at a relatively low speed (from 2 to 6 rpm). Fine powder or small pellets of solid slag and/or steel is introduced into the chamber at the selected temperature [135–138]. Propane and oxygen are usually the fuel used for the burner inside the chamber to heat it. The temperature inside the chamber can be controlled by varying the flow rate of fuel in the burner. Additionally, the temperature is measured at selected time intervals with a pyrometer to help adjust the flow. The slag can also be changed at regular intervals. Usually, a less aggressive slag is introduced into the chamber to "*clean up*" the refractory between two cycles [35, 139]. The samples can be examined by visual inspection after the test. Furthermore, dissolution, infiltration, phases, and composition can be analyzed afterward using XRD and SEM-EDS[128].

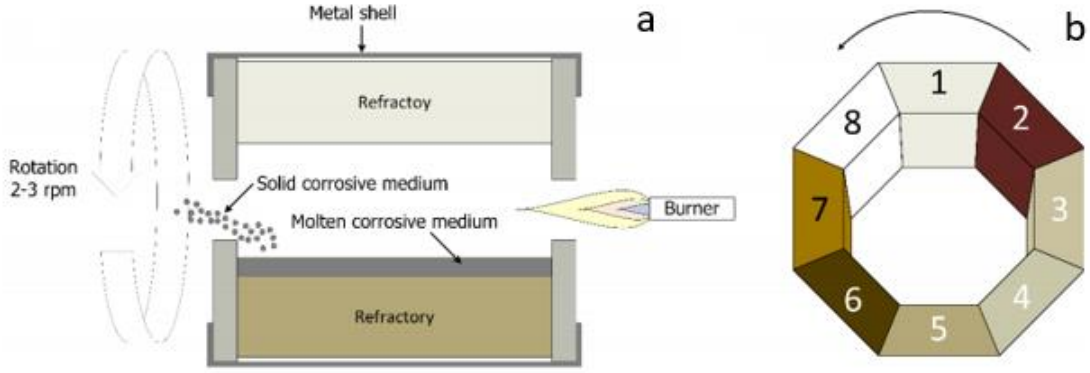

Figure 2. 31. (a)Rotating furnace and (b) crucible with 8 faces used in the rotating furnace [128].

Some of the advantages of the rotary slag test are:

- The slag would not reach saturation as it is refreshed at regularly intervals,
- The slag is stirred, and
- There is a thermal gradient inside the brick because of heating at the center of the chamber.

However, the rotary slag test has also its disadvantages:

- The temperature is quite difficult to control,
- There is a possibility of the refractories interacting between themselves,
- The test reproducibility is relatively low, and
- The test requires large quantities of slag (at least several hundred grams).

Table 2. 5 summarizes the advantages and disadvantages of the different corrosion testing methods discussed [128].

Table 2. 5 Corrosion tests parameters comparison

	Crucible test	Static finger test	Rotary finger test	Rotary slag test
Thermal gradient	No	No	No	Yes
Slag volume	Small	Large	Large	Large
Temperature control	Easy	Easy	Easy	Difficult
Slag agitation	No	No	Yes	Yes
Simplicity	Very easy	Easy	Easy	Difficult
Cost	Cheap	Average	Average	Expensive
Slag renewal	No	Possible	Possible	Yes

2.8 Conclusion

This chapter reviewed literature related to an overview on steel cleanliness, non-metallic inclusions (NMIs) and their characterisation, an overview of secondary metallurgy processes, types of slags and refractory materials used in secondary metallurgy, and a study of the interaction between refractory (MgO-C) and slag/ steel. Slag infiltration into the MgO-C refractory and the degradation mechanism of the refractory were also highlighted, as well as refractory corrosion testing methods.

Taking a cue from the above literature summaries, the following chapters focused on the experimental setup and analysis methods for a comprehensive study to understand the degradation phenomena of MgO-C refractory in the presence of synthetic slag (CMA flux). The thesis investigated the effects of different parameters on refractory corrosion. Some of the parameters that will be investigated included:

- Dwelling time
- Slag composition,
- Temperature.

Furthermore, the thesis aimed to investigate and compare the nature of the interaction of the synthetic slag with MgO-C refractories containing antioxidants, as well as those without antioxidants.

Although many of these parameters have been used to analyse refractory corrosion phenomena, they have been used in isolation. This thesis aims to analyse these parameters as an aggregate to give a comparative study of different MgO-C refractories interactions with two different slags. The experiment results and analysis using a static crucible test setup and characterisation/ analysis tools like SEM/ EDS, EPMA were be presented in the following chapters.

3. Research methodology

3.1. Overview

In this chapter, the framework, structure, and reasoning behind the design of the experiments and approach for this thesis will be presented. The design of the experiment for this masters work mainly focused on three key aspects. Furthermore, the framework of the experimental design, as well as the analysis methods for these aspects will be based on the information from the literature review section (chapter 2.6) on the topic of the interaction between refractory (MgO-C) and liquid phase (slag and/or molten steel). The first main aspect is to investigate the effect of dwelling time, i.e., the time the liquid phase (slag) is in contact with the refractory, on the corrosion of the refractory. A series of experiments to study the interaction of the liquid phase and refractory were performed using a static crucible test at various holding temperatures to investigate the effect of the dwelling time. The second major aspect is the investigation of the role of antioxidants in the refractory and how they affect the interaction at the refractory/slag interface. The literature states that antioxidants play a vital role at inhibiting the oxidation of carbon within the refractory matrix [140–142].Using the same series of experiments as the first aspect, a study of the oxidation of the carbon within the refractory will then be conducted. The third aspect was to investigate the effect of slag composition on the corrosion rate of the refractory. For this study, two different types of slags were used: a slag A which was also used in the previous two aspects, and a low MgO slag B.

A static crucible test was selected for this series of experiments because it is relatively easier to set up as detailed in the previous chapter, and it also provided adequate data for the analyses of the three aspects highlighted earlier as the scope of this thesis.

Detailed descriptions of the experimental design and approach for this thesis are discussed in the section that follows.

3.2. Materials

3.2.1 Slag

Two types of synthetic slags were used for the experiments, one with high MgO content (Slag 1) and the other with a lower MgO content (Slag 2). Both slags were made by mixing high purity silica, alumina, magnesia, calcium oxide powders, and CMA flux provided by Imerys. The slags have compositions as seen in Table 3. 1.

Table 3. 1 Chemical composition of the slags used for the tests.

	Al2O3 [%]	CaO [%]	MgO [%]	SiO2 [%]	TiO2 [%]	FeO [%]	SO3 [%]	K2O [%]	P2O5 [%]
Slag 1	13.97	51.02	9.08	24.3	0.68	0.56	0.19	0.17	0.04
Slag 2	17.04	54.8	0.69	27.89	0.09	0.07	0.02	0.02	0

3.2.2. MgO-C refractory crucibles

Commercial MgO-C refractory crucibles (15 wt.% residual C) were used in the tests. The chemical composition of these refractory crucibles is given in Table 3. 2.

Table 3. 2. Chemical composition of magnesia-carbon refractory crucibles

	MgO [%]	C [%]	Al [%]	Si [%]
REF 1	82.3	15	2.2	0.5
REF 2	85	15	0	0
REF 3	81	15	3	1

3.2.3 Si-killed steel

Commercially available Si-killed steel was used for all the series of experiments in this thesis. Although slightly different masses of steel were used for the different experiments, the steel to slag ratio was 1:1 for all the experiments. Table 3. 3 shows the chemical composition of the Si- killed steel used for the experiments.

Table 3. 3. Composition (wt%) of the industrial Si-killed steel used for the experiments

Elements	wt (%)	Elements	wt (%)	Elements	wt (%)	Elements	wt (%)	Elements	wt (%)
Fe	Balance	Ti	0,001	V	0,001	Sb	0,02	Nb	0,002
Si	0,007	Zn	0,001	Sn	0,002	P	0,06	O	0,0054
Si	0,005	C	0,003	B	0,0002	Cr	0,0142		
Mo	0,002	Mn	0,046	N	0,0029	W	0,003		
Cu	0,013	Ni	0,005	As	0,001	Al	0,002		

3.3 Experiment procedure and setup

The schematic illustration of the experiment apparatus used for the static crucible test is shown in Figure 3. 1. A cylindrical crucible made of MgO-C (inner diameter = 30 mm; outer diameter = 50 mm; height = 47 mm) was filled with slag and steel in a 1:1 mass ratio varying from 16 to 30 g as shown in Table 3.4. The crucible containing slag and steel was heated to 1620 °C at a rate of 5 °C/min using a high-temperature vertical tube furnace (GERO HTRV 100-250/18, with $MoSi_2$ heating elements). To replicate the reducing atmosphere that is typical in an industrial setting, a gas mixture of CO/CO_2 was blown into the furnace at flow rates of 0,2 L/min CO and 0,002 L/min CO_2. The oxygen partial pressure for the experiments was set to below 10^{-16} atm and was regularly monitored using a Rapidox 2100 portable zirconia oxygen gas analyser.

When the target temperature of 1620 °C was reached, the temperature was held for 1 hour and 30 minutes in some experiments, and 4 hours in others. This was to create a dwelling time variation between the experiments. The target temperature of 1620 °C was taken as the initial reaction temperature (T_0), and two dwelling times of 1 hour 20 minutes and 4 hours. Once the target temperature was reached and held for the required dwelling time, the crucible was taken out of the furnace and immediately quenched in water. After drying the crucible and its content, the crucible was cut along the vertical axis for compositional and microstructural analysis as shown in Figure 3. 2.

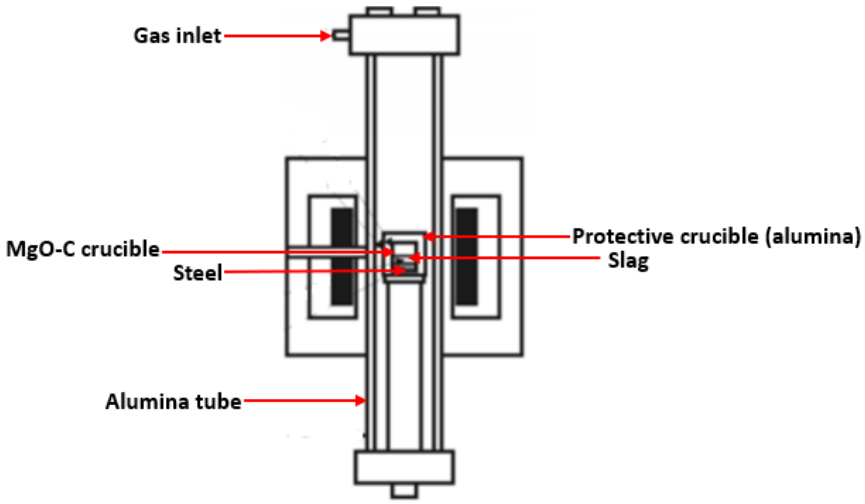

Figure 3. 1. Setup of the static crucible test for the refractory corrosion tests

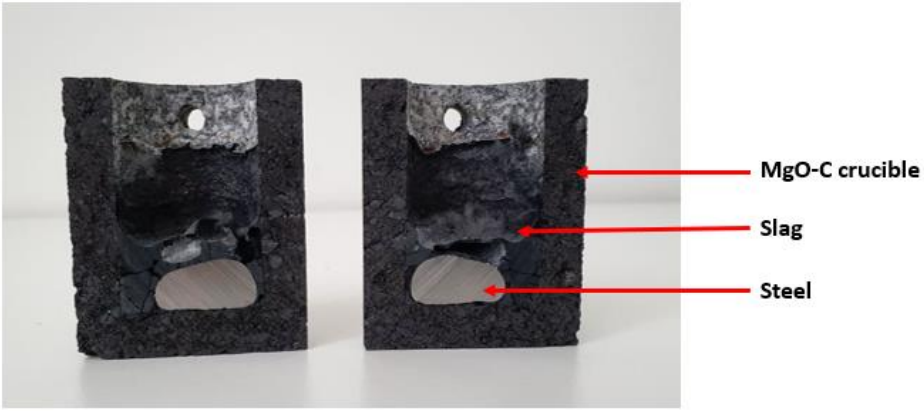

Figure 3. 2. Vertical section of a MgO-C crucible with its content (slag and steel)

3.4. Sample analysis

After cutting the crucible with its content (slag and steel) along its vertical axis, the steel was removed for further analyses. The quenched slag and refractory sections were embedded in low viscosity resin (Epofix) by vacuum impregnation to keep the refractory and slag grains in place. Once the resin was set, sections of the refractory/ slag interface were cut out. The cut pieces of samples of refractory/ slag interface were polished and coated with a conducting platinum layer for microstructural characterisation and compositional analysis. The initial compositional analyses were performed with an electron probe microanalysis (EPMA, JEOL JXA-733) operated at an accelerated voltage of 15 kV and a probe current of 15 nA in combination with an energy dispersive spectrometer (EDS). Further compositional analysis and microstructural characterisation was subsequently performed using a scanning electron microscope (Philips SEM XL-30 FEG), coupled with an EDS detector system from EDAX. Initial slags composition was analysed before the experimental test with a wavelength-dispersive X-ray fluorescence spectrometer (WDXRF) from Philips (PW2400 sequential X-ray spectrometer).

3.5. Thermodynamic calculations

Thermodynamic calculations of MgO saturation in liquid slag were performed using the FactSage 8.0 software. The equilibrium module EQUILIB was used for thermodynamic equilibrium calculation. These calculations are based on the Gibbs free energy minimisation with the FT Misc, FT Oxide and Fact PS databases. The thermodynamic simulations of the slag-refractory interactions were performed at 1620 °C. The refractory/slag interaction was modelled by continuous addition of MgO–C refractory (parameter given as α) containing 15 wt.% C into 100 g of slag. For example, if α= 100 g, then equilibrium calculations will be performed with 85 g of MgO, 15 g C, and 100 g of slag. Hence, during the FactSage simulations, the reactions between the slag phase and the refractory phase were performed in the ratio of 1:1.

4. Experiment results

4.1. General overview

In this chapter, the results of the different series of experiments are presented in four sections. The experiments are subdivided into experiments E1, E2, E3 and E4. The experiments were performed as shown in Table 4. 1. In section 4.2, the interaction of the refractory/ slag interface was presented for each experiment (E1, E2, E3 and E4) using SEM/ EDX imaging and characterisation technique.

Table 4. 1. Test data and parameters for the experiment.

	Slag	Sample	Steel [g]	Slag [g]	Target T [°C]	Dwelling time
E1-1	1	R1	27.8	27.8	1620	1h20min
E2-1	1	R2	24.2	24.2	1620	1h20min
E3-1	1	R3	25	25	1620	1h20min
E1-2	1	R1	22	22	1620	4h
E2-2	1	R2	24	24	1620	4h
E3-2	1	R3	30	30	1620	4h
E4	2	R3	26.4	26.4	1620	4h

4.2. Interaction at interface

4.2.1 Interaction at interface in experiment E1

The experiments (E1-1 and E1-2) were performed at the same target temperature of 1620 °C but at different dwelling times as shown in Table 4. 2.

Table 4. 2. Test data and parameters for the experiment E1.

	Slag	**Sample**	**Steel [g]**	**Slag [g]**	**Target T [°C]**	**Dwelling time**
E1-1	1	R1	27,8	27,8	1620	1h20min
E1-2						4 h

The refractory/ slag interface was examined in SEM/EDS for E1, and Figure 4. 1(a, b, c, and d) shows the backscattered electron (BSE) images and corroded microstructures of the samples for experiment E1.

A distinct refractory/ slag interface can be seen in Figure 4. 1(a-d). In the slag layer, some detached MgO grains and a few large metallic particles (Fe) which originate from the steel used in the experiment can be seen floating in the slag in both E1-1 and E1-2. The detached MgO grains are considered to be due to corrosion of the refractory by the slag. They occur due to the weakening of the refractory matrix as a result of the continuous dissolution of the refractory matrix by slag. Dissolved MgO in the slag, is a direct result of slag infiltration and dissolution of the refractory. This dissolution is indicated by an increase in the slag's MgO composition after the experiment. Figure 4. 1(c and d) show large periclase grains in direct contact with the slag. It can be noticed that these slag/

periclase contact areas are the origin of most of the detached MgO particles floating in the slag. E1-2 had significantly more detached MgO grains in its slag. Experiment E1-1 seemingly had no slag infiltration of the refractory matrix as highlighted in Figure 4. 1a. However, at higher magnification, as shown in Figure 4. 1c, slag infiltration can be noticed in cracks close to the refractory/slag interface. In contrast, E1-2 has slag infiltration both at areas close to the refractory/slag interface and in cracks at deeper regions of the refractory matrix as shown in Figure 4. 1 (a and b).

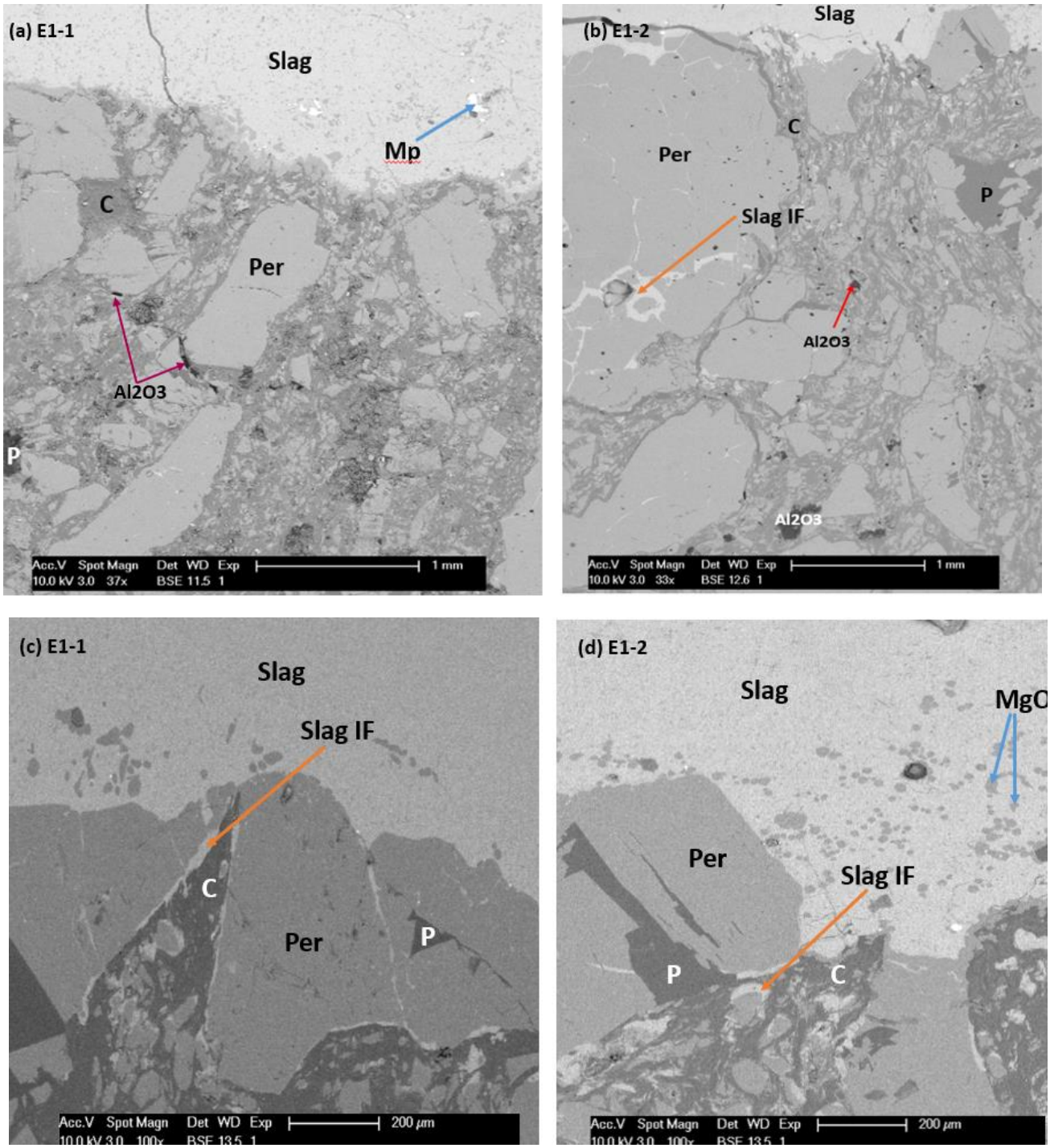

Figure 4. 1. SEM (backscattered electron) images of the refractory/ slag interface of samples of experiment E1 at different dwelling time (a) 1 hr 20 min (b) 4 hrs (c) enlarged view of the refractory/slag interface of refractory sample in experiment E1-1 (1 hr 20 min) (d) enlarged view of the refractory/slag interface of

refractory sample in experiment E1-2 (4 hr). Per: periclase grain; Mp: metal particle; C: carbon phase; Slag IF: infiltrating slag; MgO: magnesia grains; P: pores.

Pores can be noticed in the refractory matrix for both experiments (E1-1 and E1-2), especially at high magnifications as shown in Figure 4. 1(c and d). The pores in E1-2 are considerably more than those in E1-1. The pores seen in the refractory matrix is a result of volumetric shrinkage due to decarburisation. However, these pores were not filled with slag infiltrates. There is no spinel layer (magnesia-alumina spinel) at the refractory/slag interface of both experiments E1-1 and E1-2. A spinel layer typically prevents infiltration of the slag into the refractory matrix.

Al_2O_3 can be seen within the refractory matrix, as shown in Figure 4. 1(a and b). These Al_2O_3 are produced in-situ within the refractory matrix from the antioxidant (Al). When Al (antioxidants) reaches its melting point of 660°C, the molten Al reacts with the surrounding carbon in the refractory to form alumina carbide (Al_4C_3) within the refractory matrix. The resultant Al_4C_3 reacts with CO from already oxidised carbon to form a thin alumina layer (Al_2O_3) and carbon as indicated in equation 2.2 – 2.4 in section 2.5.4.4 [81, 85].

The in-situ formation reaction of reactive alumina ($Al_2O_{3(s)}$) in the matrix of MgO–C is found to improve corrosion resistance, as they protect the MgO-C brick against oxidation, by filling up the pores and forming a relatively dense zone in the oxidized areas. $MgAl_2O4$ spinel was however not noticed in both E1-1 and E1-2.

4.2.2 Interaction at interface in experiment E2

Both experiments (E2-1 and E2-2) were performed at the same target temperature of 1620 °C, with similar masses of steel and slag, but at different dwelling times as shown in Table 4. 3.

Table 4. 3. Test data and parameters for the experiment E2.

	Slag	Sample	Steel [g]	Slag [g]	Target T [°C]	Dwelling time
E2-1	1	R2	24	24	1620	1h20min
E2-2						4 h

The refractory/slag interface was examined in SEM/EDS, and Figure 4. 2 (a, b, c, and d) shows the backscattered electron (BSE) images and corroded microstructures of the samples for experiment E2.

Similar to experiment E1, a distinct refractory/slag interface can be seen in Figure 4. 2 (a-d). In the slag layer, detached MgO grains can be seen floating in both E2-1 and E2-2. Additionally, a few metallic particles (Fe), which originate from the steel used in the experiment can be seen at the refractory/slag interface in E2-1. Slag infiltration of the large periclase grains can be noticed in E2-2, while a much lower slag infiltration of the periclase grain is seen in E2-1. It can also be seen in both experiments (E2-1 and E2-2) that the carbon-containing zones remain intact and not infiltrated. The pores seen in the refractory matrix especially on the large periclase grains for both E2-1 and E2-2 is a result of volumetric shrinkage due to decarburisation.

Just like experiment E1, there is no spinel layer (magnesia-alumina spinel) at the refractory/slag interface.

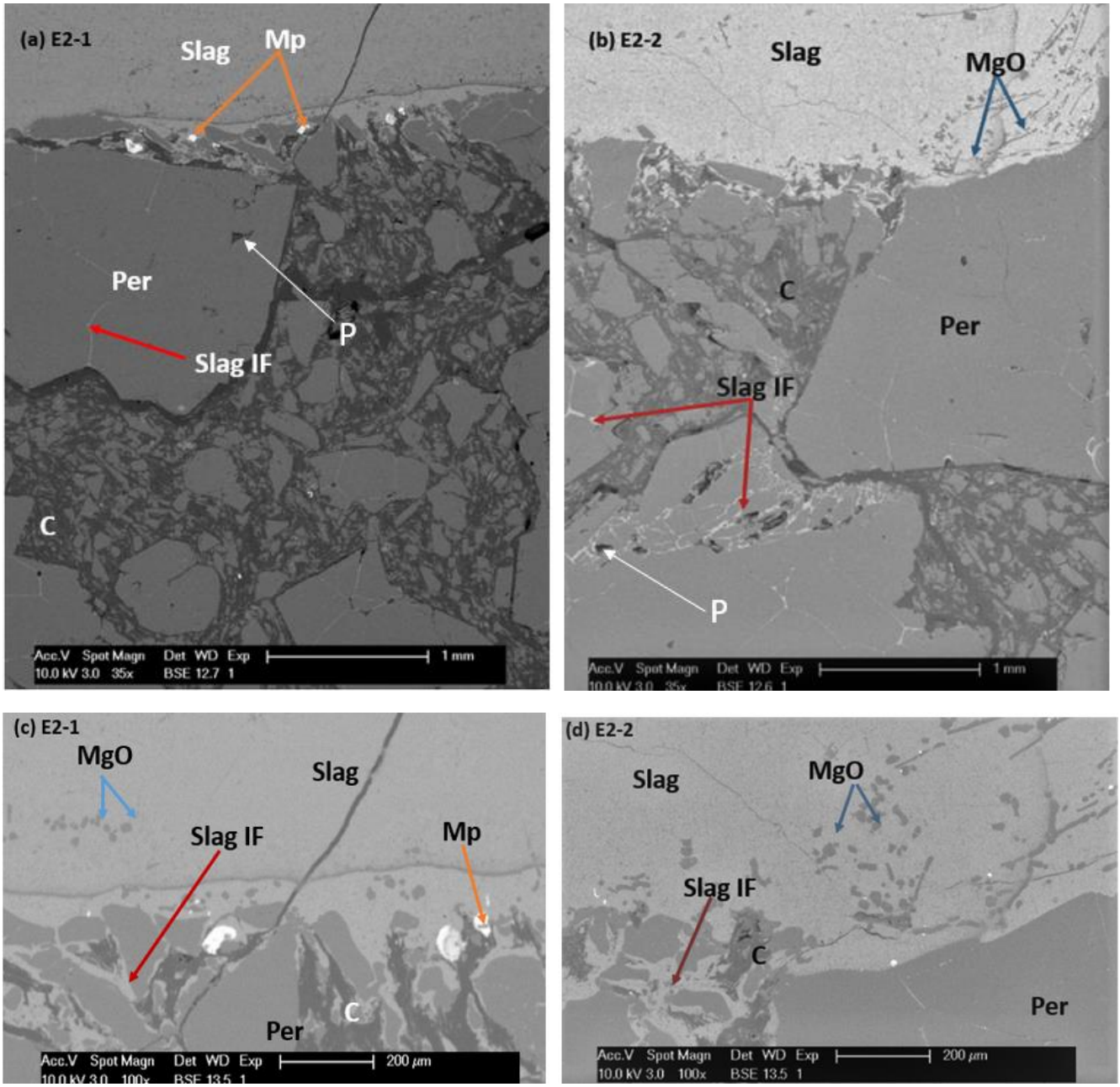

Figure 4. 2. SEM (backscattered electron) images of the refractory/slag interface of samples of experiment E2 at different dwelling time (a) 1 hr 20 min (b) 4 hrs (c) enlarged view of the refractory/ slag interface of experiment E2-1 (1 hr 20 min) (d) enlarged view of the refractory/ slag interface of refractory sample in experiment E2-2 (4 hr). Per: periclase grain; Mp: metal particle; C: carbon phase; Slag IF: infiltrating slag; MgO: magnesia grains; P: pores.

4.2.3 Interaction at interface in experiment E3

Both experiments (E3-1 and E3-2) were performed at the same target temperature of 1620 °C but at different dwelling times as shown in Table 4. 4.

Table 4. 4: Test data and parameters for the experiment E3.

	Slag	Sample	Steel [g]	Slag [g]	Target T [°C]	Dwelling time
E3-1	1	R3	25	25	1620	1h20min
E3-2						4 h

Figure 4. 3 (a-d) show SEM backscattered electron (BSE) images of the refractory/slag interface of experiment E3 at a dwelling time of 1 hour 20 min, and 4 hr respectively. The slag phases of both experiments (E3-1 and E3-2) have a relatively low amount of MgO particles floating.

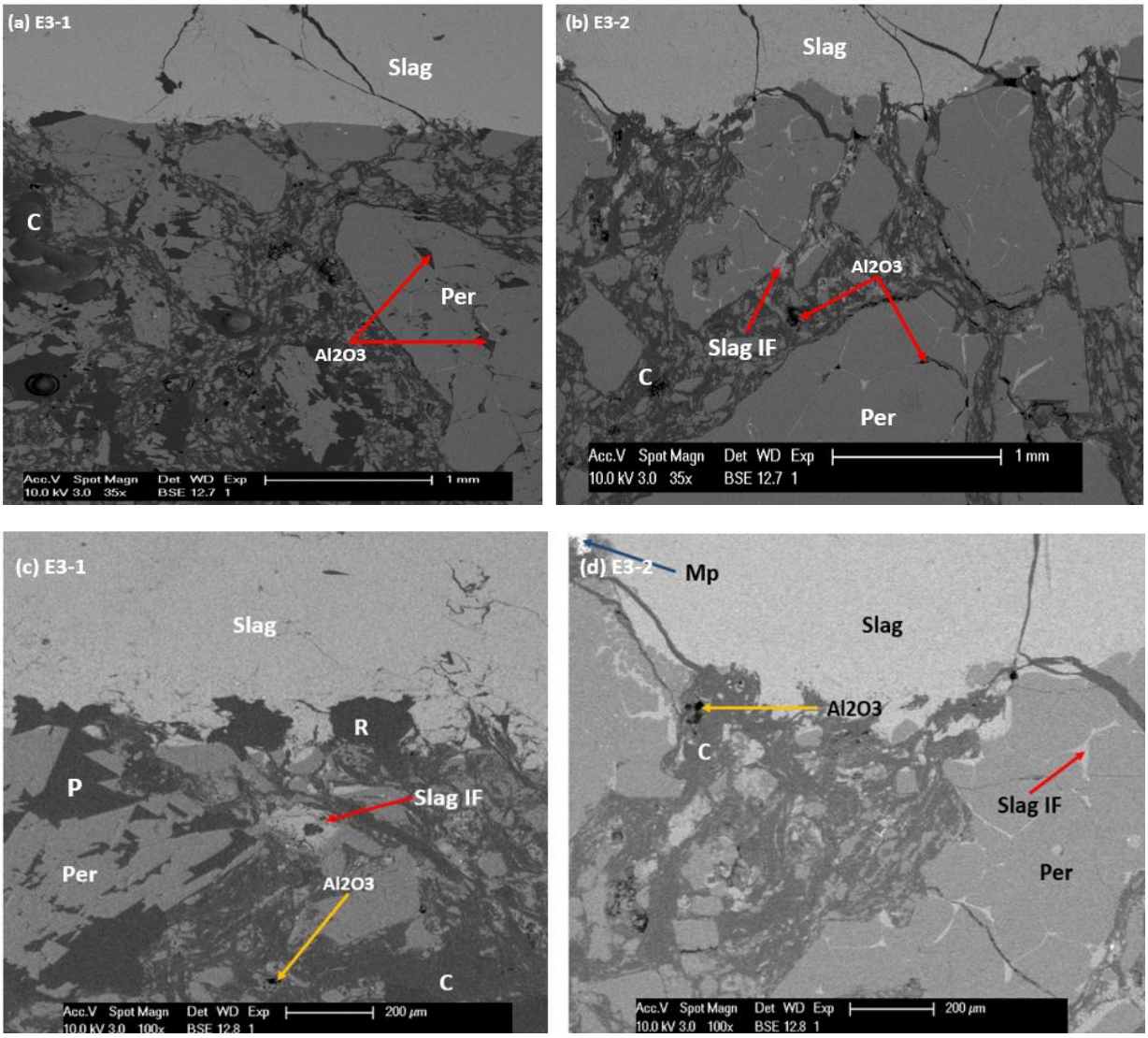

Figure 4. 3. SEM (backscattered electron) images of the refractory/slag interface of samples of experiment E3 at different dwelling time (a) 1 hr 20 min (b) 4 hrs (c) enlarged view of the refractory/ slag interface of experiment E1-1 (1 hr 20 min) (d) enlarged view of the refractory/ slag interface of refractory sample in experiment E3-2 (4 hr). Per: periclase grain; R: Resin; C: carbon phase; Slag IF: infiltrating slag; MgO: magnesia grains; P: pores.

In Figure 4. 3c (E3-1), a few large pores and resin spots can be seen at the refractory/slag interface. These pores are due to cracks from sample preparation and not as a result of decarburisation or volumetric shrinkage. The refractory/ slag interface of the sample in experiment E3-1 is less corroded as the interface looks fairly intact. Furthermore, the periclase grains in contact with the slag phase seem to be also intact and there is very minimal slag infiltration of the refractory sample as can be seen in Figure 4. 3 (a and c). This is not the case in E3-2, as slag infiltration of the periclase grains can

be noticed as seen in Figure 4. 3 (b and d). However, the areas of the refractory with carbon remain intact to a large extent.

Oxidised Al from the antioxidants in the initial composition of the refractory can be noticed in both experiments (E3-1 and E3-2) as shown in Figure 4. 3. (a-d). Also, there is no spinel layer (magnesia-alumina spinel) at the refractory/slag interface.

4.2.4 Interaction at interface in experiment E4

Experiment E4 was performed at the same target temperature of 1620 °C but at a dwelling time of 4 hr as shown in Table 4. 5.

Table 4. 5: Test data and parameters for the experiment E4.

Sample	Slag	Steel [g]	Slag [g]	Target T [°C]	Dwelling times	Target T [°C]
Ref 3	2	26	26	1620	4 hrs	1620

Figure 4. 4 shows an SEM backscattered image of the refractory/ slag interface of experiment E4. The distinct phases of periclase, carbon and slag can be seen. Also, some metallic particles (Fe) can be noticed at the refractory/ slag interface. Large particles of MgO can also be noticed in the slag. Very minimal slag infiltration can be noticed even though there are several pores and cracks in the refractory matrix. However, these pores and cracks were not infiltrated by slag. Most of the slag corrosion occurs at the interface, where the large periclase grains were in contact with the slag. The carbon phase of the refractory is also intact. Furthermore, oxidised Al can also be seen in the refractory matrix. Like the other experiments (E1, E2 and E3), there is a distinct interface between the slag phase and refractory. Also, there is a clear absence of a spinel layer (magnesia-alumina spinel) at the refractory/slag interface.

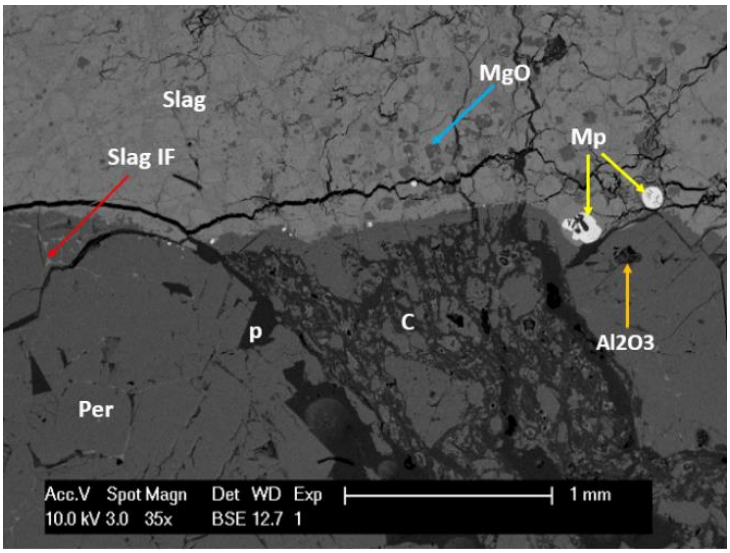

Figure 4. 4. SEM (backscattered electron) images of the refractory/slag interface of samples of experiment E4 at dwelling time 4 hrs. Per: periclase grain; C: carbon phase; Slag IF: infiltrating slag; MgO: magnesia grains; P: pores.

4.3 Slag composition

Figure 4.5 shows an area analysis used to depict the evolution estimation of the slag phase chemical composition in the vicinity of the refractory. This EDS area analysis of the slag's MgO content evolution was performed using profile areas of approximately 300 µm long and 900 µm wide to obtain an average representative value of the slag composition of the different analysed areas. This was done to perform a comparative study to the initial composition of the slag, to understand the slag evolution during the experiment. From the refractory/ slag interface, the area analysis was performed by selecting four areas as shown in Figure 4. 5. The analysis was performed while paying attention to avoid slag phase areas with high concentrations of MgO particles. Table 4. 6 shows the results of the EDS area analysis of the average chemical compositions of the slag after the experiments (E1, E2, E3 and E4). The detected elements in this analysis are Si, Al, Ca, Mg, and O, which were quantified as SiO_2, Al_2O_3, CaO and MgO.

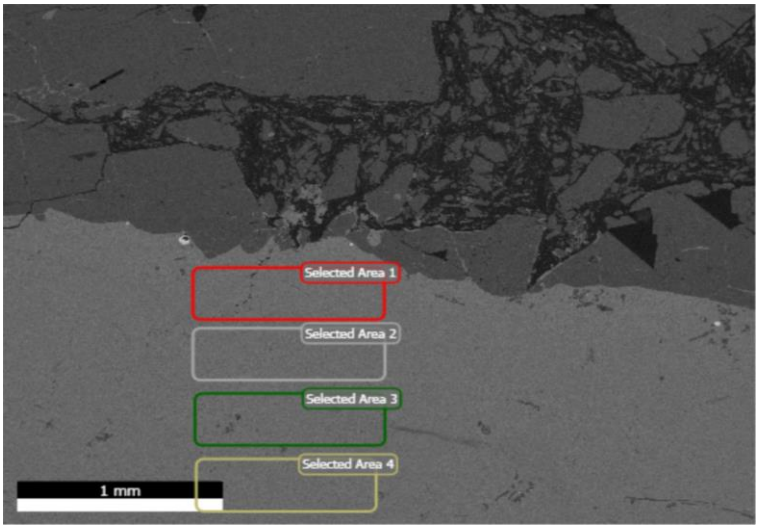

Figure 4. 5. EDS analysed area slag phase of experiment E1 at dwelling time 1 hr 30mins.

Table 4. 6: Average chemical compositions of the slag after the experiments, as determined by EDS analysis (in wt.%).

	CaO	MgO	Al2O3	SiO2
E1-1	46,5 - 50,9	10,7 - 11,3	15,6 - 16,4	22,7 - 25,8
E1-2	47 - 49,8	10,7 - 11,5	14,5 - 16	23,2 - 26,2
E2-1	42,9 - 45,5	10,7 - 11,5	17,5 - 20,6	25,5 - 26
E2-2	42,7 - 45,1	11,1 - 11,9	17,4 - 19,8	24,8 - 26,4
E3-1	46,3 - 48,6	9,7 - 11,2	16,9 - 21,8	22,2 - 25,2
E3-2	46,7 - 48,2	10,2 - 11,7	15,9 - 19,6	23,5 - 24,3
E4	44,3 - 50,1	4,5 - 6,2	18,3 - 20,7	24,1 - 26,6

As discussed in earlier in section 3.5, the calculated values will be derived from the FactSage modelling of the refractory/slag, using a continuous addition of MgO–C refractory (parameter given as α) containing 15 wt.% C into 100 g of slag. For the presentation of the result in this thesis, α=100g of MgO-C refractory material.

4.3.1 MgO concentration

Figure 4. 6 depicts the increase of the MgO slag content (wt. %) in all the experiments (E1 – E4). The MgO content in the slag after the experiment is considerably more than the slag's initial MgO content and the calculated MgO content using FactSage. It is logical to assume that the source of the additional MgO in the slag is from the dissolved periclase grains of the refractory. Although E2-2 had the highest MgO slag content increase (11.5 wt.%), it was not much different from E3-1 which had the lowest MgO content increase of 10.6 wt. %. Hence, there was no significant variation in MgO content between E1 (1 and 2), E2 (1 and 2) and E3 (1 and 2). E4 had a significantly lower MgO slag content after the experiment. However, it had the highest MgO content increase (Δ MgO) of about 5 wt. %.

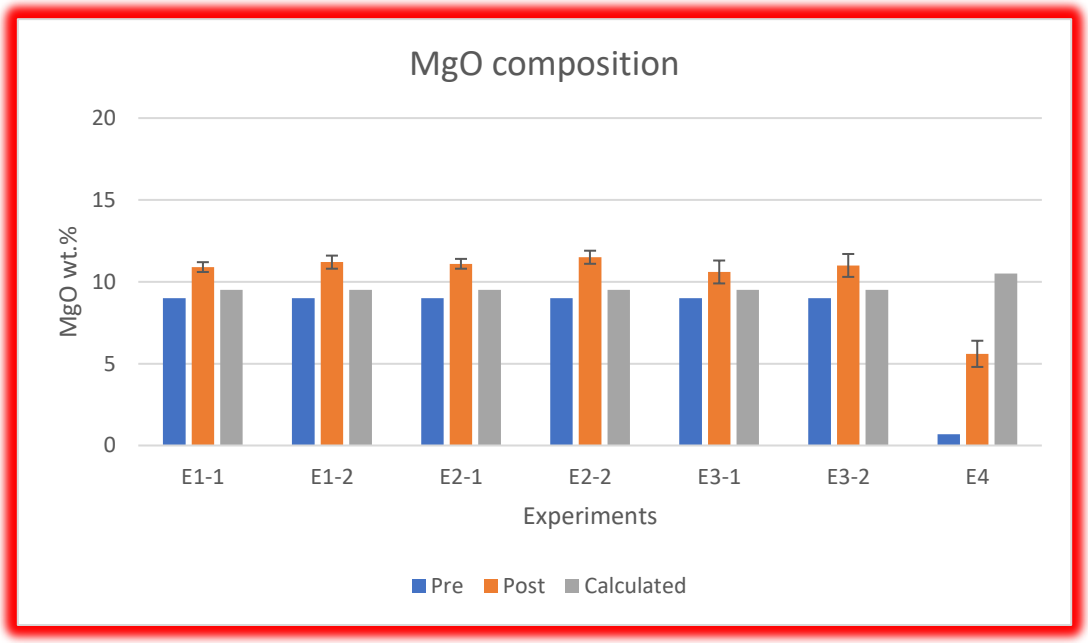

Figure 4. 6. MgO slag contents (wt.%) measured before and after the tests compared to the calculated values for α = 100 g.

The FactSage simulation to predict the saturation and evolution of the different elements in the slag was done using the procedure explained in section 3.5. The results of the FactSage simulation is shown in Figure 4. 7 and Figure 4. 8. Figure 4. 7 depicts the refractory/ slag interaction in experiment E1 (slag 1), while Fig. 4.8 shows the FactSage simulation of E4 (slag 2). Both simulation results highlight a gradual increase in the MgO slag content as α increases until it reaches a saturation of 9.5 wt.% of MgO in the slag for experiment E1. The slag MgO saturation for experiment E4 using slag 2 is 9.4 wt.% of MgO as show in Fig 4.8. The difference between the experimental and FactSage simulation results can be attributed to the presence of detached MgO grains floating in the slag.

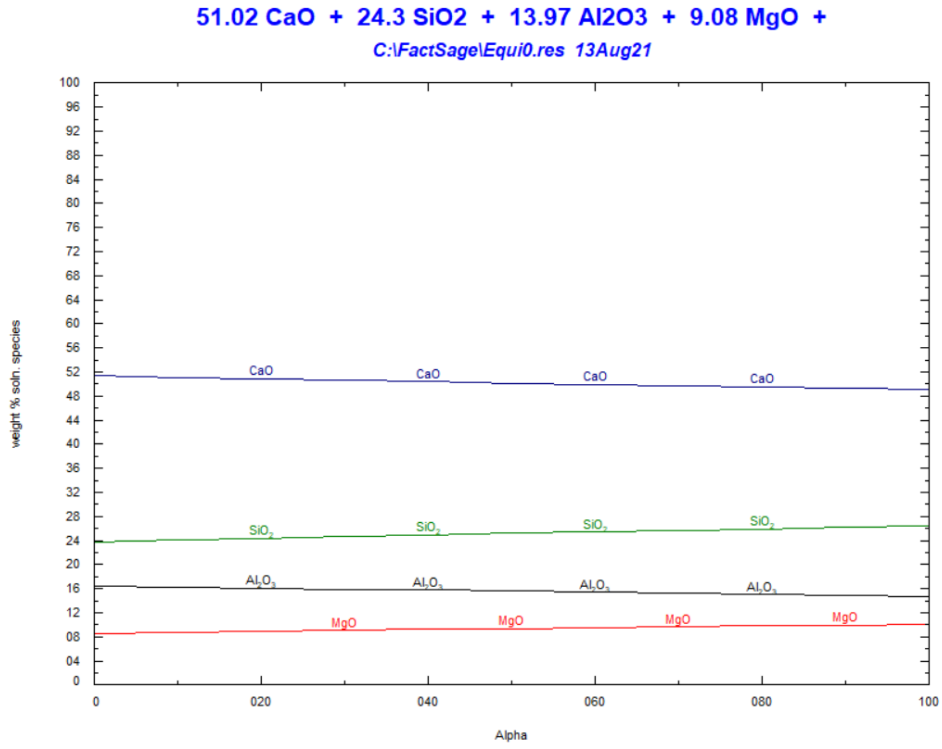

Figure 4. 7. Prediction of the evolution of the MgO,CaO, Al_2O_3 and SiO_2 content (wt.%) in the slag phase with increasing amount of MgO–C refractory (α) at 1620 °C for slag 1 in experiment E1.

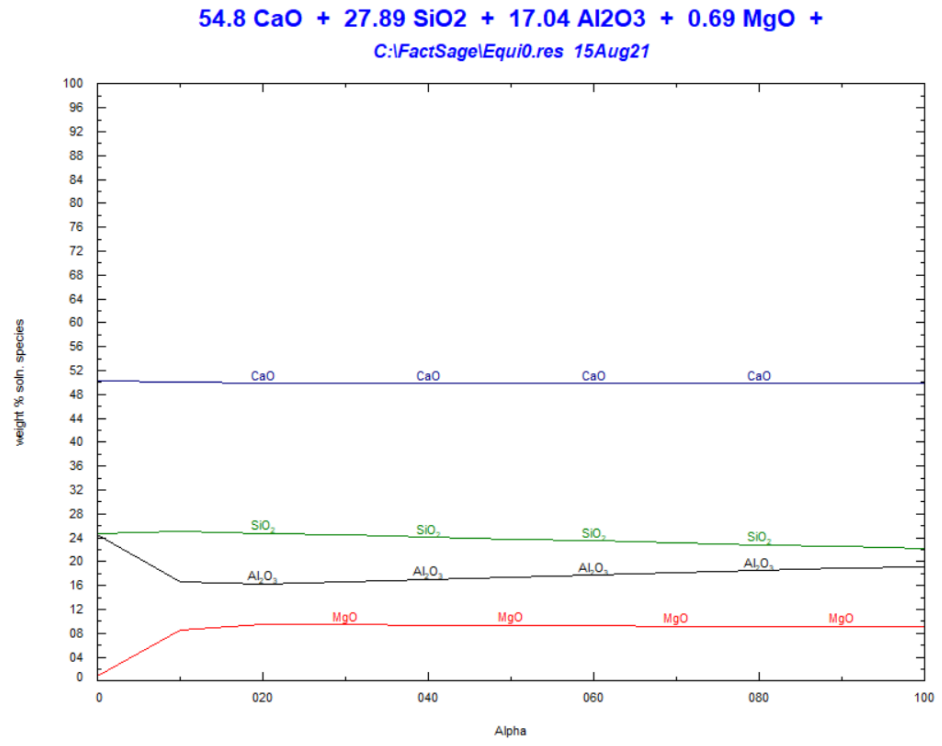

Figure 4. 8. Prediction of the evolution of the MgO,CaO, Al_2O_3 and SiO_2 content (wt.%) in the slag phase with increasing amount of MgO–C refractory (α) at 1620 °C for slag 2 in experiment E4.

4.3.2 Al_2O_3 and SiO_2 (Antioxidants) concentration

Figure 4. 9 depicts the a graphical illustration of the measured Al_2O_3 content in the slag for the different experiments (E1, E2, E3 and E4). Similarly, Figure 4. 10 indicates the SiO_2 content in the slag of the different experiments. It can be noticed that there is an increase in the alumina (Al_2O_3) content of the slag after the experiments. However, the SiO_2 content of the slag after the experiments stayed relatively the same. At high temperature (>1200 °C), Si reacts with carbon to form SiC, and also occasionally it is directly reacting with CO to form SiO_2. SiC further reacts with MgO to form M2S. The reaction is shown in equation 2.5, 2.6, and 2.7 in section 2.5.4.4 [85].

However, there was no evidence of M2S precipitation on the periclase grains or in the refractory in general for all the experiments.

The increase in alumina concentration in the slag can be correlated with the presence of antioxidants (Al) in the refractory matrix. As shown in Figure 4. 9, experiment E2 (E2-1 and E2-2) which had a minimal change in slag alumina content after the experiment, has no antioxidant in its initial refractory composition.

The increase in alumina concentration in the slag can be correlated with the presence of antioxidants (Al) in the refractory matrix. As shown in Figure 4. 9, experiment E2 (E2-1 and E2-2) which had a minimal change in slag alumina content after the experiment, has no antioxidant in its initial refractory composition.

However, there was no evidence of M2S precipitation on the periclase grains or in the refractory in general for all the experiments.

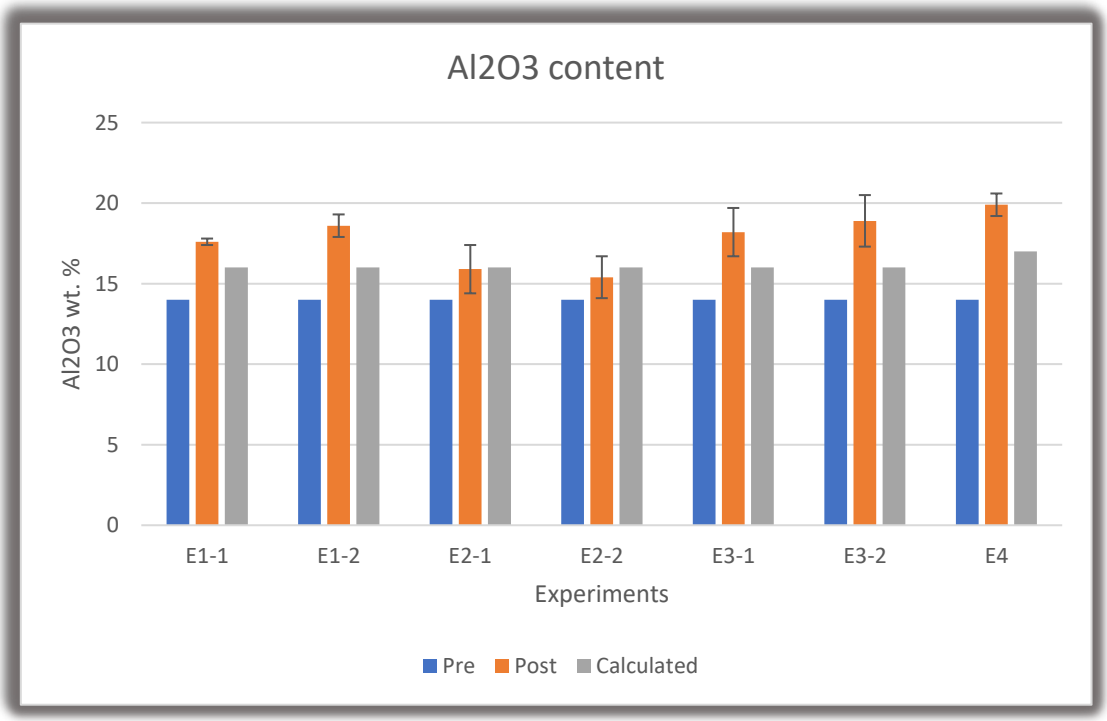

Figure 4. 9. Al_2O_3 slag contents (wt.%) measured before and after the tests compared to the calculated values for α = 100 g.

Figure 4. 10. SiO_2 slag contents (wt.%) measured before and after the tests compared to the calculated values for α = 100 g.

4.4 Penetration behavior and depth

Figure 4. 11 (a and c) show the SEM backscattered electron (BSE) images of the deeper regions of Ref 1 after experiment E1 at a dwelling time of 1 hr 20 min (E1-1) and 4 hrs (E1-2). It can be noticed in Fig. 4.11a that there is very little slag infiltration of the refractory at 5mm away from the interface with the slag. This is also depicted in Fig. 4.11b, as there is a decline in the CaO content of the refractory with increasing depth. The CaO content of the refractory can be used as an indicator for the presence of slag because increased CaO content of the refractory is a result of slag infiltration. Figure 4. 11b shows an increase of Al_2O_3 with depth. The increasing Al_2O_3 can be presumed to be oxidised antioxidant (Al) within the refractory matrix. However, SiO_2 which is also present in the refractory as an antioxidant although in a lower quantity (1 wt. %) is seen to be decreasing. This can be because Al oxidises more rapidly than Si and forms thin layers of the Al_2O_3 layer. At a longer dwelling time (4 hr), as shown in Figure 4. 11 (b and d), the Al_2O_3 and SiO_2 content of the refractory are more at the same depths in comparison to dwelling time of 1 hr 20 min.

In E1-2 there is significant infiltration of the large periclase grains at deeper regions of the refractory as can be seen in Figure 4. 11c. Additionally, small Al spinel can be seen in some of the smalls pores on periclase grains. They help reduced oxidation of these areas and filling of the pores with slags. At increased depths also, the carbon region of the refractory is seemingly intact and not infiltrated by slag.

For both E1 experiments (E1-1 and E1-2), there is clearly a decrease in slag infiltration of the refractory with increasing depth as indicated by the steady decrease in CaO content of the refractory.

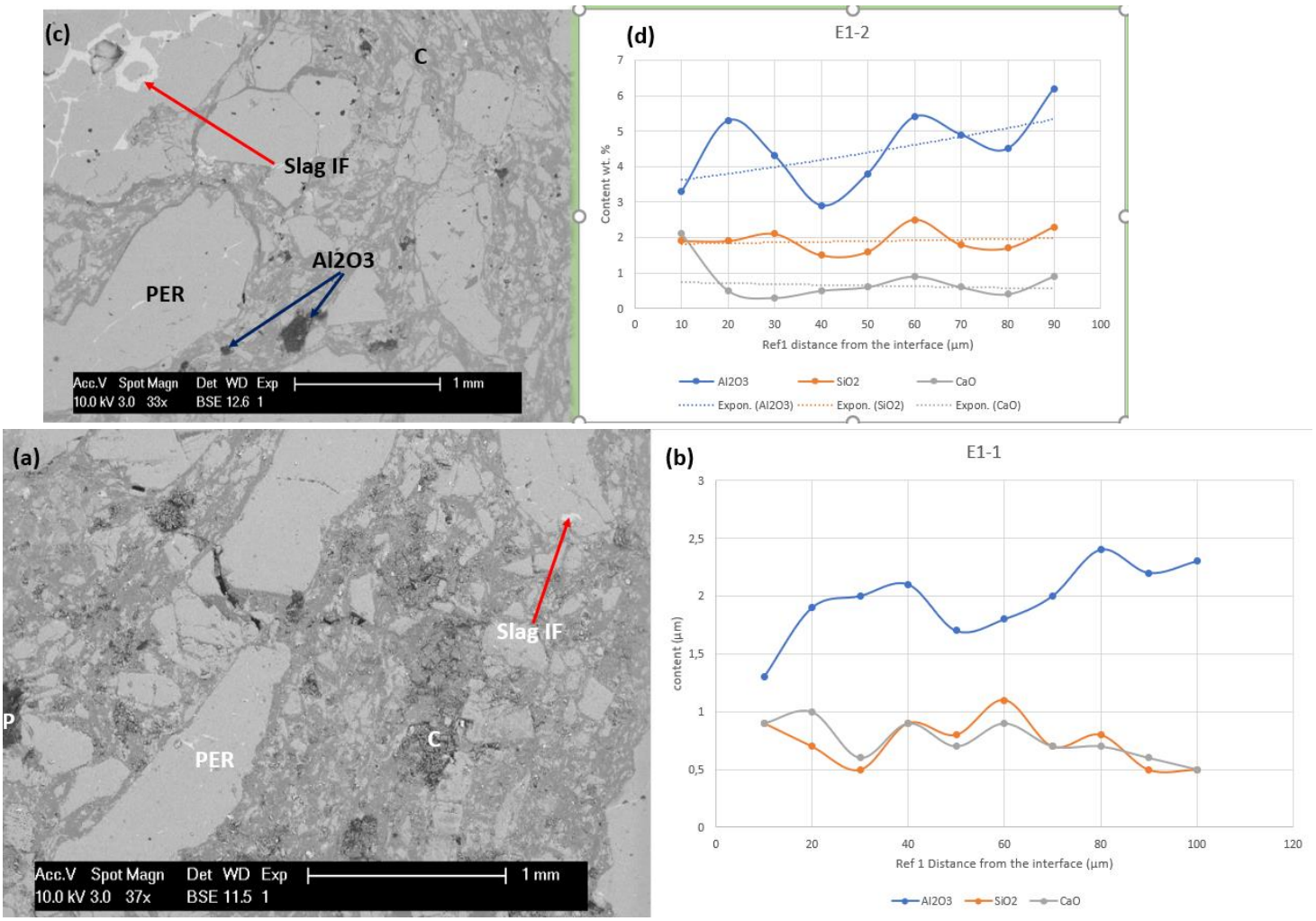

Figure 4. 11. (a and d) SEM (backscattered electron) images of the deeper regions of samples in experiment E1 at different dwelling time (a) 1 hr 20 min (c) 4 hrs. Fig 4.11 (b and d) graphical elements evolution in the refractory matrix as a function of depth. Per: periclase grain; C: carbon phase; Slag IF: infiltrating slag.

Figure 4. 12 (a and c) show BSE images of the deeper regions of Ref 2 after experiment E2 at a dwelling time of 1 hr 20 min (E2-1) and 4 hrs (E2-2). Large grains of periclase, carbon phases and pores can be seen in both BSE images (Fig. 4.12 (a and c). Additionally, it can be noticed that slag has infiltrated and filled the pores and cracks of the periclase grains in both E2-1 and E2-2. However, the carbon phase remains relatively intact. Figure 4. 12 (b and d) show a graphical representation of the evolution of the refractory's CaO, Al_2O_3 and SiO_2 content with depth. There is a sharp initial decrease in average CaO, Al_2O_3 and SiO_2 contents of the refractory between the refractory/ slag interface (0 mm) and 2mm depth. However, their concentration is steady afterwards. This indicates that more of the infiltration of the refractory by slag occurs closer to the interface, but there is still quite a level of infiltration at larger depths. The large pores as seen in Figure 4. 12 (a and C) can be attributed to volumetric shrinkage due to increased decarburisation.

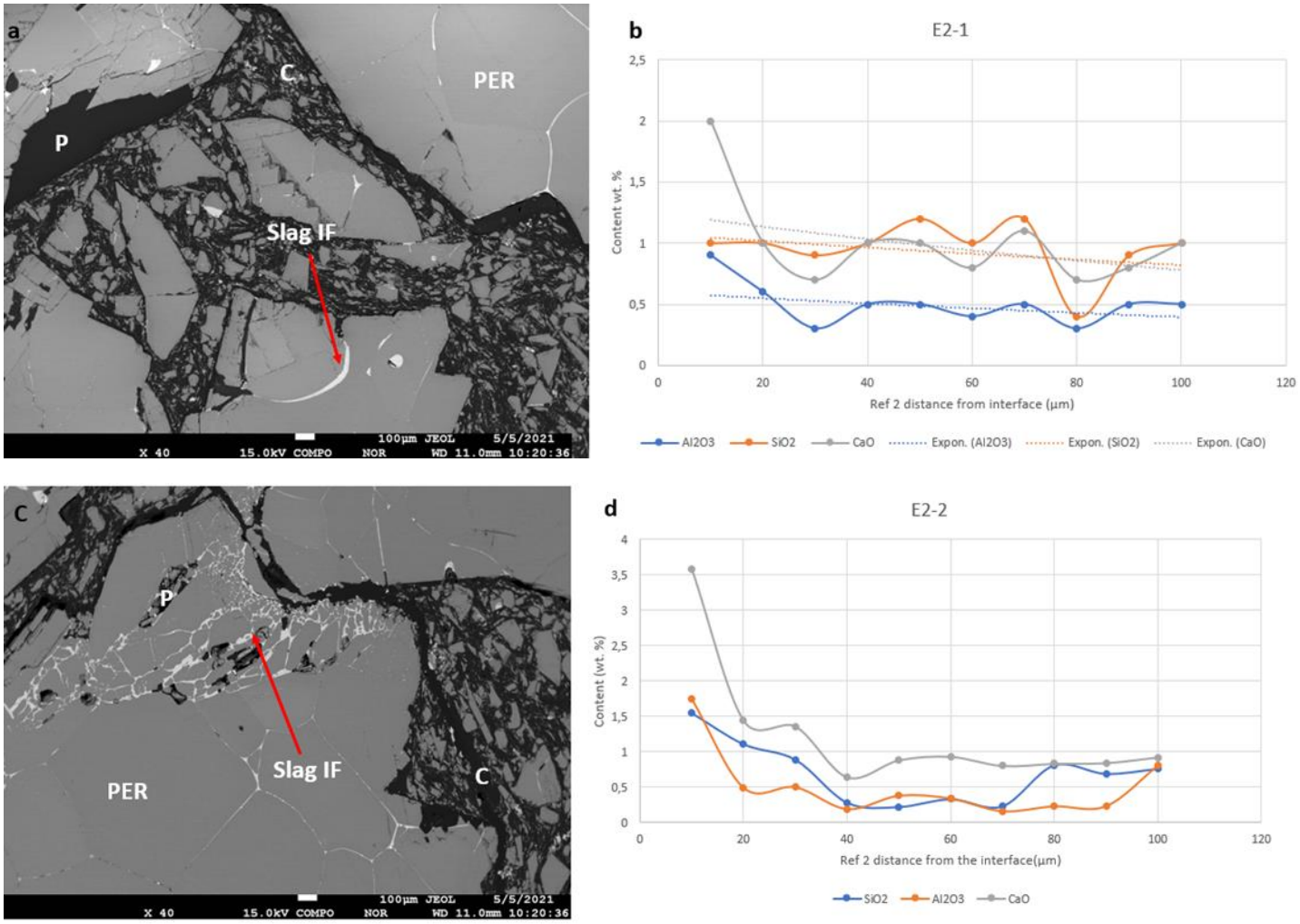

Figure 4. 12. (a and c) SEM (backscattered electron) images of the deeper regions of samples in experiment E2 at different dwelling time (a) 1 hr 20 min (c) 4 hrs. Fig 4.12 (b and d) graphical elements evolution in the refractory matrix as a function of depth. Per: periclase grain; C: carbon phase; Slag IF: infiltrating slag.

Figure 4. 13 (a and c) show the SEM backscattered electron (BSE) images of the deeper regions of Ref 3 after experiment E3-2 (slag 1) and E4 (slag 2) at a dwelling time of 4hrs. Large grains of periclase and carbon phases can be seen in both SEM images (Fig. 4.13 (a and c)). E3-2 shows little slag infiltration of the periclase grains (Fig 4.13a). In Fig 4.13c (E4), Al_2O_3 can be seen to have filled some of the small pores of the periclase grains, but there is still slag infiltration within cracks in the periclase grains. E4 on the other hand show significant slag infiltration at the deeper regions (Fig. 4.13c). This can be a result of the increased viscosity of slag 2 (0.16 Pa.s) compared to a viscosity of 0.12 Pa.s for slag 1.

Figure 4. 13 (b and d) shows the graphical representation of the evolution of the refractory's CaO, Al_2O_3 and SiO_2 content with depth during experiments E3-2 and E4. There is an increase in the Al and Si concentration in both experiments , but a decrease in the average CaO content of the refractory as it goes deeper from the refractory/ slag interface. Most of the corrosion in E4 occured at the refractory/ slag interface where slag 2 (low MgO) is in direct contact with the periclase grains as shown in Figure 4. 14.

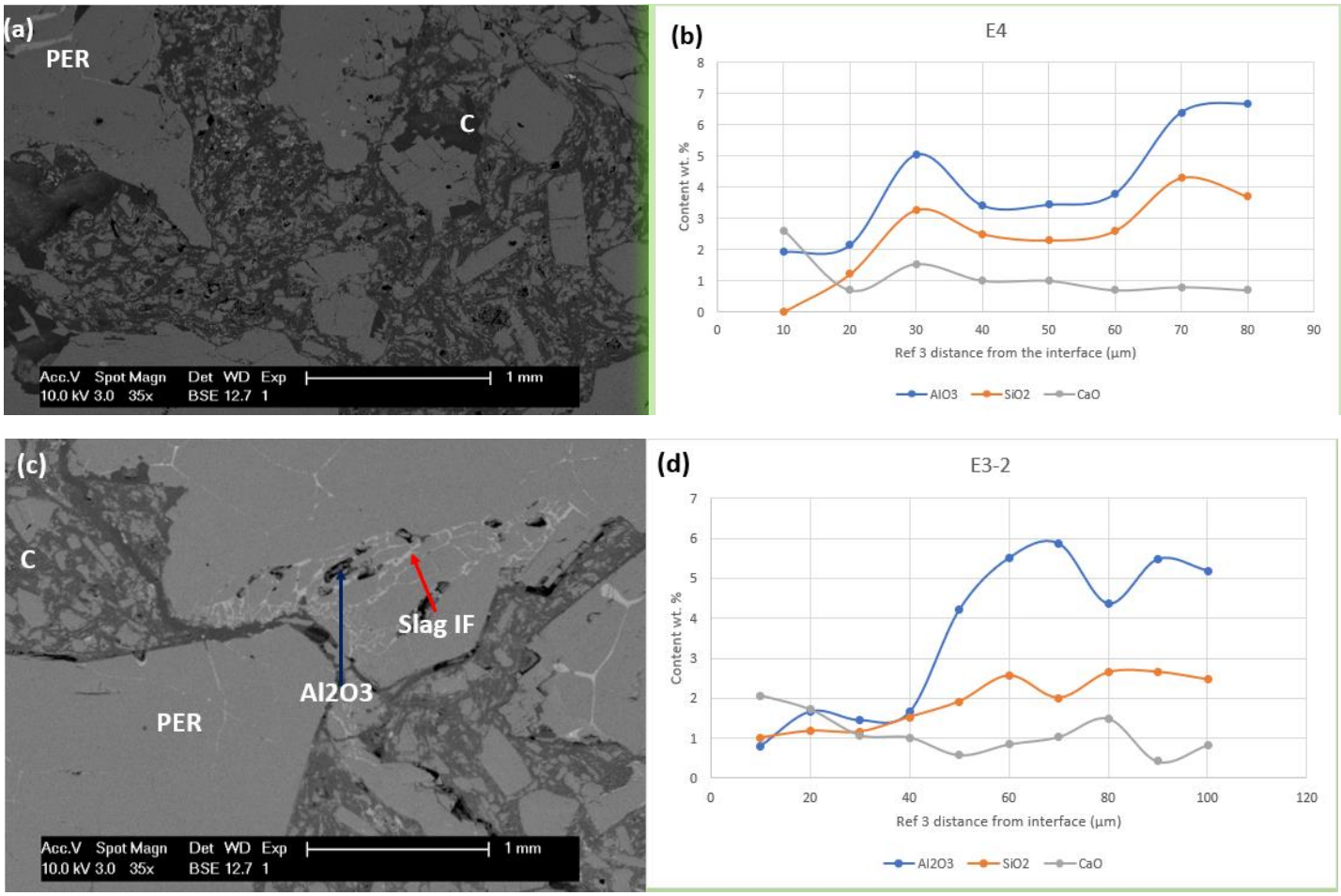

Figure 4. 13. (a and c) SEM (backscattered electron) images of the deeper regions of samples in experiment E3-2 and E4 at a dwelling time of 4 hrs. Fig 4.13 (b and d) graphical elements evolution in the refractory matrix as a function of depth. Per: periclase grain; C: carbon phase; Slag IF: infiltrating slag.

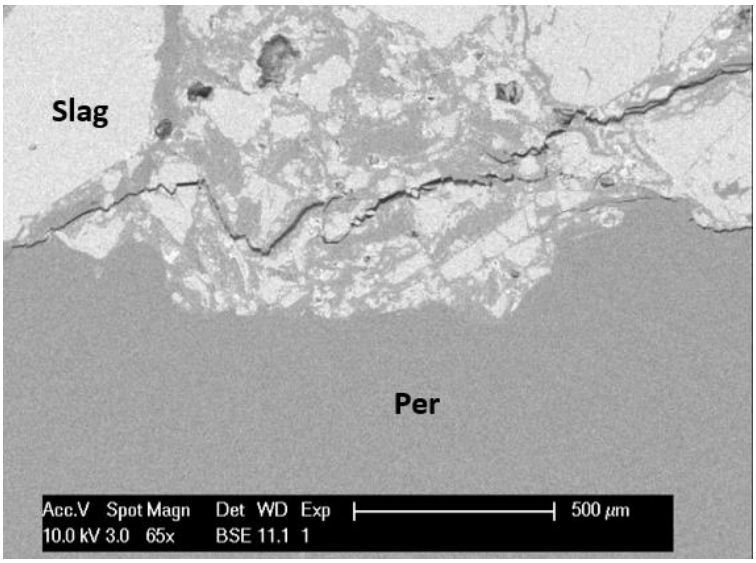

Figure 4. 14. SEM (backscattered electron) images of the refractory/ slag of a sample from in experiment E4 (slag 2) . Per: periclase grain.

5. Discussion

5.1. Slag penetration and dissolution of refractory

MgO dissolution of the refractory material by the slag was verified by SEM/EDS investigations of the samples. The slag can be seen in most of the experiments to have penetrated the refractory material. Slag penetration and dissolution of refractory can be described as a vicious cycle whereby the slag penetrates through the refractory via pore spaces within the refractory, gradually detaching and dissolving elements within the refractory leading to eventual refractory corrosion. Figure 5. 1 describes systematically the corrosion cycle of the refractory slag interaction [143].

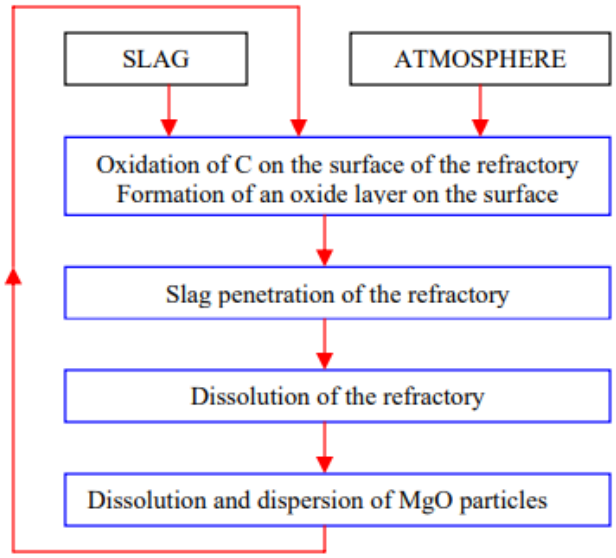

Figure 5. 1. Corrosion mechanism of a typical MgO-C refractory [143].

5.2 Absence of MA spinel

All the experiment samples showed an absence of magnesia-alumina (MA) spinels. This may be as a result of the relatively high experiment temperature of 1620°C. Reactions between the refractory and liquid slag above 1500°C do not form a MA spinel. For spinels to form, the MgO content of the slag needs to about be around 17–18 wt.%. At lower MgO contents, the slag composition will be above the MA liquidus surface, hence will be completely liquid at 1500°C [132].

5.3 The effect of antioxidants

Decarburisation is the oxidation of the carbon in the MgO-C refractory. The carbon within the MgO-C refractory is inherently susceptible to oxidation at a high temperature. All the experiments in this thesis were conducted at a relatively high temperature (1620°C). Hence the carbon in the MgO-C refractories was prone to decarbonisation. The oxidation of carbon harms the overall performance (corrosion resistance) of the MgO-C refractory [140, 141]. Decarburisation of the MgO-C refractory brick is an essential mechanism of refractory corrosion because decarburisation sites are penetration

channels for the slag. Additionally, the presence of C in the refractories reduces the refractory's wettability by molten slags [144].

After decarburisation, the structure of the MgO-C refractory is altered due to several pores formed in the refractory, leaving an avenue for the slag to penetrate the refractory structure. Hence, antioxidants (Al, Si) are added during refractory production to prevent the oxidation of carbon. It is assumed that antioxidants at high temperatures plug open pores and inhibit oxygen penetration of the sample, thereby improving its oxidation resistance [145].

Figure 5. 2 and Figure 5. 3 graphically illustrate the effect of antioxidants on the corrosion resistance of MgO-C refractories. It was revealed that the refractory grade Ref 3 with the highest amount of antioxidant (3 wt.% Al, 1 wt.% Si) had the lowest amount of dissolved MgO in the slag from the refractory after the interaction. The refractory grade with no antioxidant (Ref 2) had the highest increase in MgO concentration in the slag after the experiment. As shown in the figures, the addition of antioxidants reduces the dissolution of the MgO from the refractory into the slag. Al_2O_3 or MgAl2O4 formed in the matrix of MgO–C refractory (equation 2.3 and 2.4) would effectively protect the carbon from oxidising, and also fill the pores created, hence subsequently increase the refractory's corrosion resistance. Therefore, as depicted in Figure 5. 2 and Figure 5. 3, the refractories containing antioxidants (Ref 1 and Ref 3) demonstrated a better corrosion resistance compared to the bricks without antioxidants (Ref 2) at two different dwelling times (1hr 20 min and 4 hrs).

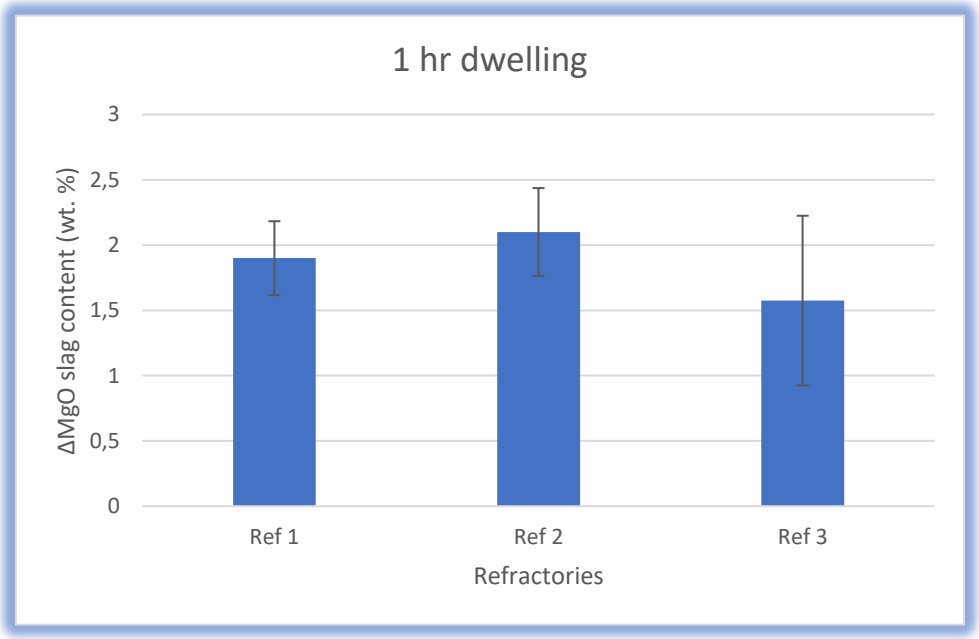

Figure 5. 2. MgO content evolution of slag 1 after interaction with the refractory samples with different amounts of antioxidants at 1 hr 30 mins dwelling time

Figure 5. 3. MgO content evolution of slag 1 after interaction with the refractory samples with different amounts of antioxidants at 4hrs dwelling time

5.4 The effect of slag composition

The effect of slag composition on the corrosion of MgO-C refractory material was investigated in this thesis by using two slags (1 and 2) with different MgO contents has shown in Table 3. 1. It can be seen from Figure 5. 4. MgO content evolution of slag 1 and 2 after interaction with the refractory samples with Ref 3 at 4hrs dwelling timeFigure 5. 4 that the corrosion rate i.e. the rate of change (increase) in MgO content in the slag is more for the slag with less initial MgO content in the slag (slag 2).

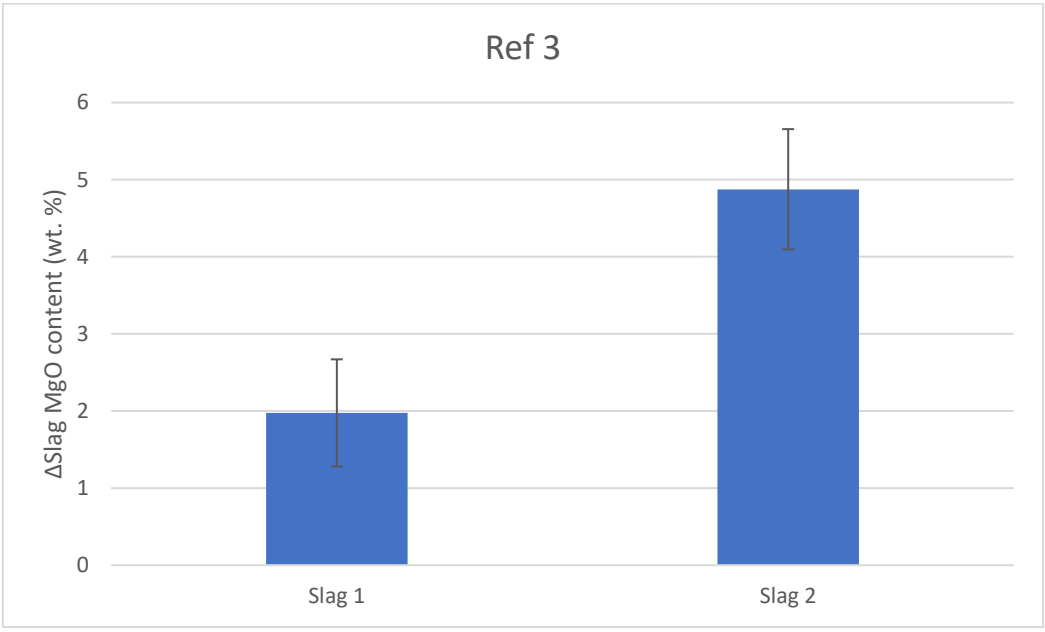

Figure 5. 4. MgO content evolution of slag 1 and 2 after interaction with the refractory samples with Ref 3 at 4hrs dwelling time

FactSage simulation results indicate that the MgO saturation of slag 1 is 9.5 wt.%, and while for slag 2 it is about 9.4 wt. % (Fig. 4.8 and Fig. 4.9). The average slag MgO content in experiment E3-2 is 11 wt. % and that of experiment E4 is 5.6 wt. %. The slag in E3-2 is apparently oversaturated with MgO and this is due to some undissolved detached MgO grains floating on the slag. Consequently, little or no corrosion by dissolution can occur. This is different for E4, as there is still room for slag dissolution of the refractory MgO grains since the saturation limit has not been reached. The lower MgO content of the slag increases the dissolution rate of the MgO–C refractory into liquid slag. This is due to the increase in the driving force for the dissolution process. The driving force of the dissolution of MgO into the slag at the refractory/ slag interface is the concentration gradient Δ (%MgO) as detailed in equation 2.16, 2.17, and 2.18 [113, 121]. The experimental results as graphically shown in Figure 2. 26Figure 2. 26. illustration of the dissolution process that leads to refractory corrosion [121]., is coherent with the equation 2.16. When the slag is saturated with the MgO, this driving force for the dissolution process goes away.

5.5 The effect of dwelling time

The effect of dwelling time on refractory corrosion via slag interaction was investigated in this masters thesis by perform three series of experiments at two different dwelling times of 1 hr 20 mins and 4 hrs as shown in Table 4.1 – 4.3. It can be inferred from the results as depicted in Figure 5. 5 that dwelling time affects the rate of corrosion of the MgO-C refractory. Experiments performed at the lower dwelling time of 1 hr 20 mins had less average slag MgO content increase (wt. %) across all the three series of experiments (E1-1, E2-1 and E3-1). Furthermore, as discussed earlier in section 4.4, experimental results as shown in Figure 4. 11 and Figure 4. 12 shows that penetration depth increased with increasing dwelling time. The experiments performed at longer dwelling time (4 hr) experienced more penetration of their refractory matrix by slag. Additionally, these penetrations could be noticed at increased depths.

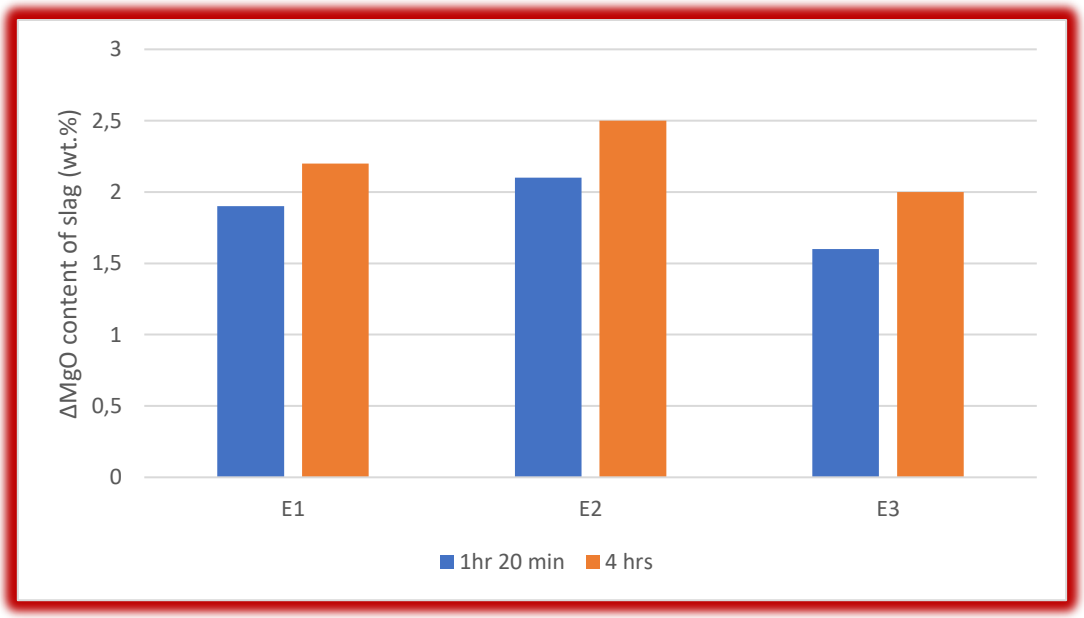

Figure 5. 5. MgO content evolution in slag 1 after interaction with the refractory samples in experiments E1, E2 and E3 atdifferent dwelling time of 1 hr 20 mins and 4hrs.

6. Conclusions

The goal of this master thesis was to make a comparative study of the corrosion and wear mechanism of different types of refractories with varying antioxidant compositions. This work was presented in three major sections that form the core of the master thesis. In the first section, the interaction at the refractory/ slag interface was studied and analysed. The major finding in this section includes:

Infiltration of slag into the MgO-C refractory was generally observed for most of the experiments. The infiltration of slag into the refractory from the experiments performed (E1, E2, E3 and E4) was largely dependent on the refractory composition (with or without antioxidants), slag composition (slag MgO content), slag viscosity and dwelling time. Refractories with antioxidants generally had less dissolution of MgO into the slag phase compared to the refractories without antioxidants.

Besides the dissolution of MgO from the refractory by the slag, detachment of periclase grains in direct contact with the slag at the refractory/ slag interface was a common phenomenon in the different experiments. These MgO grain detachments was a consequence of the weakening of large periclase grains in direct contact with the slag at the refractory/ slag interface. This was very much the case using slag 2 with a lower initial MgO content in experiment E4. There was more infiltration and detachment of large periclase grains at the interface.

There was an absence of magnesia alumina (MA) spinel at the refractory/ slag interface of the experiments due to the high temperature of the experiments, which made penetration of the slag through the refractory more likely.

The importance of the carbon phase in reducing penetration/ infiltration of slag cannot be understated. The carbon phase of the refractory sample after the experiments was not infiltrated by the slag. Carbon loss due to oxidation was not investigated in this thesis. However, pores caused by decarburisation was noticed, especially in the refractory without antioxidants (Ref 2).

In section 2, the slag composition after the refractory/ slag interaction was studied. The findings in this section are:

- Refractories with antioxidants generally had less dissolution of MgO in comparison to the refractories with antioxidants. Additionally, Ref 3 which had the highest antioxidant composition (3 wt.% of Al, and 1 wt.% of Si), had the lowest change (increase) in slag MgO content after the experiments.
- The Al_2O_3 content (wt. %) in the slag of the experiments with refractories that had antioxidants (Ref 1 and Ref 3) increased after the refractory/ slag interaction. The slag SiO_2 content stayed relatively the same from before and after the interaction. Some of the oxidised Al from the refractory can be said to have found its way into the slag phase, causing the increase in the slag alumina content after the interaction.

For section 3, the penetration behaviour and depth of penetration of the MgO-C refractory by slag were studied. The findings in Section 3 are: The experimental results indicated that the penetration rate and penetration depth increased with increasing dwelling time. Experiments performed at longer dwelling times experienced more penetration of their refractory matrix by slag. Additionally, these penetrations could be noticed at increased depths.

Another factor that influenced penetration behaviour was the initial slag composition. More viscous slag (slag 2) penetrated the refractory less than slag 1. Most of the MgO dissolution was done very close to the interface as compared to experiments using slag 1 for which penetration of the refractory matrix was still noticed at increased depths.

7. Future work

The following topics are suggested for further studies:

The experimental investigation of this thesis was carried out on the assumption that corrosion of the refractory is most critical at the slag line due to the refractory/slag interaction in this zone. However, during preheating of the ladle, as well as during stirring or degassing of molten steel in the ladle, the reaction between the MgO-C and furnace atmosphere (Argon, CO/CO2) can already cause decarburized zones in the refractory matrix. Molten slag could already infiltrate the refractory through these decarburized zones even before the dissolution of the MgO. Further studies and investigations have to be carried out to understand the behaviour of refractory materials in reducing (furnace) atmospheres like Argon and CO atmospheres.

The microstructural analysis of the experimental result in this thesis did not reveal the presence of SiC in the refractory. However, analysis and characterisation of the steel used in this thesis experiment were carried out by another colleague (Antonio Mazzon). His study revealed the presence of SiC inclusions in the steel. Hence, further studies and investigations have to be performed to understand how reaction products in the refractory can appear in the steel matrix as inclusions.

The experimental results of this thesis showed that there was a change in the slag composition after the experiment. Further studies should be done to investigate how this slag compositional change affects the slag properties and metallurgical requirements.

8. References

1. Beskow K, Tripathi NN, Nzotta M, Sandberg A, Du Sichen (2004) Impact of slag–refractory lining reactions on the formation of inclusions in steel. Ironmaking & Steelmaking. Doi:10.1179/030192304225019360
2. Bygden J, DebRoy T, Seetharaman S (1994) Dissolution of MgO in stagnant CaO-FeO-SiO2 slags. Ironmaking & Steelmaking 21(4):318–322
3. Ambedkar, K BR, Naidu, S G, Sreenivasarao, T, Varahalanaidu, G (2016) Studies on production of steel with improved cleanliness and its effect on mechanical properties. Journal of Production Engineering Vol.19(2):114–116
4. Pretorius EB, Oltmann HG, Schart BT (2013) An overview of steel cleanliness from an industry perspective. Ironmaking & Steelmaking 1-2(1):993–1026
5. Gómez-Rodríguez C, Castillo-Rodríguez GA, Rodríguez-Castellanos EA, Vázquez-Rodríguez FJ, López-Perales JF, Aguilar-Martínez JA, Fernández-González D, García-Quiñonez LV, Das-Roy TK, Verdeja LF (2020) Development of an Ultra-Low Carbon MgO Refractory Doped with α-Al2O3 Nanoparticles for the Steelmaking Industry: A Microstructural and Thermo-Mechanical Study. Materials (Basel, Switzerland). Doi:10.3390/ma13030715
6. Dekkersl R, Jokanovlc" N, Romboutl A, l BB, Wollants P (2005) Steel cleanliness during Secondary Metallurgy of High-grade Quality Electric Steels 76(7)
7. Zhang L, Thomas BG (eds) (2002) Evaluation and control of steel cleanliness. Dept of Mech. Engg., University of Illinois at Urbana-Champaign
8. Gupta A, Goyal S, Padmanabhan KA, Singh AK (2015) Inclusions in steel: micro–macro modelling approach to analyse the effects of inclusions on the properties of steel. Int J Adv Manuf Technol. Doi:10.1007/s00170-014-6464-5
9. Pérez J (2012) Inclusion control model in the ladle metallurgy furnace. Master of Science, Hamilton, Ontario, Canada
10. Sharma R (2011) Investigation of inclusion characteristics in LCAK Calcium Treated Steel. Master Thesis, Stockholm, Sweden
11. Stephen Famurewa Mayowa (2009) Improvement of the desulphurisation process by slag composition control in the ladle furnace. Master Thesis,
12. Basak S, Kumar Dhal R, Roy GG (2010) Efficacy and recovery of calcium during CaSi cored wire injection in steel melts. Ironmaking & Steelmaking. Doi:10.1179/030192309X12506804200384
13. Costa e Silva ALVd (2019) The effects of non-metallic inclusions on properties relevant to the performance of steel in structural and mechanical applications. Journal of Materials Research and Technology. Doi:10.1016/j.jmrt.2019.01.009
14. Kiessling R, Lange N (1978-89) Non-metallic inclusions in steel, 2nd edn. Metals Society. Book no.194; 411. Metals Society, London
15. Klueh RL, Shingledecker JP, Swindeman RW, Hoelzer DT (2005) Oxide dispersion-strengthened steels: A comparison of some commercial and experimental alloys. Journal of Nuclear Materials. Doi:10.1016/j.jnucmat.2005.01.017
16. Lifeng Zhang (Dr.), Brian G. Thomas (Prof.) (eds) (2003) Inclusions in continuous casting of steel, Morelia, Mich, Mexico
17. Michelic S, Bernhard C (2020) Special Metallurgical Process Technology: Secondary Metallurgy. MONTANUNIVERSITÄT LEOBEN,Chair of Ferrous Metallurgy
18. Moll, D, Wehrstedt, A (2009) Für die Bestimmung nicht metallischer Einschlüsse in Stählen mit Richtreihenbildern gilt jetzt DIN EN 10247:2007. MP Materials Testing 51(6):382–389
19. Michelic S (2020) Laboratory process in ferrous metallurgy: Inclusion Metallurgy, Leoben

20. Ren Q, Zhang L, Yang W (2018) Effect of Oxide Inclusions on the Magnetic Properties of Non-Oriented Electrical Steel. steel research int. Doi:10.1002/srin.201800047
21. Manganese sulphide inclusions in steel: Part One (2015) Total materia. https://www.totalmateria.com/page.aspx?ID=CheckArticle&site=kts&NM=443
22. Burja J, Koležnik M, Župerl Š, Klančnik G (2019) Nitrogen and nitride non-metallic inclusions in steel. Mater. Tehnol. Doi:10.17222/mit.2019.247
23. Janis D, Karasev A, Jönsson PG (2015) Evaluation of Inclusion Characteristics in Low-Alloyed Steels by Mainly Using PDA/OES Method. ISIJ International. Doi:10.2355/isijinternational.ISIJINT-2015-172
24. Bartosiaki BG, Pereira JAM, Bielefeldt WV, Vilela ACF (2015) Assessment of inclusion analysis via manual and automated SEM and total oxygen content of steel. Journal of Materials Research and Technology. Doi:10.1016/j.jmrt.2015.01.008
25. Non-metallic inclusion in steel (2018) Steel data
26. Hatto F. Jacobi (2005) The MIDAS technique for detection of macroscopic inclusions in CC 2010;Material: Fundamentals and Practical Applications. Steel research International 76(8):596–602
27. Jacobi H, Wünnenberg K (2003) Improving oxide cleanness on basis of MIDAS method. Ironmaking & Steelmaking. Doi:10.1179/030192303225001702
28. Nagaytsev, Theile, Abelt (2017) SILENOS - Steel inclusion level evaluation by numerical optical systems. MATLAB EXPO
29. On the Representativeness of Automated SEM/EDS Analyses for Inclusion characterisation with special regard to the measured sample area (2011) Susanne K. Michelic, Gerhard Wieser and Christian BERNHARD. ISIJ International 51(5):769–775
30. Pandey JC, Raj M, Roy TK, Venugopalan T (2008) A novel method to measure cleanliness in steel using ultrasonic C-Scan Image Analysis. Metall and Materi Trans B. Doi:10.1007/s11663-008-9146-6
31. Gianluca Nastasi RN (2013) Determining inclusion size distributions from OES/PDA data. Yejin Fenxi/Metallurgical Analysis 33(3):9–13
32. Lifeng Zhang and Brian G. Thomas (2003) State of the art in evaluation and control of steel cleanliness. ISIJ Int. 43(3):271–291
33. CUI Jian ZHENG Yiyu ZHU Lixin (2005) Progress of production technology of clean steel in BaoSteel. Strategic Study of Chinese Academy of Engineering 7(6):21–26
34. Li-feng Z (2004) Indirect methods of detecting and evaluating inclusions in steel. J: Iron & Steel Research International 13(2)
35. Zhang S, Lee WE (2000) Influence of additives on corrosion resistance and corroded microstructures of MgO–C refractories. Journal of the European Ceramic Society 21:2393–2405
36. T R, Kadli R, S AK (2014) Control of nitrogen pickup in steel at continuous casting using Buckingham PI theorem. International Journal of Recent Development in Engineering and Technology 3(2):150–156
37. Kailash Bathy Vodeyar Math (2012) Optimization of steel production: Ladle furnace slag and caster productivity. Masters Thesis, Montreal, Canada
38. Peter Tom Jones (2001) Degradation mechanism of basic refractory materials during the secondary refining of stainless steel in VOD ladles. Ph.D Thesis
39. Alan* E, Çetin* Z, Keler* K, Ayçiçek+ İ (eds) (2017) Effects of slag optimization on steel cleanliness in secondary metallurgy process
40. Dippenaar R (2005) Industrial uses of slag (the use and re-use of iron and steelmaking slags). Ironmaking & Steelmaking. Doi:10.1179/174328105X15805

41. Scheunis L, Campforts M, Jones PT, Blanpain B, Malfliet A (2015) The influence of slag compositional changes on the chemical degradation of magnesia-chromite refractories exposed to PbO-based non-ferrous slag saturated in spinel. Journal of the European Ceramic Society. Doi:10.1016/j.jeurceramsoc.2014.08.017
42. Lencina R, Zhang B, Malfliet A, Chen Y, Touzo B, Blanpain B, Guo M (eds) (2019) Pre-Fused vs. Blended Fluxes: Their impact on cleanliness of Low-Carbon Low-Alloy steel
43. Lencina R, Malfliet A, Touzo B, Guo M (eds) (2018) Slag conditioning of Ti-Stabilized stainless steel by using a TiO2-Rich Calcium Aluminate Flux
44. Yan P, Huang S, Pandelaers L, van Dyck J, Guo M, Blanpain B (2013) Effect of the CaO-Al2O3-Based Top Slag on the Cleanliness of Stainless Steel During Secondary Metallurgy. Metall and Materi Trans B. Doi:10.1007/s11663-013-9898-5
45. Scheunis L, Fallah Mehrjardi A, Campforts M, Jones PT, Blanpain B, Jak E (2014) The effect of phase formation during use on the chemical corrosion of magnesia–chromite refractories in contact with a non-ferrous PbO–SiO2 based slag. Journal of the European Ceramic Society. Doi:10.1016/j.jeurceramsoc.2013.12.026
46. Wöhrmeyer C, Jolly R, Brüggmann C (2011) Novel Fluxing Agents for Ladle Slags to Improve Refractory Life Time and Steel Quality. Refractories World Forum 3(3):81–86
47. Le Coq X, Dupre B, Gleltzer C, Adam R, Scheidt F, Tassot P (1990) Slag corrosion of dolomite-carbon refractories. Steel research 61(12):593–597
48. Benavidez E, Brandaleze E, Musante L, Galliano P (2015) Corrosion Study of MgO-C Bricks in Contact with a Steelmaking Slag. Procedia Materials Science. Doi:10.1016/j.mspro.2015.04.068
49. pinnacle Chemical wearing mechanism of refractory materials in a steel ladle slag line
50. Jansson S, Brabie V, Jonsson P (2005) Corrosion mechanism and kinetic behaviour of MgO-C refractory material in contact with CaO-Al2O3-SiO2-MgO slag. Scand J Metallurgy. Doi:10.1111/j.1600-0692.2005.00748.x
51. Blumenfeld P., Peruzzi S., Puillet M., de Lorgeril J. (2005) Recent improvements in Arcelor steel ladles through optimization of refractory materials, steel shell and service conditions. La Revue de Métallurgie-CIT:233–239
52. Boenzi F, Ordieres-Meré J, Iavagnilio R (2019) Life cycle assessment comparison of two refractory brick product systems for ladle Lining in Secondary Steelmaking. Sustainability. Doi:10.3390/su11051295
53. Bag M (2011) Development of Environment Friendly New Generation MgO-C Brick Using Nano Carbon
54. Jones PT (2001) DEGRADATION MECHANISMS OF BASIC REFRACTORY MATERIALS DURING THE SECONDARY REFINING OF STAINLESS STEEL IN VOD LADLES
55. Acidic refractory RS Refractories. https://refractoriesmaterials.com/acidic-refractory/
56. Refractories: Properties and types Roshni. https://www.engineeringenotes.com/engineering/refractories/refractories-properties-and-types-engineering/41897
57. Refractory brick chemical composition (2021) RESCO Product Inc. https://www.rescoproducts.com/resources/acidic-basic-neutral-refractory-brick
58. Cappel J (2007) The link between refractories, slag and steel in ferrous metallurgy. RHI Bulletin 1(1):61–69
59. A. Buhr (1999) Refractories steel secondary metallurgy. CN-Refractories 6(3):19–30
60. a WSR, a RMS, b SMJ, b RMA, b EL, b JBB, No last name!, b ERL, b CAP, b, L. E. B. Soledade, b JEG, c JAV (2000) Key features of alumina/magnesia/graphite refractories for steel ladle lining. Journal of the European Ceramic Society 20:1419–1427

61. Cho M-K, van Ende M-A, Eun T-H, Jung I-H (2012) Investigation of slag-refractory interactions for the Ruhrstahl Heraeus (RH) vacuum degassing process in steelmaking. Journal of the European Ceramic Society. Doi:10.1016/j.jeurceramsoc.2012.01.005
62. Otunniyi IO, Theko ZV, Mokoena BLE, Maramba B (eds) (2019) Major determinant of service life in magnesia-graphite slagline refractory lining in secondary steelmaking ladle furnace 655
63. Parithy Magnesia carbon refractory bricks granulometry
64. Liu C, Gao X, Kim S-j, Ueda S, Kitamura S-y (2018) Dissolution behavior of Mg from MgO–C refractory in Al-killed molten steel. ISIJ International. Doi:10.2355/isijinternational.ISIJINT-2017-593
65. Ren X-m, Ma B-y, Li S-m, Li H-x, Liu G-q, Yang W-g, Qian F, Zhao S-x, Yu J-k (2021) Comparison study of slag corrosion resistance of MgO–MgAl2O4, MgO–CaO and MgO–C refractories under electromagnetic field. J. Iron Steel Res. Int. Doi:10.1007/s42243-020-00421-0
66. Cheng Y, Zhu T, Li Y, Sang S (2021) Microstructure and properties of MgO–C refractory with different carbon contents. Ceramics International. Doi:10.1016/j.ceramint.2020.09.099
67. Bounziova J, Nagyová I, Zajac V, Hrabčáková L, Vadász P, Kamenský R (2016) Testing magnesia-carbon bricks for oxidation resistance. Acta Metall. Slovaca. Doi:10.12776/ams.v22i3.677
68. Lee KS, Jo G-H, Jung Y-G, Byeun Y (2016) Effect of carbon content on the mechanical behavior of MgO–C refractories characterized by Hertzian indentation. Ceramics International. Doi:10.1016/j.ceramint.2016.03.097
69. Huihua W, Channa W, Yingjun X, Kun J, Tianpeng Q, Jun T, Deyong W (2019) Induced electro-deposition of high melting-point phases on MgO–C refractory in CaO–Al2O3–SiO2 – (MgO) slag at 1773 K. High Temperature Materials and Processes. Doi:10.1515/htmp-2018-0035
70. Shand MA (2006) The chemistry and technology of magnesia. Wiley-Interscience, Hoboken, N.J
71. Abu-Hamatteh ZSH, Alnawafleh MA (2009) Evaluation of magnesia clinker extracted from dolomite rocks. Mineral Processing and Extractive Metallurgy Review. Doi:10.1080/08827500802665508
72. Bag M, Adak S, Sarkar R (2012) Study on low carbon containing MgO-C refractory: Use of nano carbon. Ceramics International. Doi:10.1016/j.ceramint.2011.10.086
73. PlasmaChem (2018) Surface and Nano-Technology: Nanomaterials and related products
74. Bag M, Adak S, Sarkar R (2012) Nano carbon containing MgO-C refractory: Effect of graphite content. Ceramics International. Doi:10.1016/j.ceramint.2012.02.082
75. Dr. Gerald Buchebner Basic Brick for the Steel Industry. Refractory Technology
76. Bahtli T, Murat Bostanci V, Yesim Hopa D, Yalcin Yasti S (2018) The Effect of Carbon Sources on the Thermal Shock Properties of MgO-C Refractories. ujms. Doi:10.13189/ujms.2018.060501
77. Patra SK (2014) Effect of specially formulated graphite on the thermo-mechanical properties of Al2O3-C slide gate plate refractory
78. Kuffa T, Su~ik G, Hr{ak D (2005) THE INFLUENCE OF CARBON MATERIALS ON THE PROPERTIES OF MgO REFRACTORIES
79. Pagliosa C, Freire N, Cholodovskis G, Pandolfelli VC (2014) MgO–C Bricks Containing Nano-boron Carbide
80. Liu Z, Yu J, Yang X, Jin E, Yuan L (2018) Oxidation Resistance and Wetting Behavior of MgO-C Refractories: Effect of Carbon Content. Materials (Basel, Switzerland). Doi:10.3390/ma11060883
81. Gokce AS, Gurcan C, Ozgen S, Aydin S (2008) The effect of antioxidants on the oxidation behaviour of magnesia–carbon refractory bricks. Ceramics International. Doi:10.1016/j.ceramint.2006.10.004
82. Atsuhisa Iida, Masayoshi Kakihara, Minoru Suto, Hidenori Tada (2016) Improvement of MgO-C Bricks for BOF Based on Microstructure Investigation

83. Luz AP, Souza TM, Pagliosa C, Brito MAM, Pandolfelli VC (2016) In situ hot elastic modulus evolution of MgO–C refractories containing Al, Si or Al–Mg antioxidants. Ceramics International. Doi:10.1016/j.ceramint.2016.03.080
84. Campos KS, Lenz e Silva GFB, Nunes EHM, Vasconcelos WL (2012) The influence of B4C and MgB2 additions on the behavior of MgO–C bricks. Ceramics International. Doi:10.1016/j.ceramint.2012.04.009
85. Zhang S, Marriott NJ, Lee WE (2000) Thermochemistry and microstructures of MgO-C refractories containing various antioxidants
86. Chen L, Chen W, Hu Y, Chen Z, Xu Y, Yan W (2018) Effect of Al antioxidant in MgO–C refractory on the formation of Al 2 O 3 -rich inclusions in high-carbon steel for saw wire under vacuum conditions. Ironmaking & Steelmaking. Doi:10.1080/03019233.2016.1261245
87. Trick KA, Saliba TE (1995) MECHANISMS OF THE PYROLYSIS OF PHENOLIC RESIN IN A CARBON/PHENOLIC COMPOSITE
88. Wang* J-G, Guo Q-G, Liu L, Song J-R (2002) Study on the microstructural evolution of high temperature adhesives for graphite bonding
89. Prof. Dr. Ing. W. SCHULLE, Dor. Dr. Ing. habil. J. ULBRICHT (1992) Influence of different carbonaceous binders on the properties of refractories
90. Aneziris CG, Borzov D, Ulbricht J, Suren J, Dern H (2004) Phenolic Resins with Carbo-Resin Additions for Improved MgO-C Refractories. KEM. Doi:10.4028/www.scientific.net/KEM.264-268.1767
91. Maldhure AV, Wankhade AV (2017) In-situ development of carbon nanotubes network and graphitic carbon by catalytic modification of phenolic resin binder in Al 2 O 3 –MgO–C refractories. Journal of Asian Ceramic Societies. Doi:10.1016/j.jascer.2017.04.010
92. Jun* L, LiHongXia, Feng Haixia (2015) Influence of carbores binder on the strength of Magnesia-Carbon materials
93. Sarkar R, Sohn HY (2018) Interactions of alumina-based and magnesia-based refractories with iron melts and slags. Metall and Materi Trans B. Doi:10.1007/s11663-018-1300-1
94. Svantesson JL, Glaser B, Ersson M, White JF, Imris M, Jönsson PG (2020) Study of dynamic refractory wear by slags containing very high FeO contents under steelmaking conditions. Ironmaking & Steelmaking. Doi:10.1080/03019233.2020.1827672
95. Wagner C, Wenzl C, Gregurek D, Kreuzer D, Luidold S, Schnideritsch H (2017) Thermodynamic and experimental investigations of high-temperature refractory Corrosion by Molten Slags. Metall and Materi Trans B. Doi:10.1007/s11663-016-0861-0
96. Lee WE, Zhang S (1999) Melt corrosion of oxide and oxide–carbon refractories. International Materials Reviews. Doi:10.1179/095066099101528234
97. Mukai K (1992) Wetting and marangoni effect In iron and steelmaking processes. ISIJ Int. 32(1):19–25
98. The marangoni effect Multiphysics Cyclopedia. https://www.comsol.com/multiphysics/marangoni-effect
99. Brabie V (1997) A study on the mechanism of reaction between refractory materials and aluminium deoxidised molten steel. Steel research 68(2):54–60
100. Chen Y, Wang J, Zhang L Transient Interaction between Molten Iron, Alumina Lining Refractory and Slag
101. Li Y, Yang W, Zhang L (2020) Formation Mechanism of MgO Containing Inclusions in the Molten Steel Refined in MgO Refractory Crucibles. Metals. Doi:10.3390/met10040444
102. Jurgen Cappel (2007) The Link Between Refractories, Slag, and Steel in Ferrous Metallurgy
103. Sunayama H, Kawahara M Oxidation Rate Of Magnesia-Carbon Refractory Under Low Oxygen Partial Pressure

104. Jansson S, Brabie V, Bohlin L (eds) (2004) Corrosion mechanism and kinetic behaviour of refractory materials in contact with CaO-Al2O3-MgO-SiO2 slags
105. Blond E, Schmitt N, Hild F, Blumenfeld P, Poirier J (2007) Effect of Slag Impregnation on Thermal Degradations in Refractories. J American Ceramic Society. Doi:10.1111/j.1551-2916.2006.01348.x
106. Jansson S (2008) A Study on the influence of steel, slag or gas on refractory reactions. Doctoral Thesis, Stockholm Sweden
107. Watanabe A, Takahashi H, +, Nakatani' F (1986) Mechanism of dense magnesia layer formation near the surface of magnesia-carbon brick
108. Ji H, Hong Y, Ahn J, Chung* Y (2017) Interaction between molten metal and MgO-C refractory during RH Degassing process in steelmaking, Rep. of Korea
109. Harada A, Miyano G, Maruoka N, Shibata H, Kitamura S-y (2014) Dissolution behavior of Mg from MgO into molten Steel deoxidized by Al. ISIJ Int. Doi:10.2355/isijinternational.54.2230
110. Schwerdtfeger* K (1983) Present state of oxygen control in aluminum deoxidized steel. Arch. Eisenhuttenwes. 54(3):87–98
111. Guo M, Parada S, Jones PT, Boydens E, Dyck JV, Blanpain B, Wollants P (2009) Interaction of Al2O3-rich slag with MgO–C refractories during VOD refining—MgO and spinel layer formation at the slag/refractory interface. Journal of the European Ceramic Society. Doi:10.1016/j.jeurceramsoc.2008.07.063
112. Harmuth H (2021) Continuous refractory wear. Continuous refractory wear, Leoben, Austria
113. Huang A, Harmuth H, Doletschek M, Vollmann S, Feng X (2015) Toward CFD modeling of slag entrainment in gas stirred ladles. steel research int. Doi:10.1002/srin.201400373
114. Riaz S, Mills KC, Bain K (2002) Experimental examination of slag/refractory interface. Ironmaking & Steelmaking. Doi:10.1179/030192302225003477
115. R S, C FM (eds) (1996) Glazing of steel ladles. 39th International colloquium on refractories, Aachen, Germany
116. da Cruz RT, Bragança SR (2015) Evaluation of the protective C2S layer in the corrosion process of doloma-C refractories. Ceramics International. Doi:10.1016/j.ceramint.2014.12.028
117. Cruz RT, Bielefeldt WV, Bragança SR (2017) Influence of ladle slag composition in the dissolution process of the dicalcium silicate (C2S) layer on doloma-C refractories. Ceramics International. Doi:10.1016/j.ceramint.2017.08.076
118. ZushuLI, Tao KMZ (2000) Reaction between MgO-C refractory, molten slag and metal. ISIJ Int. 40:101–105
119. Wei R, Lv X, Yue Z, Xiang S (2017) The dissolution kinetics of MgO into CaO-MgO-Fe2O3 slag. Metall and Materi Trans B. Doi:10.1007/s11663-016-0842-3
120. McCauley RA (2013) Corrosion of Ceramic Materials 60. Emerald Group Publishing Limited
121. Vollmann S, Harmuth H (2010) Investigation of refractory corrosion of a gas-stirred steel ladle by simulation. AST. Doi:10.4028/www.scientific.net/AST.70.199
122. Fruehan RJ, Martonik LJ (1976) The Rate of reduction of MgO by carbon. Metallurgical Transaction 78:537–542
123. Kitamura S-y (2017) Dissolution behavior of lime into steelmaking slag. ISIJ International. Doi:10.2355/isijinternational.ISIJINT-2017-109
124. Umakoshi M, Mori* K, Kawai* Y (1984) Dissolution rate of burnt dolomite in molten Fe2O-CaO-SiO2 slags. ISIJ Int. 24:532–539
125. Huang F, Liu C, Maruoka N, Kitamura S-Y (2015) Dissolution behaviour of MgO based refractories in CaO–Al 2 O 3 –SiO 2 slag. Ironmaking & Steelmaking. Doi:10.1179/1743281215Y.0000000003

126. National Standards Authority of Ireland (4th 2006) Methods of test for dense refractory products: Guidelines for testing the corrosion of refractories caused by liquids, Ireland (ICS 81. 080)
127. Lee WE, Zhang S (eds) (2004) Direct and indirect slag corrosion of oxide and oxide-c refractories 7
128. Reynaert C, Sniezek E, Jacek S (2020) Corrosion test for refractory materials intended for the steel industry. Ceramics-Silikáty 64(3)
129. Tang HY, Wu GH, Wang Y, Li JS, Lan P, Zhang JQ (2017) Comparative evaluation investigation of slag corrosion on Al2O3 and MgO-Al2O3 refractories via experiments and thermodynamic simulations. Ceramics International. Doi:10.1016/j.ceramint.2017.09.034
130. Braulio MAL, Martinez AT, Luz AP, Liebske C, Pandolfelli VC (2011) Basic slag attack of spinel-containing refractory castables. Ceramics International. Doi:10.1016/j.ceramint.2011.02.007
131. Pena P, Criado E, Bakali JJ, Baudín C (2011) Dynamic corrosion of Al2O3–ZrO2–SiO2 and Cr2O3-containing refractories by molten frits. Part II: Microstructural study. Journal of the European Ceramic Society. Doi:10.1016/j.jeurceramsoc.2010.11.024
132. Guo M, Parada S, Jones PT, van Dyck J, Boydens E, Durinck D, Blanpain B, Wollants P (2007) Degradation mechanisms of magnesia-carbon refractories by high-alumina stainless steel slags under vacuum. Ceramics International. Doi:10.1016/j.ceramint.2006.03.009
133. Chen L, Malfliet A, Jones PT, Blanpain B, Guo M (2016) Degradation mechanisms of alumina–silica runner refractories by carbon steel during ingot casting process. Ceramics International. Doi:10.1016/j.ceramint.2016.03.139
134. Um H, Lee K, Kim K-Y, Shin G, Chung Y (2014) Effect of carbon content of ferromanganese alloy on corrosion behaviour of MgO–C refractory. Ironmaking & Steelmaking. Doi:10.1179/1743281212Y.0000000098
135. Hon M-H, Hsu C-C, Wang M-C (2008) Corrosion of magnesia–chrome brick in molten MgO–Al2O3–SiO2–CaO–FetO slag. Materials Chemistry and Physics. Doi:10.1016/j.matchemphys.2008.02.001
136. Korgul P, Wilsod Dr, Lee'* WE (1997) Microstructural analysis of corroded alumina-spinel castable refractories. Journal of the European Ceramic Society 17(1):77–84
137. Chena S-K, Chengb M-Y, Linb S-J, Koc Y-C, No last name! (2002) Thermal characteristics of Al2O3–MgO and Al2O3–spinel castables for steel ladles. Ceramics International 28(1):811–817
138. Ko Y-C (2002) Role of spinel composition in the slag resistance of Al2O3–spinel and Al2O3–MgO castables. Ceramics International 28:805–810
139. Bavand-Vandchali M, Golestani-Fard F, Sarpoolaky H, Rezaie HR, Aneziris CG (2008) The influence of in situ spinel formation on microstructure and phase evolution of MgO–C refractories. Journal of the European Ceramic Society. Doi:10.1016/j.jeurceramsoc.2007.07.009
140. Ghosh A, Jena S, Tripathi HS, Haldar MK, Reddy VP, Ghosh J, Das SK, Rao AKR, Ray P (2013) The influence of metallic antioxidants on some critical properties of Magnesia-carbon refractories. refractories WORLDFORUM 5(4):69–74
141. Sadrnezhaad SK (2011) Effect of Si antioxidant on the rate of oxidation of carbon in MgO–C refractory. IJE. Doi:10.5829/idosi.ije.2011.24.04b.06
142. Sadrnezhaad SK, Nemati ZA, Mahshid S, Hosseini S, Hashemi B (2007) Effect of Al antioxidant on the rate of oxidation of carbon in MgO-C refractory. J American Ceramic Society. Doi:10.1111/j.1551-2916.2006.01391.x
143. Sune Jansson (2005) A study on molten steel/slag/refractory reaction during ladle stel refining. Doctorate Thesis

144. Tabatabaie-Hedeshi SM, Bavand-Vandchali M, Naghizadeh R (2020) Characterization and post-mortem analysis of Al2O3-MgO-C refractories used in steelmaking ladle furnaces. Engineering Failure Analysis. Doi:10.1016/j.engfailanal.2020.104697
145. Bavand-Vandchali M, Golestani-Fard F, Sarpoolaky H, Rezaie HR, Aneziris CG (2008) The influence of in situ spinel formation on microstructure and phase evolution of MgO–C refractories. Journal of the European Ceramic Society. Doi:10.1016/j.jeurceramsoc.2007.07.009

Appendix A: Interaction at interface

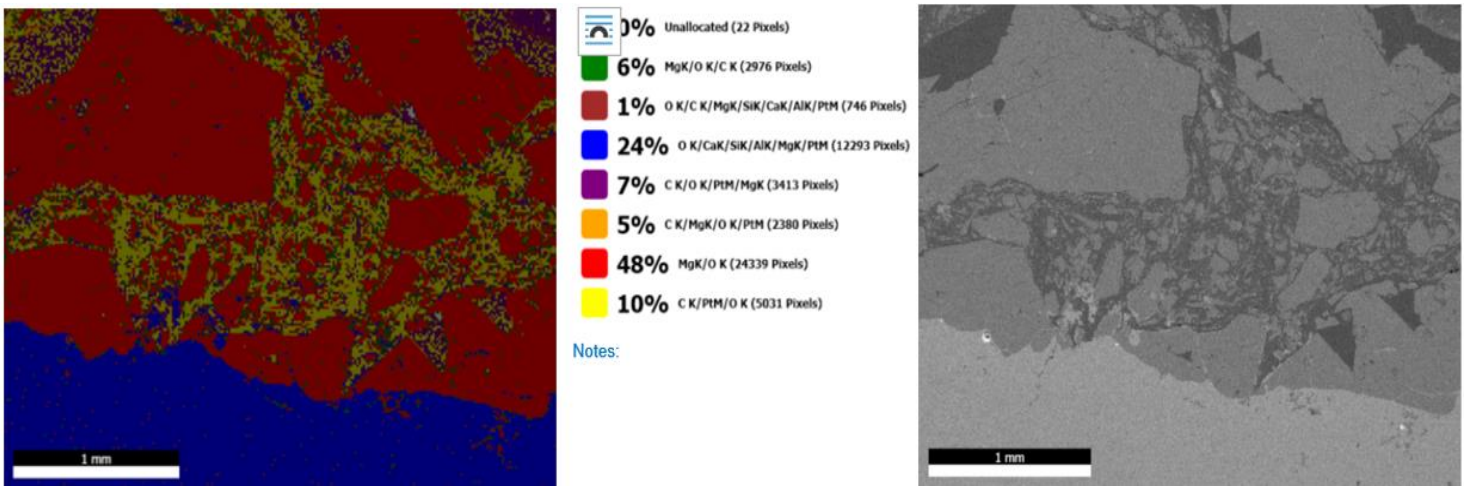

Fig A.1: EDS mapping image of the refractory/slag interface of experiment E1-1 (Ref 1 and slag 1; 1 hr 20 mins dwelling time)

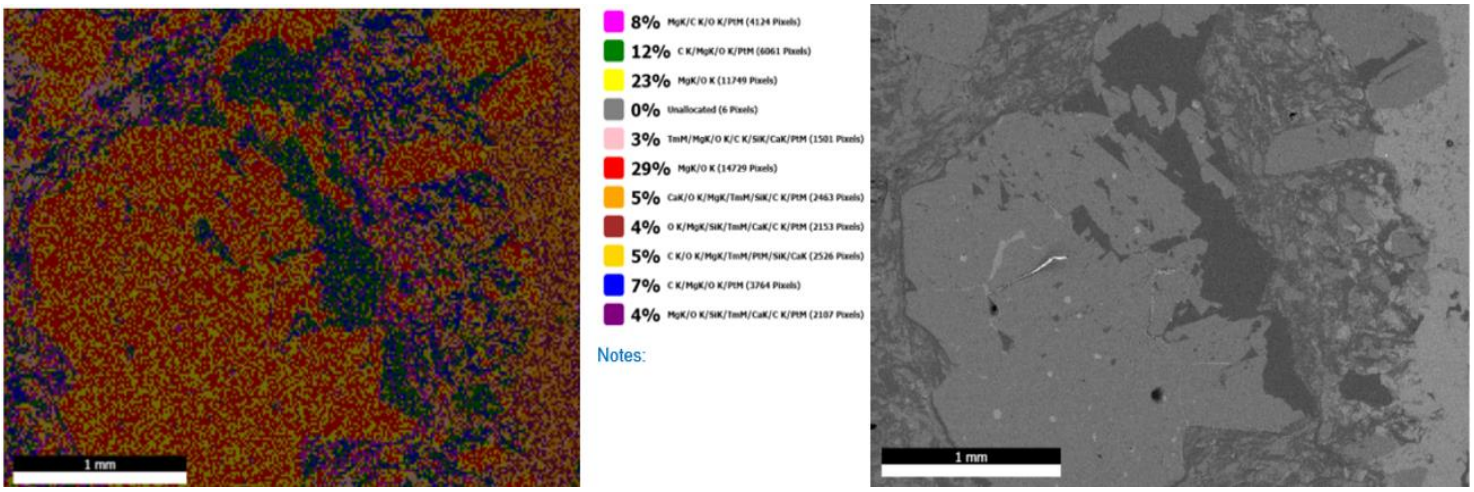

Fig A.2: EDS mapping image of the refractory/slag interface of experiment E1-2 (Ref 1 and slag 1; 4 hrs dwelling time)

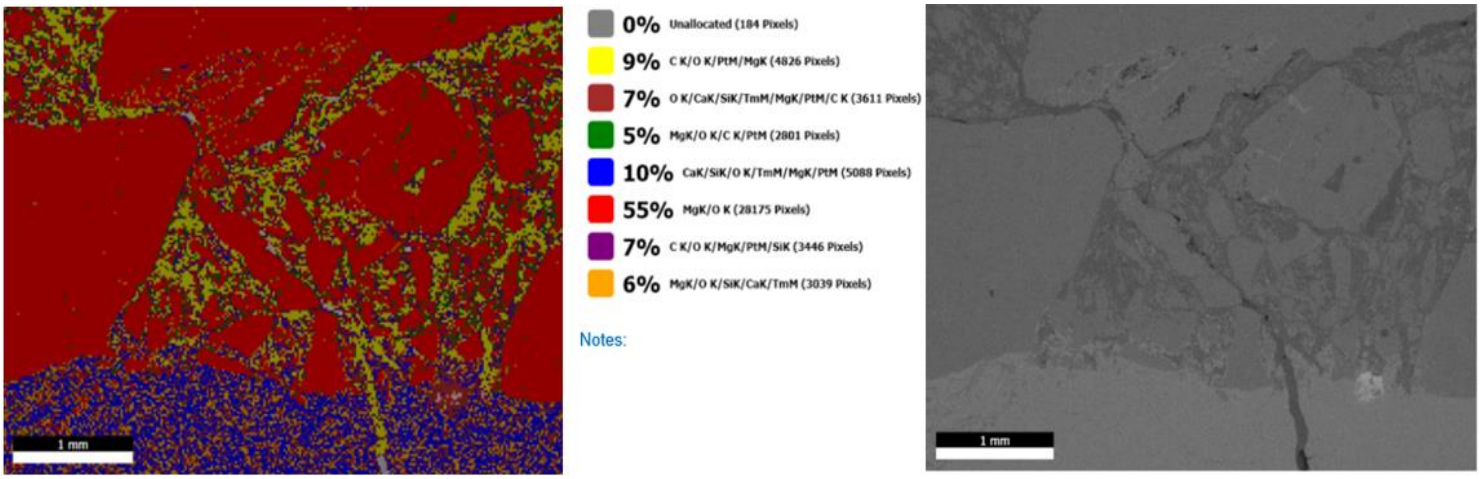

Fig A.3: EDS mapping image of the refractory/slag interface of experiment E2-2 (Ref 2 and slag 1; 4 hrs dwelling time)

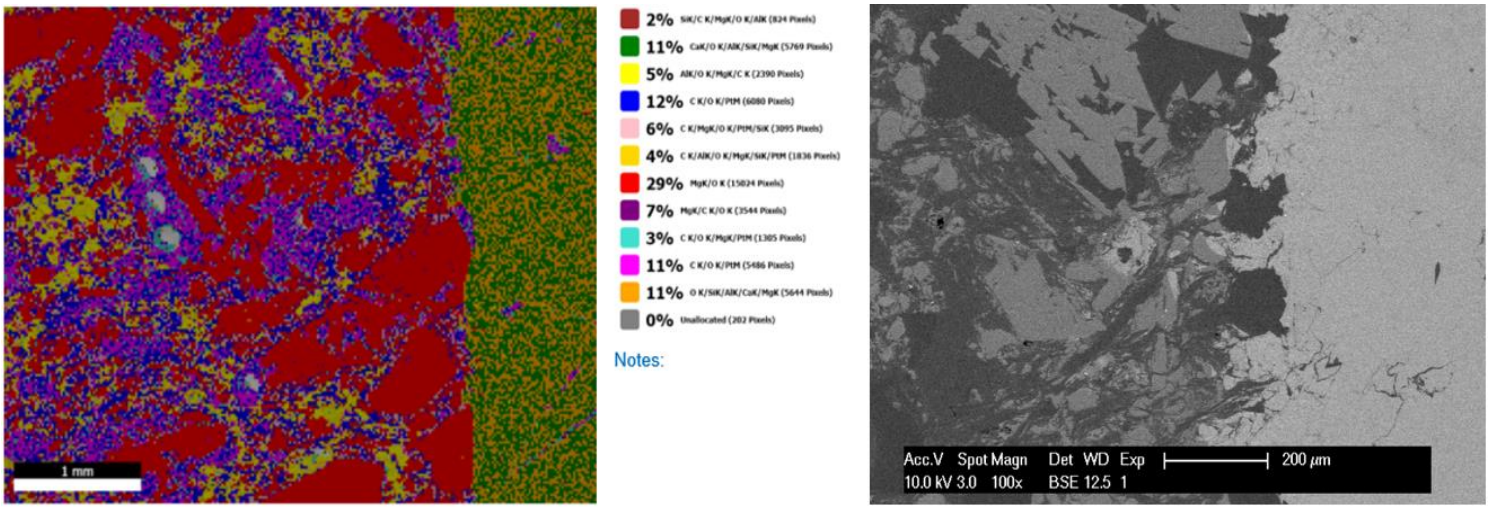

Fig A.4: EDS mapping image of the refractory/slag interface of experiment E3-1 (Ref 3 and slag 1; 1 hr 20 mins dwelling time)

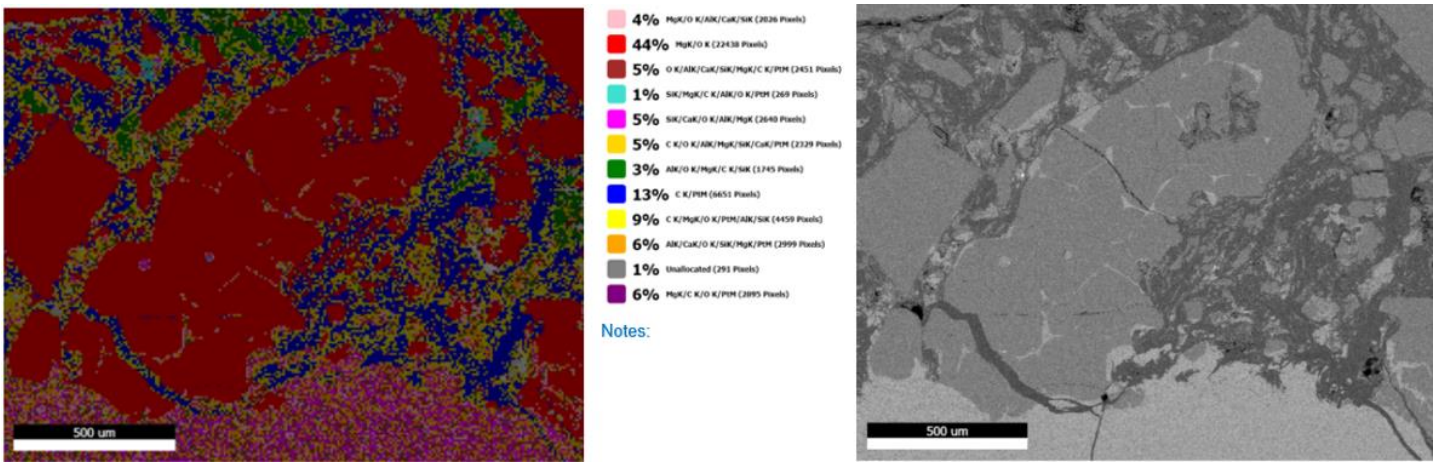

Fig A.5: EDS mapping image of the refractory/slag interface of experiment E3-2 (Ref 3 and slag 1; 4 hrs dwelling time)

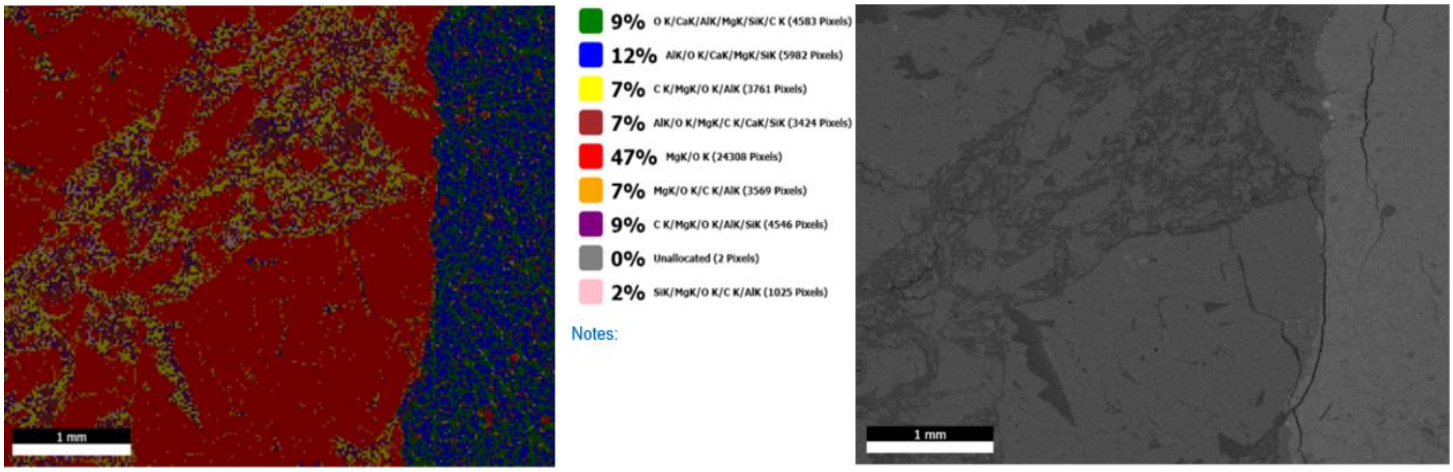

Fig A.6: EDS mapping image of the refractory/slag interface of experiment E3-2 (Ref 3 and slag 2; 4 hrs dwelling time)

Appendix B: Slag composition

Table B.1: Average slag composition of E1-1 (after experiment) as a function of distance from refractory/slag interface

Distance for interface (µm)	CaO (wt%)	MgO (wt%)	Al2O3 (wt%)	SiO2 (wt%)
0	46.4	10.7	17.1	25.7
300	45.5	11.3	17.4	25.8
600	48.3	10.9	16.6	24.3
900	49.9	10.7	16.7	22.7

Table B.2: Average slag composition of E1-2 (after experiment) as a function of distance from refractory/slag interface

Distance for interface (µm)	CaO (wt%)	MgO (wt%)	Al2O3 (wt%)	SiO2 (wt%)
0	48.3	11.5	15.6	24.6
300	49.8	11.4	15.6	23.2
600	49.0	11.2	14.5	25.3
900	47.0	10.7	16.0	26.2

Table B.3: Average slag composition of E2-1 (after experiment) as a function of distance from refractory/slag interface

Distance for interface (µm)	CaO (wt%)	MgO (wt%)	Al2O3 (wt%)	SiO2 (wt%)
0	44.5	11.2	18.2	26.0
300	45.5	11.5	17.5	25.5
600	44.2	11.0	19.1	25.8
900	42.9	10.7	20.6	25.7

Table B.4: Average slag composition of E2-2 (after experiment) as a function of distance from refractory/slag interface

Distance for interface (µm)	CaO (wt%)	MgO (wt%)	Al2O3 (wt%)	SiO2 (wt%)
0	44.9	11.9	18.4	24.8
300	45.1	11.7	17.4	25.6
600	43.8	11.2	18.9	26.1
900	42.9	11.1	19.6	26.4

Table B.5: Average slag composition of E3-1 (after experiment) as a function of distance from refractory/slag interface

Distance for interface (µm)	CaO (wt%)	MgO (wt%)	Al2O3 (wt%)	SiO2 (wt%)
0	46.9	10.9	16.9	25.2
300	48.6	11.2	17.1	23.0
600	46.0	10.5	19.1	24.4
900	45.3	9.7	19.8	25.2

Table B.6: Average slag composition of E3-2 (after experiment) as a function of distance from refractory/slag interface

Distance for interface (µm)	CaO (wt%)	MgO (wt%)	Al2O3 (wt%)	SiO2 (wt%)
0	48.2	11.7	15.9	24.3
300	48.2	11.4	16.7	23.7
600	47.8	10.6	18.0	23.6
900	46.7	10.2	19.6	23.5

Table B.7: Average slag composition of E4 (after experiment) as a function of distance from refractory/slag interface

Distance for interface (µm)	CaO (wt%)	MgO (wt%)	Al2O3 (wt%)	SiO2 (wt%)
0	46.5	6.2	19.5	27.8
300	46.9	6.1	19.2	27.8
600	45.8	5.5	20.9	27.8
900	47.6	4.5	19.9	28.0